JAERI-Review
95-021

ANNUAL REPORT OF NAKA FUSION RESEARCH ESTABLISHMENT

from April 1, 1994 to March 31, 1995

November 1995

Naka Fusion Research Establishment

日本原子力研究所
Japan Atomic Energy Research Institute

本レポートは，日本原子力研究所が不定期に公刊している研究報告書です。
入手の問合わせは，日本原子力研究所技術情報部情報資料課（〒319-11 茨城県那珂郡東海村）あて，お申しこみください。なお，このほかに財団法人原子力弘済会資料センター（〒319-11 茨城県那珂郡東海村日本原子力研究所内）で複写による実費領布をおこなっております。

This reports are issued irregularly.
Inquiries about availability of the reports should be addressed to Information Division Department of Technical Information, Japan Atomic Energy Research Institute, Tokaimura, Naka-gun, Ibaraki-ken 319-11, Japan.

編集兼発行　日本原子力研究所
印　　刷　ニッセイエブロ株式会社

JAERI-Review 95-021

Annual Report of Naka Fusion Research Establishment from April 1, 1994 to March 31, 1995

Naka Fusion Research Establishment

Japan Atomic Energy Research Institute
Naka-machi, Naka-gun, Ibaraki-ken

(Received October 27, 1995)

Research and development activities at Naka Fusion Research Establishment, JAERI, are reported for the period from April 1, 1994 to March 31, 1995.

The main objectives of the JT-60 experiments are: confinement improvement, impurity control and divertor studies, steady-state studies, and energetic particle physics. In FY 1994 the highest fusion-triple-product of $1.2\times10^{21}m^{-3}\cdot s\cdot keV\cdot$ was marked in high-β_p H-mode plasma through the optimization of target plasma, heating profile and first wall condition. Regarding steady operation, the triple fusion product of $4.4\times10^{20}m^{-3}\cdot s\cdot keV$ was sustained for 1.5sec in the ELMy phase of the high-β_p H-mode. Plasma current of 1MA was sustained by non-inductive full current with NB(37%) and with bootstrap current(74%). Helium ash exhaustion, simulated with helium beam injection, demonstrated that wall pumping with the solid target boronization reduced the helium content to one-third of that without boronization and kept constant accumulation(5%) and the helium neutral pressure in the divertor(1×10^{-3} Pa). JFT-2M experiments progressed in the momentum transport study by applying an external helical field and toroidal momentum input with NBI, and also, the boundary plasma study through the introduction of an electric field in the scrape-off layer(SOL) by the divertor biasing. A design of divertor modification for a closed divertor study was carried out with keeping the divertor biasing capability being kept. The study in Plasma Theory and Computation focused on the stability of the

Editors: Nagashima T. (Chief), Naito O., Ogiwara N., Saigusa M., Seki M., Murasawa M., Uehara Y.

Toroidal Alfven Eigenmode(TAE) mode as well as analyses of confinement and heating process, MHD equilibrium and stability analyses. Progress in the DIII-D experiments was obtained in the studies of divertor radiation, advanced tokamak and VH-mode plasma.

As for the fusion technology research, activities are focused on the Research and Development (R&D) for ITER EDA: superconducting magnets, neutral beam heating, radio frequency heating, plasma facing components, reactor structure, remote maintenance, shielding branket, tritium processing, tritium safety and fusion safety. In the development of pulsed poloidal field coils, R&D for mass-production of a 9.6ton Nb_3Sn conductor was completed and fabrication of a 9.6ton Nb_3Sn for 13T was started for ITER. In the development of the DC toroidal field coils, a high performance Nb_3Al strand was also developed. The full-sized conductor with 1152 strands successfully produced 39kA at 11.6T and 7.1K. Construction of a MeV-class ion source test facility was completed and the negative H beam was successfully accelerated up to 580keV with a drain current of 110mA for 1sec. Stable, high efficiency, high power generation was demonstrated in a gyrotron with beam energy recovery. By the application of an electron retarding potential, efficiency was enhanced from 30 to 50% at 610kW for 50msec and 400kW for 4sec at 110GHz. Development of an ITER-relevant 170GHz gyrotron was started. A new tritium removal system using gas separation membranes was studied so as to develop a more compact and cost-effective system for a fusion reactor. A divertor mockup consisting of a flat-plate unidirectional CFC(carbon fiber reinforced carbon composite) armors brazed onto W/Cu composites successfully endured a heat load of 25MW/m^2, 30sec for more than 1000 thermal cycles. Special emergency bearing resistant to large lift forcing was fabricated and tested for the ceramic turbo-viscous pump designed for ITER. The R&D efforts of the reactor structure development focused on the fabrication and testing of a full-scaled section model of double-walled vacuum vessel. Fabricability of the HIPped(Hot Isostatic Pressing) first wall of the ITER shield blanket was investigated through the fabrication of test specimens and partial mockups.

Based on the Outline Design approved in March 1994 by the ITER Council a sensitivity study was conducted by the new director and JCT in close collaboration with four Home Teams in order to determine the optimum way to achieve a reduction in the cost of ITER while minimizing the impacts regarding its performance margins. Japanese Home Team carried out a part of the ITER design based on task agreements, mainly in the field of vacuum vessel, first wall and blanket, initial assembly, etc. The DREAM tokamak reactor concept was improved focusing on the reactor internals and safety.

Keywords: Fusion Research, JAERI, JT-60, JFT-2M, DIII-D, Plasma Physics, Fusion Engineering, Fusion Technology, ITER, Fusion Reactor Design, Annual Report

那珂研究所年報（平成６年度）

日本原子力研究所
那珂研究所

（1995年10月27日受理）

原研・那珂研究所における平成６年度（1994年４月～1995年３月）の研究開発活動について報告する。

ＪＴ－60の主な実験目的は、閉じ込め特性の改善、不純物制御、ダイバータに関する研究、定常化研究、及び、高エネルギー粒子物理の研究である。1994年度の実験ハイライトは、高βpHモードのプラズマにより、核融合積$1.2\times10^{21}m^{-3}\cdot s\cdot keV$が記録された。定常化の観点では、高$\beta$pHモードのエルミー期間中に核融合積$4.4\times10^{20}m^{-3}\cdot s\cdot keV$が維持された。無誘導電流により１ＭＡの完全プラズマ電流が中性粒子入射による電流（37％）とブートストラップ電流（74％）により維持された。ヘリウム灰排気に関連して、ヘリウムビームの入射により、ボロナイゼーションの場合の壁による排気をシミュレートし、ボロナイゼーションを行わない場合の１／３にヘリウム量が低減し、ダイバータでのヘリウム分子の圧力は1×10^{-3}Paに達した。また、ＪＦＴ－２Ｍ実験では、外部ヘリカル磁場の印加、及び、中性子粒子入射によりトロイダル方向にモーメンタムを与えることにより、モーメンタムの輸送に関する研究、及び、ダイバータへの電圧印加によるスクレープ層での電界の導入によるプラズマ境界物理の研究が進展した。また、クローズ型ダイバータの設計がダイバータへの電圧印加とともに進められた。プラズマ理論・数値解析では、アルフヴェン固有モードの研究を中心に、プラズマの閉じ込め、加熱機構の解析、ＭＨＤの平衡や安定性の解析が行われた。日米協力によるＤⅢ－Ｄの実験では、ダイバータ放射、先進的トカマク、ＶＨモードプラズマで進展があった。

核融合炉工学については、国際熱核融合実験炉（ＩＴＥＲ）の工学設計活動（ＥＤＡ）に関連して、超電導磁石、中性粒子入射加熱、高周波加熱、プラズマ対向機器、炉構造、遠隔保守、遮蔽ブランケット、トリチウムの処理と安全、核融合炉の安全に関する技術を中心に開発研究（Ｒ＆Ｄ）が進んでいる。超電導パルス磁石については、高性能のNb_3Al導体が開発され、11.6T，7.1Kにおいて39kAの通電が実証された。高エネルギー負イオンビームの開発では、580keVで110mA（引き出し電流値）を1秒間加速するのに成功した。高周波技術では、周波数110GHzジャイロトロンにおいて、エネルギー回収により出力 610kW、50msにおいて効率を30％から50％に高効

那珂研究所：〒311－01　茨城県那珂郡那珂町向山801-1
編集者：永島　孝（責任者）、内藤　磨、荻原　徳男、三枝　幹雄、関　昌弘、
村沢　道彦、上原　勇相

率化するとともに、高効率運転による 400kW、４秒という長パルス試験にも成功した。ＩＴＥＲ用の170GHzジャイロトロンの開発を開始した。ＩＴＥＲ用として開発した１m長のダイバータ試験体（ＣＦＣ材料）による試験では、25MW/m^{2}の熱流束で30秒間、1000サイクルの試験に耐えた。新しいトリチウム回収技術として、気体分離膜による方法が開発されたが、これはよりコンパクトで経済的な方法として有望なものである。ＩＴＥＲに関連する炉構造開発として、２重壁構造の大型部分モデルの製作が行われ、第一壁・遮蔽ブランケットの熱間静水圧加工（ＨＩＰ）による製作性について試験体と部分モデルにより製作技術が確立した。

1994年３月のＩＴＥＲ理事会に承認された概要設計に基づき、感度研究が新しい所長とＩＴＥＲ中央共同チームと各極の国内チームとの密接な協力により進められ、性能を下げずにコストを軽減する方策が検討された。日本国内チームは、タスク契約に基づき、特に、真空容器、第一壁・ブランケット、初期組立等の設計に貢献した。核融合動力炉に関しては、ＤＲＥＡＭトカマク炉の概念検討を進め、安全性等について進展があった。

Contents

目　　次

付　　録

Foreword

Japan Atomic Energy Research Institute (JAERI), Naka Fusion Research Establishment (Naka), have been conducting fusion experiments on JT-60, JFT-2M, and DIII-D (US-Japan collaboration) regarding their physics activities. As for the technology, activities have been focused on R&D for the International Thermonuclear Experimental Reactor (ITER)-Engineering Design Activity (EDA). In addition, JAERI have been organizing the Japanese Home Team involving Japanese industries, which is giving strong support to the Joint Central Team (JCT) of ITER-EDA.

The aim of the JT-60 program is to study confinement improvement, impurity control with a magnetic divertor, steady-state operation and energetic particle physics. The JFT-2M and DIII-D are continuing studies on the advanced tokamak concepts with higher stability limits and an ingenious profile control. The study in theory and computation has been carried out on the topics of confinement analyses, MHD stability and burning physics.

As for the ITER technology R&D, ongoing activities are superconducting magnets, neutral beam heating, radio frequency heating, plasma facing components, reactor structure, remote maintenance, shielding blanket and tritium technology. Also based on the Outline Design issued in March 1994 by the ITER Council the sensitivity study was conducted by the director and JCT in close collaboration with four Home Teams.

The highlight of the JT-60 experiment was the highest fusion-triple-product of 1.2×10^{21} $m^{-3} \cdot S \cdot keV$, marked in high-β_p H–mode. Remarkable progress was also made regarding studies on steady-state operation, helium-ash exhaust, etc. related to ITER physics R&D. In ITER engineering R&D, a full-size conductor with high performance Nb_3Al strands demonstrated 39 kA at 11.6 T and 7.1 K. The development of a negative ion source and a high efficiency gyrotron both for ITER showed that significant progress had been made.

The JAERI Fusion Program is based on the Third Phase Basic Program of Fusion Research and Development laid down by the Atomic Energy Commission of Japan in 1992. All of JAERI's Naka programs can supply essential information for preparing the next generation core devices such as ITER. Since October 1992 JAERI, Naka have provided a Joint Work Site for the JCT of ITER-EDA, as well as in Garching and San Diego.

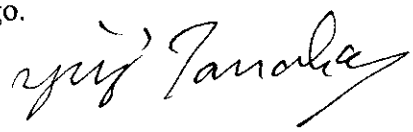

Yuji Tanaka
Director General
Naka Fusion Research
Establishment, JAERI

I. JT-60 PROGRAM

1. Overview

JT-60 is a single null divertor tokamak with capability of plasma current $I_p < 6$ MA, toroidal magnetic field $B_t < 4.4$ T, aspect ratio A =3.2–4.5, and shape parameters $\delta < 0.3$, $\kappa < 1.8$. Additional heating of the neutral beam (NB), 36 MW, lower hybrid (LH), 7 MW, and ion cyclotron (IC), 7 MW, were installed. Main objectives of the JT-60 project are: (1) confinement improvement, (2) impurity control and divertor studies, (3) steady-state studies, and (4) energetic particle physics. On the basis of these studies, contribution to the ITER physics R&D and providing a database for the conceptual design of fusion power reactors like SSTR are being sought.

The highest fusion triple product $n_D(0)\ T_i(0)\ \tau_E$ of 1.2×10^{21} keV s m^{-3} was marked during FY 1994 in high-β_p H-mode plasma through the optimization of target plasma, heating profile, and first wall condition. The high performance of high-β_p H-mode plasma could be achieved by the formation of the internal thermal barrier, which was first observed in JT-60 in the plasma inside as well as in the plasma periphery. From the aspect of steady operation, the triple fusion product of 4.4×10^{20} keV s m^{-3} was sustained for 1.5 s in the ELMy phase of the high-β_p H-mode.

Plasma current of 1 MA was sustained by non-inductive full current drive with NB (37%), and with bootstrap current (74%). The results have demonstrated the plasma conditions for the Steady-State Tokamak Reactor (SSTR). Non-inductive current drive was also sustained by LH wave injection with two multi-junction launchers and by tangential NB. Maximum driven current of 3.6 MA (LH), 0.6 MA (NB) and maximum drive efficiency η_{CD} of 0.35×10^{20} A $W^{-1}m^{-2}$ (LH), 0.075×10^{20} A $W^{-1}m^{-2}$ (NB) were achieved, respectively. Current profile control with LH and NB could also be demonstrated.

Helium ash exhaustion, simulated with the helium beam injection, showed that wall pumping with the solid target boronization reduced the helium content to one-third of that without boronization and kept the helium accumulation constant in the core plasma (5%) and the helium neutral pressure in the divertor (1×10^{-3} Pa). The results look quite promising for the ITER design.

Radiative divertor was produced by strong gas puff in L-mode plasma, which produced a divertor radiation fraction having an input power of up to 70%. Although 40% of the input power was radiated at the divertor in ELMy H-mode, optimization to prevent the neutral particle influx was required from viewpoint of sustaining the improved confinement in a core plasma.

Improved confinement and steady-state operation research will be undertaken with a negative-NB experiment starting early in 1996, and with a closed divertor installation late in 1996.

2. Operation of the JT-60

2.1 Tokamak

2.1.1 Operation and maintenance of the JT-60 machine

Operation and maintenance of the JT-60 machine have been carried out almost on schedule. In relation to vacuum leakage, it was observed that a diagnostic window and an insulated joint of RF had cracked. Water leakage of the drift tube of the tangential neutral beam injector could also be observed. These damaged parts were repaired immediately, and then we were able to recover JT-60 to an efficient extent. Moreover, three main turbo molecular pumps were exchanged for new pumps, and the programmable controller of the exhaust section was changed. Regarding the gas injector, the damaged bellows of the gas injector was also changed, and a new piezoelectric actuator gas injection valve was developed. Pellets of deuterium, neon and mixture for them were also developed, and the projection tests were successful. We could also find the crack in the cooling tube of the toroidal coil, which caused water leakage in 1992, using a newly developed fiber scope. V coil joint-bars were installed for the experiment of high triangularity configuration plasma. In October 1994, a water cooling experiment for divertor tiles was carried out successfully. In the *in-situ* boronization system, deuterium gas injection was added, and then, the 6th boronization was performed using this newly modified system in March 1995.

2.1.2 Operation results of plasma facing components

Various wall conditioning methods have been used in JT-60. Especially, boronization has been used successfully to reduce any oxygen impurity. We have two methods for boronization. One is a boronization system using decaborane, and the other is, the so-called, solid target boronization (STB) using B_4C-converted CFC divertor tiles installed along the toroidal ring. The wall conditioning time after the vacuum vessel vent has been actually shortened using these methods. Six boronization experiments have been carried out so far. In the 6th boronization test using a gas mixture of deuterium and helium in glow discharge instead of helium only, a reduction in hydrogen in the boron film could be achieved. On the other hand, the B_4C-converted CFC tiles installed in December 1993 served the real-time STB due to the strong evaporation of the B_4C-converted layer. Figure I.2.1-1 shows severe melting surfaces of the B_4C tiles. As a result of STB, a low concentration level of impurities was able to be achieved.

Water cooling experiment of the divertor tiles, which was carried out in October 1994, showed that the water cooling of the divertor tiles was also effective in reducing the impurity production.

From the measurements of the tritium content in the graphite first wall tiles removed from JT-60 in November 1993, a total quantity of tritium which remained in the graphite first wall was estimated to be 1.6×10^{10} Bq. This value corresponds to about 50% of the tritium generated from July 1991 until October 1993 in JT-60.

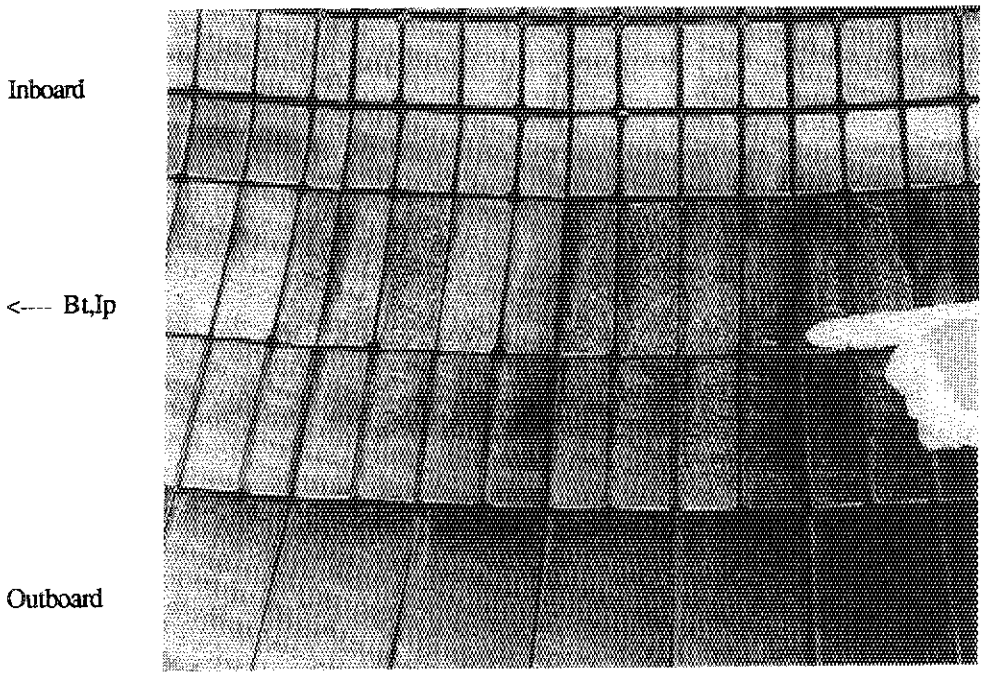

Fig. I.2.1-1. A typical view of the divertor tiles after operation until October 1994, showing severe melting surfaces of B_4C tiles installed in December 1993.

2.2 Control system

The control system continuously works in the JT-60 experiments according to the required schedule. Two functions were newly developed this fiscal year for the real-time feedback control system to fulfill the experimental objectives: (a) high triangularity plasma operation, and (b) neutron production rate feedback control. Since the high triangularity plasma operation was expected to improve energy confinement and suppress ripple loss, a feedback control algorithm for plasma triangularity was developed and installed in the equilibrium control computer system. In a fusion power plant, its neutron production rate must be controlled so as to regulate the electric power output. To test this controllability, a function was added to the feedback algorithms in which the neutron production rate could be controlled to the reference waveform by NBI for the actuator.

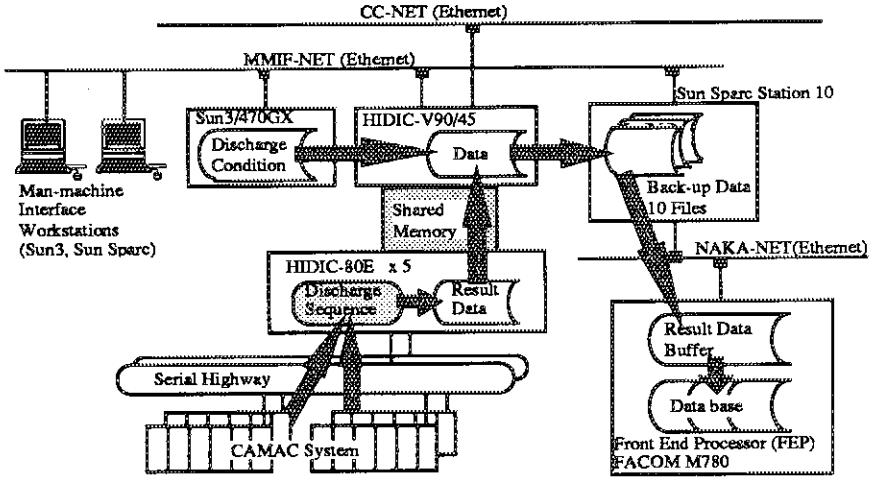

Fig.I.2.2-1. A new data transfer route from JT-60 to the database system.

For maintenance of the control system, annual inspections are being carried out for the computer system, control boards, and the signal processing system for plasma control during the shutdown period from November to December. JT-60 discharge result date is transferred to the general purpose computer (FACOM M-780, Fujitsu Ltd.) from the central control system (HIDIC 80E, Hitachi Ltd.) through a special channel interface. To rejuvenate the system, those computers are supposed to be replaced by workstations having high capability at a lower price. For the first step, the data transfer route through a network, Ethernet, was developed as shown in Fig. I.2.2-1.

2.3 Power supply

The JT-60 power supply systems, namely, the toroidal field power supply (TFPS), the poloidal field power supply (PFPS) and the motorgenerator for the heating system (H-MG) operated on schedule under the JT-60 experimental plan this fiscal year. The power distribution system and emergency power supply also operated smoothly. As preventive maintenance, the capacitor banks of the constant voltage constant frequency (CVCF) inverter and the smoothing capacitors in the uninterruptible power supply system were replaced, respectively.

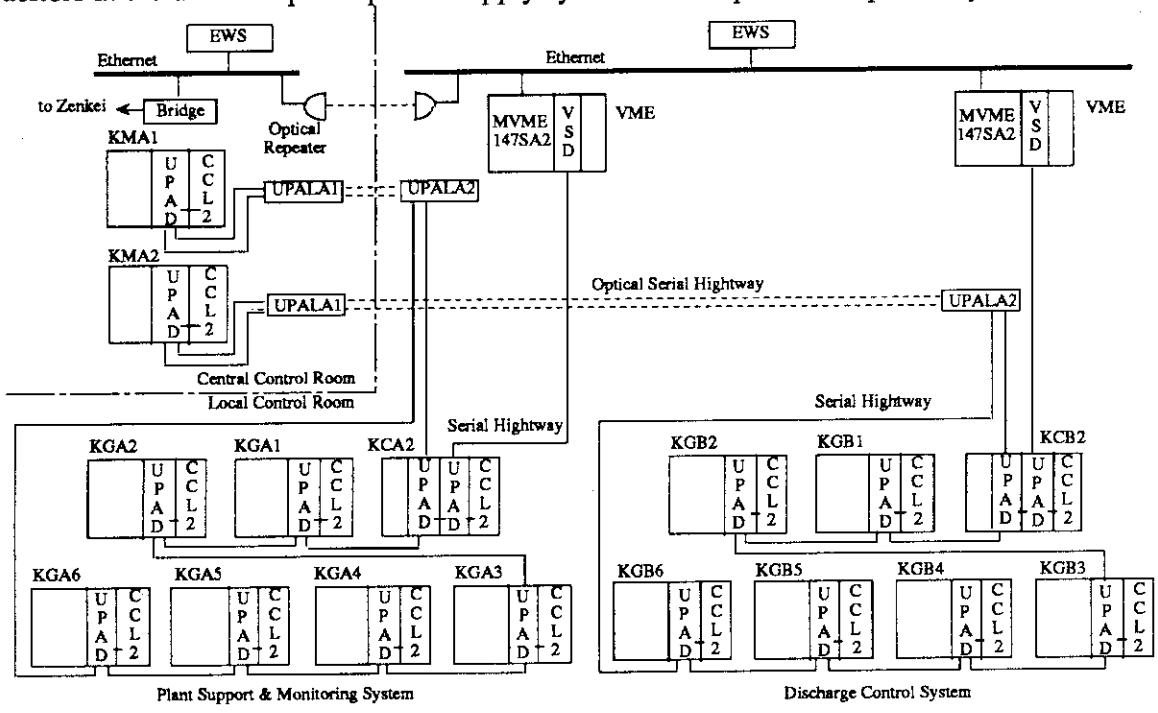

Fig.I.2.3-1. New control system for PFPS.

For PFPS, the rejuvenation of the CAMAC control system was completed in January, 1995 [2.3-1]. All of the CAMAC-based 16-bit microcomputers and memory (ROM/RAM) modules were replaced by VMEbus-based 32-bit microcomputers as shown in Fig.I.2.3-1.

Modern engineering workstations are dedicated for data communication with the JT-60 central control computer system (Zenkei) via an Ethernet LAN and for human interface in the operation of PFPS. After this renewal the operational efficiency has been improved, because the troubles due to the CAMAC-based microcomputers were decreased to a great extent.

PFPS was also modified as regards the construction of the test facilities for the central solenoid (CS) model coil under the ITER EDA program. PFPS was used as a pulse power supply in this test, where the operation pattern with a long pulse up of to 75 s which can be seen in Fig.I.2.3-2 (a) is required from the viewpoint of both magnetic field strength and its change rate. However, the maximum period of operation time in the OH-coil power supply (OHPS) was 25 s in the JT-60 high power pulse operation. This comes from the thermal limit of the field windings of the motor generator (P-MG), whose output voltage is normally 18 kV. The thyrister converters and snubber resistors have no thermal limits regarding this operation pattern. Then, a new operation mode where the output voltage of MG is 11 kV was added in the automatic voltage regulator (AVR) of the exciting control boards. The long pulse operation of PFPS using a dummy load coil after modification were successful as shown in Fig.I.2.3-2 (b).

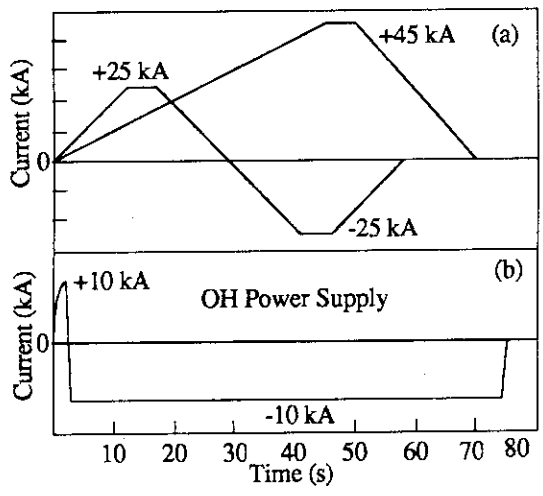

Fig. I.2.3-2. (a) Waveforms of the coil current required for the CS model coil. (b) Test results using a dummy load coil.

Some modifications in H-MG and the power distribution system were carried out for supplying electric power to the negative-ion-based NBI system under development.

Reference

[2.3-1] Kimura T., Nucl. Instr. and Meth. in Phys. Res. A **352** (1994) 125.

2.4 Neutral beam injection system

The JT-60 neutral beam injection system (JT-60 NBI), consisting of four tangential and 10 quasi-perpendicular beam line units, was operated almost on schedule under the JT-60 experimental plan in this fiscal year. Beam injections into JT-60 were performed successfully at a beam energy of 80 to 100 keV with beam species of D, H, and ^{4}He. Moreover, ^{3}He beams were injected into the JT-60 plasma in order to investigate the Toriton burning performance.

The pumping capability of the mixed gas, ^4He and D_2, was examined by cryo-sorption using an argon-condensed layer in a quasi-perpendicular beam line cryopump(#1). The sorption pumping speed for the mixed gas was about 700 m^3/s, while, the speed for only the ^4He gas was about 480 m^3/s. The amount of the adsorbed mixed gas during the test was 123 Pam3. It was confirmed that the NBI cryopumps were applicable for density control in the closed type divertor system.

2.5 Radio-frequency system

2.5.1 LHCD system

The lower hybrid current drive (LHCD) system for JT-60 consists of three sub-systems and has been operated at the frequency range of 1.74 - 2.23 GHz. Each sub-system could inject RF power of 2 - 3 MW. The system has two multijunction launchers. The 24 x 4 multijunction launcher (CD-1') is driven by one sub-system and the other launcher (CD-2) by two sub-systems. The CD-2 launcher consists of 4 x 4 multijunction modules. Each module has 12 sub-waveguides lined up toroidally. Both the launchers were greatly useful to study the current profile control and wave absorption mechanism.

A launcher is one of the most important components to decide the capability of injection of RF power to the plasma in the LHCD system. Injection of RF power with short pulses into a vacuum is very effective for conditioning the launcher quickly and keeping its high power injection ability. Then, in this fiscal year, we have improved the RF control system to make it easier to inject RF power into a vacuum in the interval of tokamak discharges. A new control system was added into the existing control system, as shown in Fig. I.2.5-1. It consists of a workstation, VME-bus involving a timing generator and an exclusive selector. The existing system mainly works for the injection into the plasma. The graphical user interface and a mouse key-in are adopted in the additional system so that it is designed to operate the LHCD system easily and quickly.

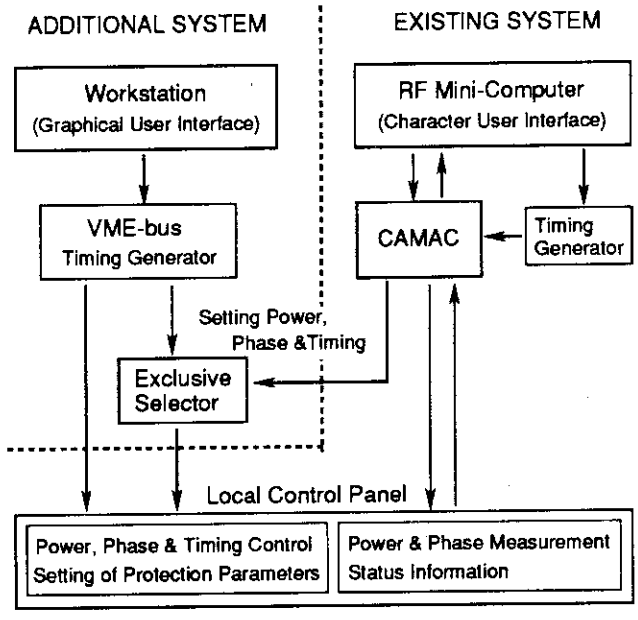

Fig.I.2.5-1. Diagram of the modified LHCD control system.

2.5.2 ICRF system

The ion cyclotron range of frequencies (ICRF) system for JT-60 was operated well at 116 MHz in FY 1994. The output power of the ICRF system was increased from 6 to 8 MW for 3 sec last fiscal year. Then, this fiscal year the system could inject power levels of 6 MW into plasmas

stably with P11 and P12 antennas, and it contributed to studies for TAE modes, behaviour of energetic ions up to several MeV and so on. Also, the injection of 5 MW level assisted in the generation of H-mode plasma at a high plasma current 4 MA in combined NBI and ICRF heating, suppressing sawtooth oscillation in the core plasma by ICRF power. It is noted that the power was injected at a large gap (0.15 m) between the separatrix and the antenna Faraday shield even in H-mode plasmas.

Hot spots on the Faraday shield were observed by a TV camera for special experimental conditions [2.5-1]. After the experiment, small melting marks were found (about 5 mm in width, about 15 mm in length) on the limited section of Faraday shield surface, which seemed to be caused by energetic ion bombardment. Therefore, we have equipped an infra red (IR) TV camera system for measurement of temperature profile on the P11 antenna surface, as can been seen in Fig.I.2.5-2. The camera is contained in a shield box to reduce any effect due to a magnetic field, X-ray and neutron irradiation. The box consists of soft iron plates 15 mm thick, lead plates 6 mm thick, polyethylene plates 25 mm thick and stainless steel plates 1 5 mm thick. The IR TV camera system has shown clear data of temperature profiles, but it is still under calibration.

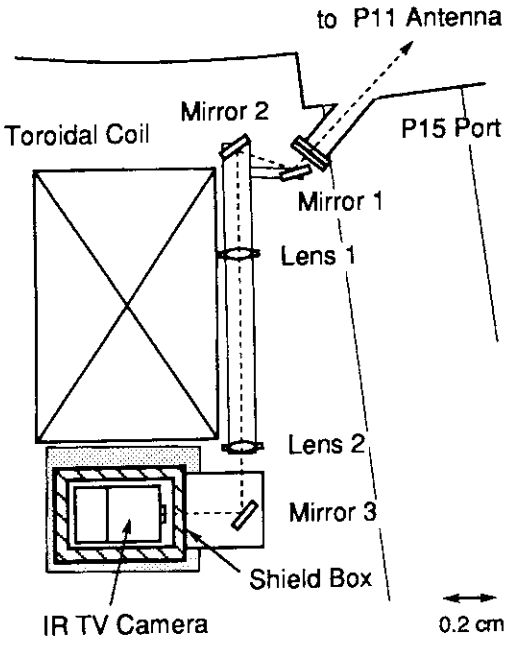

Fig.I.2.5-2. Arrangement of an IR TV camera system for measurement of temperature profiles on the P11 antenna surface.

Reference

[2.5-1] FUJII T., SAIGUSA M., KIMURA H., et al., "Performance of toroidally wide-separation loop antennae for JT-60 ICRF experiments", Proc of 5th Inter. Toki Conf. on Plasma Physics and Controlled Nuclear Fusion, Toki (1995) 377.

2.6 Diagnostic system

The recent progress of the diagnostic system development has been carried out under the following system. A newly introduced YAG laser Thomson scattering system has been successfully operating with high repetition measurements of the electron temperatures. Under successful cooperation with the international institutions and organizations, new neutron detectors and a high energy neutral particle analyzer are contributing to the research of heating and confinement mechanisms of plasma. Also, in the interferometry, remarkable progress has been made.

2.6.1 YAG laser Thomson scattering system

The YAG laser Thomson scattering system is being developed in order to measure the time evolution of electron temperature (T_e) and density profile with pseudo-continuously. The system consists of a Nd-YAG laser (1064 nm, 2 J, 10 Hz) and 20 polychromators of 6 spectral filter channels, in addition to the existing optics (light collection and laser incidence) of the ruby laser system. Configuration of this is shown in Fig. I.2.6-1. The preliminary results show that this system has a potential of wide dynamic range (20 eV-10 keV) for T_e measurements. The scattered spectra of the near infrared region are measured with Si Avalanche Photo Diode (APD) detectors, the sensitivity of which is larger than 20 A/W at 1064 nm. Since the gain of APD varies sensitively regarding temperature, APDs are mounted on a Peltier temperature control element to minimize the thermal variation of APD sensitivity. Many advantages are expected in the infrared region concerning the Thomson scattering diagnostics; one is the low influence of photon noise by strong line spectra such as D_α/H_α and by the radiation of Bremsstrahlung. Another important advantage is the hardness to window darkening caused by the coating effect of the plasma discharge, compared with the shorter wavelength region.

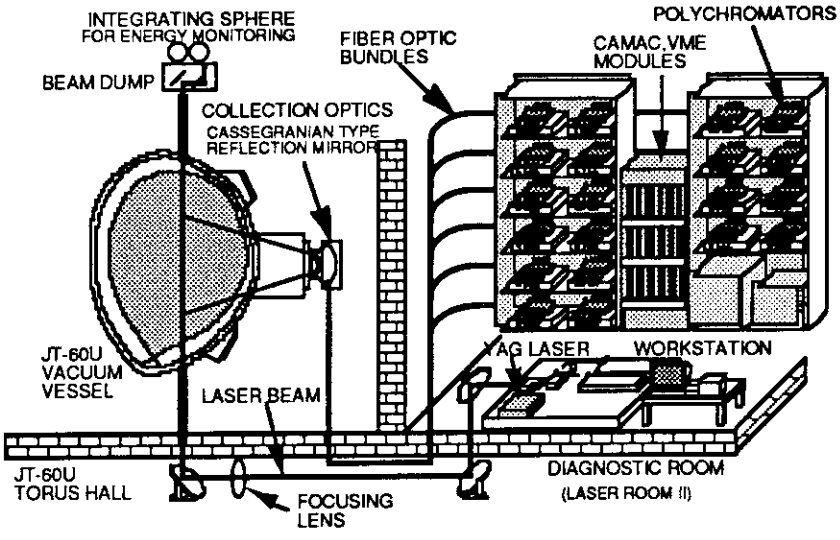

Fig. I.2.6-1. Schematic view of YAG laser Thomson scattering system

2.6.2 14 MeV neutron measurements using scintillating fiber detectors

The time resolved triton burnup measurements have been performed using a new type 14 MeV neutron detector based on scintillating fibers, as part of US-Japan tokamak collaboration efforts. Two sets of detectors have been installed at a distance of 1.7 m outside the toroidal field coil position as shown in Fig. I.2.6-2. The scintillating fiber detectors have been calibrated by the shot-integrated 14 MeV neutron yield measured with the neutron activation technique using a pneumatic foil transfer system [2.6-1]. The foils are irradiated at 20~30 cm outside of the plasma. The counts of the scintillating fiber detectors and the 14 MeV neutron yield measured with the neutron activation technique have good linearity in the range of 14 MeV neutron yield 10^{12}- 10^{15} /shot.

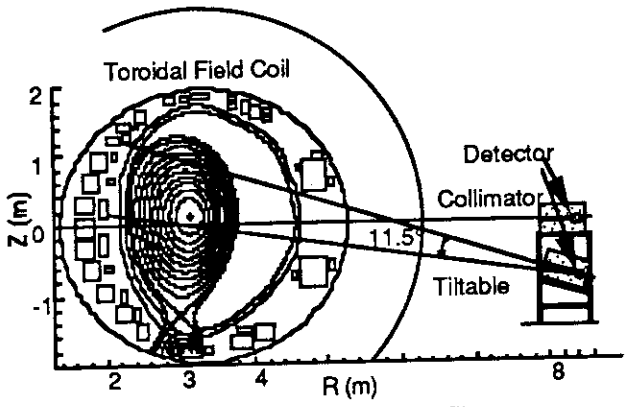

Fig. I.2.6-2. Schematic view of scintillation fiber neutron detectors with horizontal and tiltable sightlines.

The scintillating fiber detector system operates in the background of the DD neutrons which are ~100 times brighter than the DT neutron signal, at the counting rate of up to 100 MHz. The peak DT neutron rate at the time of the neutral beam (NB) turn-off is as high as 2% of the total neutron rate measured by the ^{235}U fission chambers. After NB turn-off, 14 MeV emission decays exponentially in many shots. The typical decay time constant is 400-500 ms for high β_p plasmas. The time-dependent 14 MeV neutron emissivity was simulated by a simple classical slowing down model in which Tritons were allowed to slow down according to the classical energy loss theory. The diffusivity of fast triton, D_{triton}, was estimated to be 0.05-0.15 m^2/s and increased as the toroidal ripple rate increased.

2.6.3 Neutral particle diagnostics in a MeV range

An alpha particle analyzer, which was provided by the Ioffe Institute from Russia to investigate confinement properties of energetic ions such as alpha particles, was installed [2.6-2, 2.6-3]. In ICRF heating experiments, the energy spectrum of energetic atomic hydrogen was successfully measured up to 1.5 MeV using the analyzer. A typical energy spectrum is shown in Fig. I.2.6-3. Higher harmonic (2 to $5\omega_{CH}$) beam ion acceleration was investigated in combination

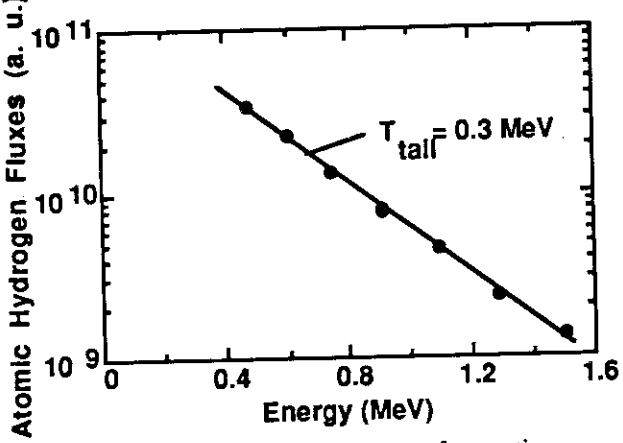

Fig. I.2.6-3. Typical energy spectrum of energetic atomic hydrogen fluxes in ICRF heating.

with the ICRF and H^0 beam heating. The tail temperature determined in 0.25 – 0.75 MeV increased with the harmonic number and this tendency was consistent with the calculation from the Fokker-Planck code [2.6-4]. Another neutral particle analyzer for the measurement of beam ions produced by the 500 keV beam was newly introduced from the Ioffe Institute and installed in JT-60.

2.6.4 Dual CO_2 laser interferometer

The tangential CO_2 laser interferometer of JT-60 has been modified to a dual CO_2 laser system with close wavelengths of 10.6 and 9.27 μm [2.6-5] from the previous 10.6 [CO_2] and 3.39 μm [HeNe] two color combination system [2.6-6]. Two color configuration is necessary to cancel the optical path change by mechanical vibration in the interferometric measurement. The new system has the advantages on practical problems such as hardness to window darkening, monitoring easiness of the laser beam, and simplified configuration of optical layout design by using very close wavelengths. The dual CO_2 system has been operating very successfully. The measurement stability enables us to study about even a major disruption which had been until now almost impossible with the conventional FIR interferometric system. The results are shown in Fig. I.2.6-4. The figure shows the relation of I_p decay and n_e jump, such as a shorter decay of I_p corresponds for a larger change in n_e.

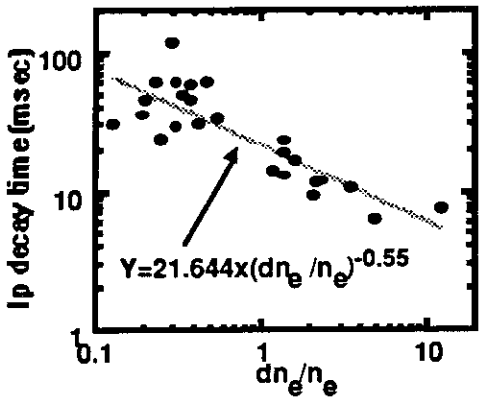

Fig. I.2.6-4. The decay time relation at disruption.

On the contrary, a serious disadvantage has appeared. The density information in the detected phase is reduced to about 10% compared with the ideal wavelength combination. To avoid this problem, an ultra-high resolution phase discriminator module is now under development, which has the property of 1/10000 fringe resolution and time response of 1 μs. The resolution is 100 times better performance than the conventional discriminator. The preliminary examination of prototype module was achieved with sufficient resolution.

References

[2.6-1] Hoek M., Nishitani T., Ikeda Y. et al., Rev. Sci. Instrum. **66**, 885 (1995).
[2.6-2] Kusama Y., Afanassiev V. I., Petrov S. Y. et al., "Direct Measurement of MeV-range Atomic Hydrogen using a Charge-exchange Neutral Particle Analyzer in ICRF-heated JT-60U Plasmas", JAERI-Research 94-036.
[2.6-3] Kusama Y., Nemoto M., Satoh M. et al., Rev. Sci. Instrum. **66**, 339 (1995).
[2.6-4] Afanassiev V. I., Kusama Y., Nemoto M. et al., "Measurement of atomic hydrogen fluxes in MeV-energy range on ICRF-heated JT-60U plasmas", presented in 22th EPS Conf. on Controlled Fusion and Plasma Physics, July 1995, Bournemouth, UK.
[2.6-5] Kawano Y., Nagashima A. et. al., "Development of Dual CO2 Laser Interferometer for Large Tokamak", JAERI-Research 95-023 (1995).
[2.6-6] Kawano Y., Nagashima A. et. al., Rev. Sci. Instrum. **63**, 4971 (1992).

3. Experimental results and analysis

3.1 Disruptions and plasma control

In JT-60, disruption studies have been continued to achieve disruption avoidance and the softening of disruption conditions such as a divertor heat load and electromagnetic force (EMF).

Disruptions in JT-60 are classified into six types, which are caused by (1) density limit, (2) error field (mode locking), (3) β_p collapse, (4) low l_i during the plasma current ramp-up, (5) high l_i during the plasma current ramp-down and (6) vertical instability. For all types of disruptions, we identified the parameter regions or operation phases. Operational scenarios were successfully avoided for all six types of disruptions in JT-60 [3.1-1]. The slowing down of the plasma-current-quenching could reduce the EMF and the growth rate of vertical displacement event (VDE). As a result, the halo current was also suppressed. These studies are one of the key issues of ITER physics R&D.

3.1.1 Amelioration of disruption conditions [3.1-2]

Disruption mechanism was investigated using density limit disruptions. First, MARFE occurs in some cases with increasing density. Having reached 100% radiation, contraction of the temperature profile can be observed. During the energy quenching (few milliseconds), the stored energy is reduce rapidly. After that, a large amount of heat flux (~ 150 MW/m^2 in JT-60) flows onto the divertor plates and the divertor temperature ($T_{div.}$) increases. Then, a sudden intense burst of carbon appears when $T_{div.}$ exceeds the critical value, and a large amount of carbon impurity causes the plasma to cool down. As a result, the plasma temperature drops suddenly and the plasma current terminates with fast current decay.

It was confirmed that the high electron temperature (T_e) after energy quenching is a key to the softening of the current quenching for density limit disruptions. No current-quenching was observed with T_e >~ 300 eV for hydrogen plasma in both JET and JT-60 with carbon tiles. The threshold stored energy to avoid current quenching (W_{th} > W, W is the stored energy just prior to the energy quenching) was confirmed and its scaling fitted the data of JFT-2M and JT-60 derived for OH plasma. Using the scaling of peaking factor of divertor heat load [3.1-3], the scaling of W_{th} was proposed for OH plasma expressed as follows:

$$W_{th} = a \cdot C^{-1} \cdot \Delta T \cdot t^{0.5} n_e^{0.45} q_{eff}^{0.67} R^{2.65} \qquad (3.1\text{-}1)$$

where, a is the proportional coefficient, C the constant that depends on the material, ΔT is the increased temperature during energy quenching and t is the energy quenching time. The W_{th} is determined experimentally to be 0.3 MJ and $a \cdot C^{-1} \cdot \Delta T \cdot t^{0.5}$ ~ 3×10^3 [J/m^2] in the case of CFC divertor tiles. Very low Wth of 5 MJ for ITER with carbon tiles was roughly predicted from this scaling.

The killer pellet injection was examined so as to reduce the heat load on the divertor plate during energy quenching. The maximum heat flux at energy quenching could be reduced to 5~20 MW/m^2 (100~200 MW/m^2 during normal energy quenching) by injecting a neon-ice-pellet of 3 mmΦ (0.8 km/s) into the NB heated plasma (I_p = 1.6 MA, P_{NB} = 12 MW). Fast current quenching was obtained by a sudden drop in T_e from 3 keV to < 100 eV. Total amount of injecting neon (impurity) should be optimized for a heat load reduction and slow current quenching at the same time.

3.1.2 VDE avoidance [3.1-4]

VDE mechanism during the I_p quenching phase was clarified in which rapid I_p quenching can accelerate the vertical displacement due to the up-down asymmetric eddy current induced in the vacuum vessel and the degradation of n-index. As is consistent with the Tokamak Simulation Code (TSC) prediction, VDE avoidance could be achieved in JT-60 by optimization of the initial vertical position of the magnetic axis.

3.1.3 Halo current study [3.1-5]

An estimation of the toroidal asymmetry is very important for the design of a vacuum vessel, especially, plasma facing components, because the halo current can locally exert a strong force on the vacuum vessel and vessel components.

Three carbon tiles located in the lower inner side of the vacuum vessel were fractured during density limit disruptions in JT-60. A EMF of 10 kN corresponding to an halo current of 20 kA is necessary to break the CFC tiles. Toroidally, the symmetric halo current was inconsistent because the total halo current would exceed the plasma current by over 400%. A toroidal asymmetry factor (f_{as}) was estimated to be 2.5, corresponding to the maximum total halo current of ~ 0.26 I_p, to explain the observation result.

3.1.4 Neutron feedback control

A new neutron feedback system to control fusion reactivity began to operate. The neutron emission rate can be successfully controlled during the NB injection period, in which the stored energy is kept constant for 2.5 s at the same time.

References

[3.1-1] Yoshino R., Neyatani Y., Isei N. et. al., J. Plasma and Fusion Research **70**, 1081 (1994).
[3.1-2] Yoshino R., Neyatani Y., Isei N. et al., in "Proc. 15th Int. Conf. on Plasma Physics and Controlled Nuclear Fusion Research", Seville, 1994, IAEA-CN-60/A-5-II-2
[3.1-3] Itami K., Shimada M., Asakura N. et al., in "Proc. 14th Int. Conf. on Plasma Physics and Controlled Nuclear Fusion Research", Würzburg, 1992, Vol.1, p.391, IAEA, Vienna, 1993.
[3.1-4] Nakamura Y., Yoshino R. and Neyatani Y., "Mechanism of Vertical Displacement Event in JT-60U Disruptive Discharge", 22nd EPS, Bournemouth, 1995.
[3.1-5] Neyatani Y., Yoshino R. and Ando T., "Effect of Halo Current and its Toroidal Asymmetry during Disruptions in JT-60U", Fusion Technology in press.

3.2 High-β_p mode and high-β_p H-mode study

High-β_p regime has become a new paradigm of the tokamak reactor developments, since it has the potential of significantly enhancing the economical attractiveness in the tokamak fusion reactors. As pressure and current profiles are strongly coupled owing to the neoclassical bootstrap current effects, the profile control is considered as an essential issue to make such an advanced tokamak concept feasible. Therefore, it is crucially important to demonstrate a sustained high pressure plasma with highly enhanced confinement and stability under a large fraction of the bootstrap currents, which is the eventual goal of this regime in JT-60.

The high-β_p research has been consistently carried out in JT-60 since its upgrade in 1991. The high-β_p regime, in which the high-β_p mode and high-β_p H-mode were studied, was produced in elongated divertor discharges with a high aspect ratio configuration relevant to the advanced reactor concept, configured to achieve central deposition of the nearly perpendicular neutral beam injection. In the experimental campaign of FY 1994, significant progress was made in clarifying a mechanism of the peaked profile formation and improving the fusion performance in the high-β_p regime. The highlights were represented in the discovery of the internal transport barrier (ITB) in high-β_p mode plasmas and an achievement of a new world record of the highest fusion triple product up 12% over last year in high-β_p H-mode plasmas.

The existence of an internal transport barrier (ITB), named on the analogy of an edge transport barrier in the H-mode, was for the first time discovered in high-β_p mode plasmas with deuterium neutral beam injection in JT-60 [3.2-1]. Based on a detailed analysis of ion temperature profiles from charge exchange recombination spectroscopy measurements, the ITB was characterized by a prominent increase in the ion temperature just inside the intermediate place of the plasma minor radius. ITB was found to have a significant reduction in the effective thermal diffusivity and was maintained exceeding the time scale of energy confinement. Figure I.3.2-1 shows typical temperature, density and toroidal rotation velocity profiles of a high-β_p mode discharge where ITB is placed near r/a~0.55 at t=5.9 s. As seen in the time evolution of the ion temperature (T_i) and toroidal rotation velocity (V_t) profiles, the values of T_i and V_t inside ITB are remarkably increased in spite that those outside ITB are saturated at levels as low as in the L-mode plasmas.

Although ITB was observed for a variety of plasma currents and toroidal fields, a clear positive correlation between the location of ITB and the inverse safety factor $1/q_{eff}$ was found. This implies that the current density profile plays an important role in the formation of ITB. Another important occurrence condition was the NB power deposition characteristics; the central beam deposition scheme was much more effective for creating ITB than the off-axis deposition scheme when the total beam power exceeded a threshold power to produce ITB. These findings should provide us with important clues for a better understanding of the ITB mechanism.

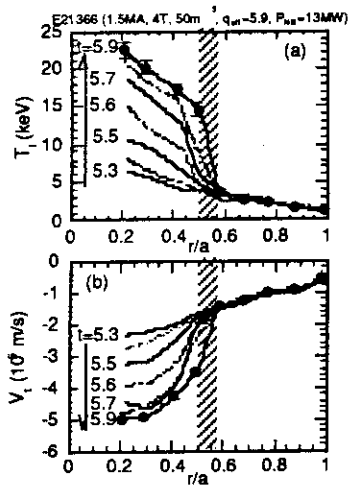

Fig. I.3.2-1. Evolution of ion temperature and toroidal rotation velocity profiles showing the internal transport barrier at r/a~0.55.

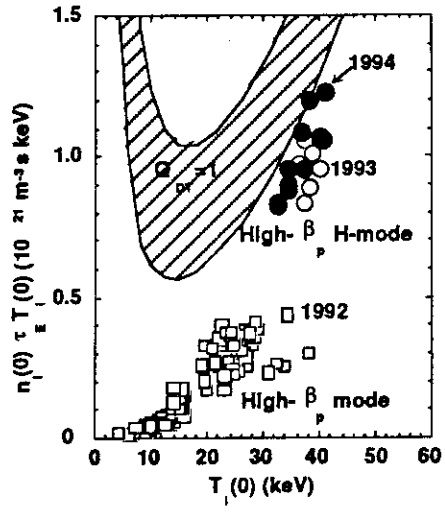

Fig. I.3.2-2. Progress in the fusion triple product as a function of the central ion temperature achieved inmode high-β_p and high-β_p H-mode discharges.

As a primary experimental subject of JT-60, a high performance campaign was carried out in the high-β_p H-mode regime by extending the confinement and fusion performance at higher plasma currents during 1994 than had been explored during 1993. The combination of the edge pedestal formation in the H-mode with a peaked profile formation in the high-β_p mode made it possible to improve the β limits with the resulting pressure profile broadening in the core region. Suppression of the sawtooth oscillations and avoidance of locked MHD modes were necessary for improvements in performance, but limited the maximum plasma current of this regime. In 1994, intensive optimization of the pressure profile was attempted by adjusting the beam deposition profiles to slightly enhance off-axis beam heating so as to improve the stability limited by β_p-collapses due to the low-n kink-ballooning modes. The optimum plasma current was substantially extended up to 2.3 MA with deuterium recycling control utilizing intensive boronization with a new world record for the fusion triple product 1.2×10^{21} $m^{-3}\cdot s\cdot keV$ at $T_i(0)$ = 39 keV, and the maximum central ion temperature up to 41 keV as shown in Fig. I.3.2-2 [3.2-2].

Searching for the route to a self-ignited fusion plasma in support of the advanced tokamak concept, extensive international collaboration between JT-60 and TFTR Teams continued since 1993 for common characterization of the high-β_p regime in JT-60 and the supershot regime in TFTR. The similarity in confinement and fusion reactivity characteristics with a highly peaked pressure profile in the two regimes was quantitatively shown where common scalings for the neutron rate and the total stored energy were proposed as $S_{DD}\propto P_{abs}^{2.0}H_{ne}V_p^{-0.9}$ and $W_{tot}\propto P_{abs}V_pH_{ne}^{0.2}$, respectively, using the absorption power (P_{abs}), the plasma volume (V_p) and the peakedness of the neutral beam fueling profile (H_{ne}) [3.2-3].

References

[3.2-1] Koide Y., Kikuchi M., Mori M. et al., Phys Rev. Lett. **72**, 3662 (1994).
[3.2-2] Kikuchi M. and JT-60 Team, Proc. 14th IAEA Int. Conf. in Sevillia (1994), IAEA-CN-60/A-1-I-2.
[3.2-3] Park H. and TFTR Team, Ishida S. and JT-60 Team, Proc. 14th IAEA Int. Conf. in Sevillia (1994), IAEA-CN-60/A-2-4-P-1.

3.3 H-mode studies

3.3.1 H-mode transition study

Among the various the experimental documents on the H-mode transition, significance of the edge plasma temperature has been disputed as one of the most important key parameters. Theoretical considerations take this quantity in terms of the edge ion collisionality, defined as ν_i^* ($= \nu_{ii} R_p q_{95}/\epsilon^{2/3} v_{th}$). Critical ν_i^* at which the poloidal flow velocity makes a sudden change is estimated to be around unity by the classical predictions. However, quantitative agreement with the theory has been not yet been documented. As a candidate for this discrepancy, we have proposed the influence of impurities, which should naturally have an influence on the transition conditions. We have investigated the effect of ion-impurity collision theoretically in terms of the normalized viscosity coefficient, assuming the ion distribution function is non-Maxwellian at the edge. Accordingly, we have replaced ν_i^* with $\nu_{i\,eff}^* = \nu_i^* (Z_{eff} n_e / Z_i^2 n_i)$. The cumulated data in JT-60 exhibiting the value of $\nu_{i\,eff}^*$ ranges from 1 to 2, regardless of the ion species and the ion diamagnetic drift directions. However, it decreased in the low density regime below 1.2×10^{19} m^{-3}, which may well be related to the low density transition limit. Therefore, it can be said that $\nu_{i\,eff}^*$ is primary but is not only the sole necessary condition [3.3-1].

The reduction in the turbulent density fluctuations has been clearly observed in the H-mode transition, as seen in other tokamaks, and it can be scaled with the normalized radial electric field gradient $\nabla E_r = \nabla(E_r/B_\phi)/(C_s/R_o)$. Theoretical expectations indicate that the fluctuation intensity should scale with $(\Delta\omega_t/\omega_s)^{2/3}$, where ω_t and ω_s are respectively the decorrelation and shear frequency. However, we have not yet obtained any agreement with this theoretical estimate. Edge density fluctuations were measured with a microwave reflectometer, and the poloidal flow velocity profile was measured with a charge exchange recombination diagnostic of the CVI line. It has been documented that remarkable shear was formed at $\rho = 0.99$, of which the width was merely a few cm. The coherence spectra of density fluctuations at two spatially separated positions were analyzed in the L- and H-modes. Larger decorrelation frequency together with the enhanced coherence in the L-mode is related to the increased edge turbulence diffusivity, based on the "random walk estimate": viz., D_{rw} = (coherence length)^2/(autocorrelation time). In addition, we have also found that the coherence length is more than several times the poloidal Larmor radius in the L-mode, while it is much shorter in the H-mode. This result can be related to the Bohm-like transport in the edge region of the L-mode plasmas, and the relation to the global non-dimensional scaling studies will have to be addressed, which is concerned only with the B or B^2 dependence [3.3-2].

To attain the conditions prerequisite for the transition, the edge confinement properties would be of a critical issue of interest, which is directly related to the necessary heating power. ITER design is based on the threshold power scaling P_{th} (MW) = $0.04\overline{n_e}$ (10^{20} m^{-3}) B_T(T) S(m^2), where $S = 4\pi^2 Ra\{(1+\kappa^2)/2\}^{0.5}$. Our results indicated that ITER scaling is considerably

underestimated, and the scaling obtained was either $0.34 R_p^{1.4} a^{0.4} B_T^{1.5}$ or $0.39 R_p^{1.5} a^{0.5} B_T^{1.25}$. However, it should be remarked that the JT-60 data was accumulated mainly in limited low density regime of $\overline{n_e} = 1.0\text{-}2.5 \times 10^{19}$ m^{-3}. Therefore, the I_p dependence, which is related to the influence of edge neutrals and would become effective in the high density regime, was not resolved. In addition, an increase in P_{th} for the low density regime induces restrictions on the ITER operating scenario of reducing the density to reduce the power threshold [3.3-3].

3.3.2 ELM study

We were able to find from the 1.5-D time-dependent transport code that the ballooning mode is the major candidate for the causality of ELMs in JT-60. It was also documented that the edge pressure gradient ∇P right before the ELM onset is proportional to the ballooning parameter, defined as $B_T^2 l_i / (R_p q_{95}^2)$. Here, ∇P was divided by the poloidal ion Larmor radius to represent the edge pressure gradient., and the definition of ballooning parameter was derived from the definition of the normalized pressure gradient, $\alpha (= \nabla P \{B_T^2/(2\mu_o R_p q_{95}^2)\}^{-1})$. This is convincing if the value of the local magnetic shear is replaced by l_i, and the stability limit is in the first regime in JT-60. Since the ballooning parameter is rewritten as $I_p^2 \cdot l_i$, it is also noteworthy that the edge pressure is largely limited by I_p. Also, we have documented that edge ∇P can be increased by the edge toroidal shear flow [3.3-4,5].

3.3.3 Particle confinement study

The particle confinement properties was also analyzed with the neutral particle transport code DEGAS. The value of τ_p^{main} was less than 1.5 times τ_E in the ELM-free H-mode ($\tau_E/\tau_E^{ITER\text{-}89P} = 1.4$ to 1.9). This result indicates that particles can be controlled even in plasmas with improved energy confinement, provided that efficient pumping capability is available [3.3-6].

References

[3.3-1] Fukuda T., Kikuchi M., Koide Y. et al., Plasma Phys. Control. Fusion **36**, A87 (1994).
[3.3-2] Fukuda T., Proc. US-Japan Workshop (P-231) on Development of Millimeter- and Submillimeter-Wave Technology for Diagnostic Applications for Large Plasma Devices, Tsukuba (1994) 3 - 1.
[3.3-3] Sato M., Kikuchi M., Fukuda T. et al., Proc. 15th Int. Conf. on Plasma Physics and Controlled Nuclear Fusion Research CN-60 / A-2-II-4 (1994).
[3.3-4] Kamada Y., Ushigusa K., Naito O. et al., Plasma Phys. Control. Fusion **36**, A123 (1994).
[3.3-5] Fukuda T. and the JT-60 Team, Phy. Plasmas **2**, 2249 (1995).
[3.3-6] Takenaga H., Shimizu K., Asakura N. et al., "Particle Confinement Study in Hot Ion H-mode Discharges of JT-60U," in print for Nucl. Fusion.

3.4 Steady-state high performance

One of the main purposes of JT-60 is demonstrating the concept of steady-state highly integrated performance, which means simultaneous sustainment of i) high confinement (high H-factor = $\tau_E/\tau_E^{ITER89P}$), ii) high power density (high β_N), iii) high bootstrap fraction (high β_p) and iv) high efficiency of heat and particle exhaust. For the condition iv), the ELMy H-mode is a candidate for the steady-state operation. Since MHD instabilities restrict the above conditions, expanding the stability window is a critical issue, for which control of current and pressure profiles are essential. We optimized discharges from the two important aspects: 1) sustainment of high fusion product and 2) sustainment of full non-inductive current drive at MA-class of I_p.

3.4.1 Sustainment of high fusion product in the ELMy high-β_p H-mode

In the high-β_p H-mode, high values of $n_D(0)\tau_E T_i(0)$=3-5×10^{20}m^{-3} skeV and Q_{DT}=0.25-0.36 were sustained for up to 1.5 s (5×τ_E) with B_t~4.4 T, I_p~2.3 MA, q_{eff}~4.2, P_{NB}~30 MW, $T_i(0)$=24-39 keV, $n_D(0)$=4.5-5.5×10^{19} m^{-3}, τ_E=0.28-0.32 s, H-factor=2-2.2, β_p=1.1-1.4, β_N=1.7-2.0 and bootstrap fraction 35-45% (Figs. I.3.4-1,2) [3.4-1]. The data were taken in the ELMy phase with a negligibly small dW/dt. The NB heating profile was controlled so as to be broad enough to suppress a β_p-collapse. In this series of high-power-heated discharges, the enhanced plasma wall interaction terminated the steady-state: When surface temperature of divertor tiles exceeded 1100 K, the carbon influx from the target tiles increased drastically. This event was observed just after start in a reduction in the stored energy observed simultaneously with an increased Dα signal. The strong carbon accumulation in the main plasma accelerated the confinement degradation. We observed a carbon influx at one ELM event correlated with the pulsed particle flux rather than the heat pulse to the target. This generation mechanism of carbon impurity will be hereafter analyzed based on the ELM characteristics.

3.4.2 Full noninductive current drive in high β_N ELMy H-mode [3.4-1]

Full noninductive current drive by combining the bootstrap current I_{BS} with beam driven current I_{NB} (I_{BS}/I_p~74%, I_{NB}/I_p~37%) could be sustained for 0.7 s with highly-integrated performance (β_p=2.6, β_N=2.9, H-factor=2.5) at I_p=1 MA, B_t=3 T, q_{eff}=7.1, q_{95}=5.2, P_{NB}~20 MW including 4 MW of co-tangential NB (Fig. I.3.4-3). The discharge region obtained (q_{95}, β_N, β_p, H-factor, I_{BS}/I_p) was almost the same as the design region of SSTR[3.4-3]. In the case of full noninductive current drive at Ip=0.5 MA, low $\langle T_e\rangle$~1 keV allowed sufficient current diffusion and negative magnetic shear seemed to be produced in the central region. A comparison between the monotonic q(r) and q(r) with negative shear suggests that confinement (mainly in the ion channel) can be improved by small or negative central magnetic shear, if the discharge is stable.

3.4.3 Essential method for optimizing stability and confinement

The above results were obtained when low-(m,n) kink-ballooning modes (e.g. β_p-collapse) were suppressed in the central region and control of ELMs (high-n ballooning mode)

was adequate. For optimization, there are four key factors [3.4-1,2]. The first is the current profile j(r). Basically a peaked j(r) is beneficial, because the H-factor, β_p-limit and pressure limit for an ELM-onset increase with l_i. However, more detailed j(r)-control is needed at high I_{BS}/Ip [3.4-1]. The second is pressure profile p(r). Maximum β_N is obtained at a medium peakedness of p(r), because too peaked p(r) triggers a β_p-collapse and too broad p(r) decreases β_N due to the ELMs. By optimizing j(r) and p(r), values of β_p, $\varepsilon\beta_p$ and β_N reached 4.7, 1.2 and 4.8, respectively. The third is the NB power to control the ELM frequency. The last factor is q_{eff}. Since the H-factor and the β_N & β_p-limits increase with q_{eff}, high q operation is essential to achieve a high bootstrap fraction. By summarizing these effects, we found optimum sets of (j(r), p(r), q_{eff}) for the experiments in Sections 3.4.1 and 3.4.2.

References

[3.4-1] Kamada Y. et al., Plasma Phys. Cont. Nucl. Fusion Research. Proc.15th Int. Conf., Seville, 1994, IAEA, Vienna, A-5-I-5 (1995) , see also Kamada Y. et al., Nucl. Fusion, **34**, 1605 (1994).

[3.4-2] Neyatani Y. et al., Proc. 20th European Conf. on Controlled Fusion and Plasma Phys. (Lisboa 1993) EPS, Geneva, ptI, p215 (1993).

[3.4-3] Seki M. et al., Plasma Phys. Cont. Nucl. Fusion Research. Proc.13th Int. Conf., Washington DC, 1990, IAEA, Vienna, Vol.III 473 (1991).

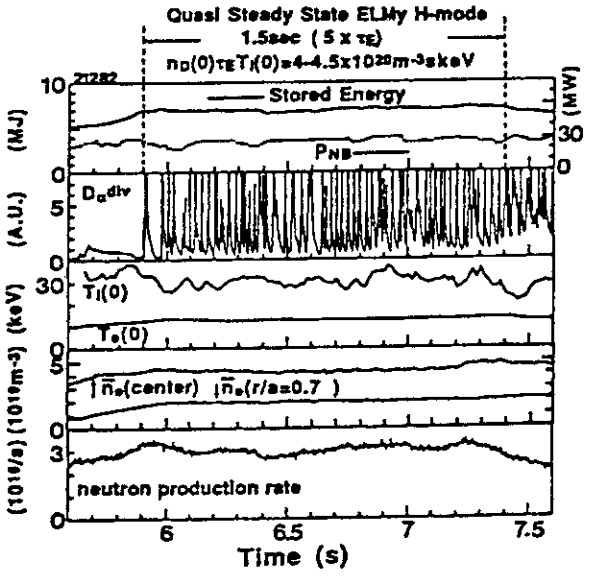

Fig. I.3.4-2. Typical waveforms for a quasi steady state ELMy H-mode with high $n_D(0)\tau_E T_i(0)$=4-4.5×10^{20} m^{-3}skeV sustained for 1.5 s (5×τ_E).

Fig. I.3.4-3. Evolution of fully current driven discharge (I_p=1MA, B_t=3T , q_{eff}=7.1, q_{95}=5.2). Bootstrap fraction of 78% and the beam driven current of 37% were obtained with highly integrated performance: β_p=2.6, β_N=2.9, H-factor=2.5 and $n_D(0)\tau_E T_i(0)$=0.8 ×10^{20} m^{-3} skeV.

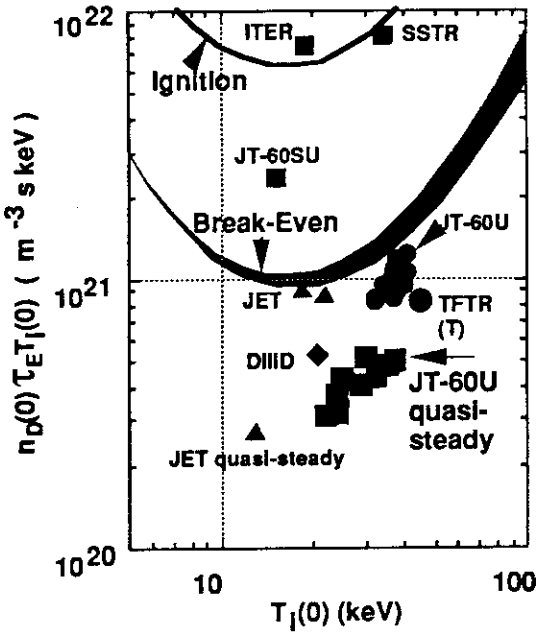

Fig. I.3.4-1. Values of $n_D(0)\tau_E T_i(0)$ obtained in quasi steady-state ELMy H-mode, which is ~1/2 of transiently obtained maximum value.

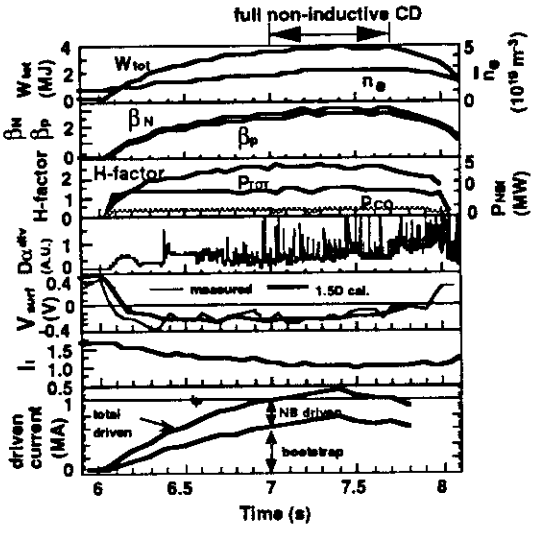

3.5 Impurity and divertor characteristics

3.5.1 Divertor characteristics

The behavior of principal divertor plasma parameters such as the ion flux, electron temperature and particle recycling in the divertor were investigated under the condition of a remote radiative cooling in L-mode and ELMy H-mode discharges. The fraction of divertor radiation loss was similar irrespective of the ion grad-B drift direction, and the ion flux to the separatrix strike points starts to decrease just before a MARFE onset. The electron temperature in the divertor ($T_{e,div}$) decreases to around 10 eV. Under a relatively symmetric total power flow onto the outer and inner divertor fans, an outboard-dominated heat load onto the target and a nearly symmetric one were observed for the ion grad-B drift towards and away from the target, respectively. This is due to the asymmetries in the particle recycling and radiation loss profiles. From the viewpoint of the in-out asymmetry in the heat and particle fluxes, operation with the ion grad-B drift away from the target plate is desirable, provided that attached conditions are maintained. Formation of a remote radiative divertor with the radiation loss in the divertor $P_{rad,div}$ of about 40% was achieved in the ELMy H-mode operation. Reduction of $T_{e,div}$ (20 - 40 eV), under the remote radiative cooling condition in the ELMy H-mode, is similar to that in the L-mode [3.5-1, 3.5-2].

In discharges with the ion grad-B drift toward the divertor, as the electron density increases, a strongly radiative region is formed between the outer separatrix strike zone and the X-point. The divertor radiation loss fraction of the input power depends on the electron density of the main plasma, NB heating power and safety factors, and reaches the level of radiation loss power found in the MARFE. During the MARFE, the maximum radiation peak stays near the X-point. In the discharges with the ion grad-B drift away from the divertor, while the radiation peak moves to the inboard side of the main plasma, $P_{rad,div}$ decreases due to detachment of the divertor plasma. However, there is no significant difference in the maximum radiation loss level between the two types of discharges [3.5-3].

The characteristics of heat and particle fluxes in ELMy H-mode plasmas under low recycling conditions were investigated in a comparative manner. It was confirmed that the multiple peak structure of heat flux during ELM activity has a role in reducing the average value of a peak heat flux at the divertor. In ELM free H-mode plasmas, divertor heat and particle fluxes showed a weak asymmetry. To characterize heat and particle flux during ELM activity, the ELM part and the steady-state part of heat flux and particle fluxes were analyzed. A large in-out asymmetry of the peak ELM heat flux density was found. The asymmetry is almost unaffected by the ion grad-B drift direction. In contrast, ELM particle flux shows a similar asymmetry with that during the ELM free phase. The in-out asymmetry of the steady-state and parts of the ELM particle flux is equally reversed when the ion grad-B drift direction is reversed [3.5-4].

3.5.2 Impurity behavior in the divertor

A two-dimensional impurity code based on Monte Carlo techniques (IMPMC) was developed to study the impurity behavior in divertor plasma. This model was applied to the carbon impurity in NB heated plasmas. Comparison of calculated spatial profile of C IV line radiation with the measured one indicates that diffusion coefficient $D_\perp$ is around 1 m^2/s [3.5-5]. The impurity source profiles in the low density plasma can be explained by the deuterium ion physical sputtering and self-sputtering. In contrast, in high density plasmas, the physically sputtered impurities from target plates are reduced because of the low incident energy of the deuterium ions. Chemical sputtering by neutral particles which strike the divertor plate in the private region becomes dominant in high density plasmas. It is found that methane sputtered from the divertor plate in the private region enhances the radiation near the X-point. This enhanced radiation near the X-point possibly triggers a MARFE. Since the shielding is less effective for the carbon originating from the private region, it is necessary to reduce the neutral flux to the wall in the private region to avoid a MARFE. One method is to close the private region with a dome-like structure. The effectiveness of this structure is now under investigation with a code [3.5-6].

3.5.3 Helium transport and exhaust

To simulate the behavior of helium (He) ash in a fusion reactor, helium transport and exhaust were investigated in the ELMy H-mode and high-β_P ELMy H-mode using He beams. Helium transport coefficients in the ELMy H-mode plasmas were found to be D_A=1 - 2 m^2/s and C_V=1.0 - 1.5 using a neutral beam of 60 keV He atoms as a source of central fueling, and D_A=1 m^2/s and C_V=1.0 - 1.5 using a short pulse He gas puff as peripheral fueling [3.5-7]. No helium accumulation was observed during the ELMy H-mode. The He recycling flux in the divertor during the ELMy H-mode was about one order of magnitude less than that in the L-mode with the same rate of He gas fueling. The neutral pressure of helium in the divertor region during the high-β_P ELMy H-mode was 5 times lower than that during the L-mode in the He beam experiment. Helium removal from the core plasma was observed due to wall pumping caused by Solid Target Boronization (STB). The He neutral pressure and He content in the main plasma were reduced by the He exhaust to 1/3 of those without STB. This demonstrates that He ash can be actually exhausted and an allowable He content is sustained by He pumping in an enhanced confinement regime such as the high-β_P ELMy H-mode [3.5-8].

References

[3.5-1] Asakura N. and JT-60 Team, IAEA Seville 1994, IAEA-CN-60/A4-I-3.
[3.5-2] Asakura N., Itami K., Hosogane N. et al., J. Nucl. Mater **220-222**, 395 (1995).
[3.5-3] Hosogane N., Itami K., Asakura N. et al., J. Nucl. Mater **220-222**, 420 (1995).
[3.5-4] Itami K., Hosogane N., Asakura N. et al., J. Nucl. Mater **220-222**,203 (1995).
[3.5-5] Shimizu K., Kubo H., Takizuka T. et al., J. Nucl. Mater **220-222**, 410 (1995).
[3.5-6] Shimizu K., Hosogane N., Takizuka T. et al., IAEA Seville 1994, IAEA-CN-60/D-P-I-2.
[3.5-7] Sakasai A., Kubo H., Hosogane N. et al., J. Nucl. Mater **220-222**, 405 (1995).
[3.5-8] Sakasai A. and JT-60 Team, IAEA Seville 1994, IAEA-CN-60/A2/4-P-12.

3.6 A study on fast ions

The analysis of fast ion behavior is one of the most important issues in obtaining stationary tokamak reactors. In JT-60, many experimental data concerned with high energy ions have been measured and analyzed using numerical codes. These results are used for studying the operation method and also used for ITER physics R&D.

3.6.1 Ripple loss study

The total ripple loss of beam-injected ions and the banana drift loss fraction were successfully evaluated [3.6-1].

Then, the direct measurement of the banana drift loss was researched by using an IRTV camera. Banana drift loss ions were thought to hit the outer upper region of the first wall, from a theoretical prediction. The IRTV measurements showed a vertical belt-like heat deposition, as predicted, along the edge region of armor tiles located between adjacent toroidal field coils. The total loss power was evaluated to be ~80 kW. Using the OFMC (Orbit Following Monte Carlo) code, we calculated the total power loss through the banana drift loss of the beam ions. The OFMC results showed good agreement between the measurements and the calculation (50±14 kW). Consequently, it was concluded that the experimentally observed heat deposition was caused by the banana drift loss of the beam ions [3.6-2].

Heat deposition on the first wall due to the ICRF-induced loss of beam ions was investigated by changing the position of the resonance layer in the ripple-trapping region. A heat spot appeared on the first wall of the same major radius as the resonance layer of the ICRF waves. The broadening of the heat spot in the major radius direction was consistent with that of resonance layer due to Doppler broadening. The heat spot was considered to be formed by the ICRF-induced ripple-trapped loss of the beam ions [3.6-3].

3.6.2 TAE modes during ICRF heating

Toroidicity induced Alfvén eigen (TAE) modes are thought to be a harmful instability in a fusion reactor because of enhancing the significant loss of energetic alpha particles. High-n TAE modes were observed during the second harmonic minority ICRH experiments in JT-60. Those TAE modes were

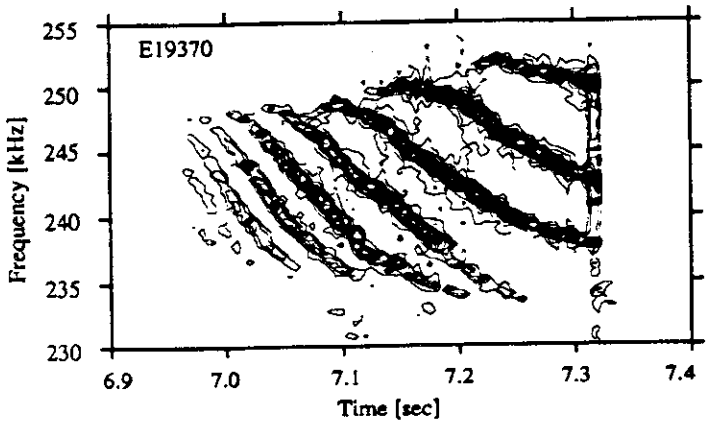

Fig. I.3.6-1. Time evolution of TAE mode frequency spectra at I_p = 4 MA.

thought to be excited by the precessional magnetic resonance and the bounce resonance of trapped fast ions produced by ICRH. The degradation of energy confinement was observed after the appearance of the TAE modes. The plasma stored energy decreased by about 10% during TAE mode excitation, while the population of MeV ions decreased by over 50% [3.6-4]. The number of excited TAE modes increased along with the plasma current. In high current discharges over 3.5 MA, many TAE modes appeared and disappeared sequentially by increasing the toroidal mode number one by one during the sawtooth free periods. Figure I.3.6-1 shows that nine TAE modes were observed at a plasma current of 4 MA. This phenomenon could be explained from the structure of Alfvén continuum gaps and Doppler shift of toroidal plasma rotation during an ICRF pulse [3.6-5]. The threshold value of fast ion beta for TAE modes excitation increased with the internal inductance due to the enhancement of Alfvén continuum damping [3.6-6].

References

[3.6-1] Tobita K. et al., Nucl. Fusion **34**, 1097 (1995).
[3.6-2] Kusama Y. et al., to be published in Nucl. Fusion Supplement (Proc. 15th Int. Conf. on Plasma Physics and Controlled Nuclear Fusion Research, IAEA-CN-60/A-2-IV-5 (IAEA, Vienna)).
[3.6-3] Kusama Y. et al., J. of Nucl. Mater. **220-222** 438 (1995).
[3.6-4] Kimura H. et al., Physics Letters A **199**, 86 (1995).
[3.6-5] Saigusa M. et al., Plasma Phys. Control. Fusion **37**, 295 (1995).
[3.6-6] Saigusa M. et al., to be published in Nucl. Fusion Supplement (Proc. 15th Int. Conf. on Plasma Physics and Controlled Nuclear Fusion Research, IAEA-CN-60/A-3-I-5 (IAEA, Vienna)).

3.7 LHRF and ICRF experiments

3.7.1 ICRF experiments

High I_p H-mode was exploited by combining second harmonic hydrogen minority ICRF heating and deuterium NBI heating (see Fig. I.3.7-1). Sawtooth was successfully stabilized by on-axis ICRF heating even at a low q (q_{eff}=2.7) and at relatively high internal inductance (l_i=1.1) discharge [3.7-1]. The resulting stored energy reached the highest level for the H-modes in JT-60 (~8 MJ). Up to 5 MW of ICRF power was coupled to ELM-free H-mode plasmas keeping a distance between the separatrix and the Faraday shield (S-F gap) up to ~15 cm.

Higher harmonic beam ion acceleration (from 2nd to 4th harmonics) was investigated by combining ICRF and H^0 NBI heating using a charge exchange neutral analyzer capable of MeV-range measurements. The scanning of the toroidal field (1.6–3.8 T) with a fixed frequency (116MHz) showed that the ion tail temperature increased by increasing harmonic number up to the 4th harmonics and then decreased at the 5th harmonics. This tendency is consistent with calculation of a 1-D full wave code incorporating a Fokker-Planck code. Reduction in the ion tail temperature at the 5th harmonics may be due to a competitive power absorption by electrons.

Antenna coupling and heating response were examined for different antenna phasing for the second harmonic minority heating. The 180°-phasing had the smallest coupling resistance but the highest heating efficiency. On the contrary, 0°-phasing had the largest coupling resistance but the lowest heating efficiency [3.7-2]. Compared to 180°-phasing, 135°-phasing had larger coupling resistance with comparable heating efficiency, so it seems to be promising for a future device. The heating efficiency as well as the coupling resistance degraded as the S-F gap increased. The edge ion temperature measured by a charge exchange neutral analyzer was enhanced as the S-F gap increased and as the phase difference decreased. It is inferred that the wave absorption in the core is degraded due to the decreasing parallel refractive index (N_z), resulting in multi-reflection and scattering of the fast waves and eventually edge power absorption through the production of tail ions at the edge.

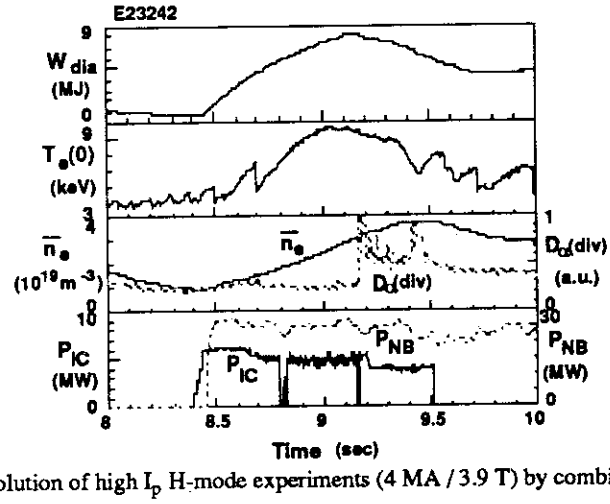

Fig. I.3.7-1. Time evolution of high I_p H-mode experiments (4 MA / 3.9 T) by combined ICRF+NB heating.

3.7.2 LHRF experiments

A good coupling (reflection < 10%) of LH waves was obtained even for a relatively long plasma-wall distance of ~20 cm. Also, it was found that the scrape-off plasma, extended and sustained by the rf power itself, contributed to the good coupling.

Concerning the absorption of LH waves, three major results were obtained. First, when two waves of different phase velocities were injected simultaneously, the resultant wave absorption profile became much broader than that for the case of the faster wave injection [3.7-3]. The enhancement of faster wave absorption at the plasma edge is attributed to the filling of the spectral gap by the slower wave. Second, using the two launchers located at different poloidal positions, we investigated the influence of the launching position on the wave absorption profile. It was found from the measurements of the hard X-ray profile and the internal inductance, that the absorption profile was broader for 45°-launching than that for 0°-launching. This is consistent with the results of a ray-tracing calculation which predicts a larger $N_{||}$-upshift and a broader wave absorption profile. Third, by systematically scanning of the magnetic field and the plasma current, it was found that the wave absorption profile was more peaked for a higher safety factor and that the effect of the safety factor was stronger than that of the electron temperature in the current range of 1–2 MA. These results are consistent with the ray tracing results which show almost the same ray trajectories for the same safety factor but with a different current and magnetic field.

The opposite current drive was demonstrated by applying the LH wave to a plasma with a reverse ohmic-current direction. As shown in Fig. I.3.7-2, the dependence of peakedness of the hard X-ray profile for an opposite current drive was similar to that of normal case (i.e., similar wave absorption profile), but the response of the internal inductance was opposite (i.e., opposite direction of LH-driven current). These results suggest that the LH current profile control is effective even when the wave absorption is restricted to the plasma edge.

References

[3.7-1] Kimura, H. et al., Fusion Engineering and Design **26**, 95 (1995).
[3.7-2] Saigusa, M. et al., Nucl. Fusion **34**, 276 (1994).
[3.7-3] Ide, S. et al., Phys. Rev. Lett. **73**, 2312 (1994).

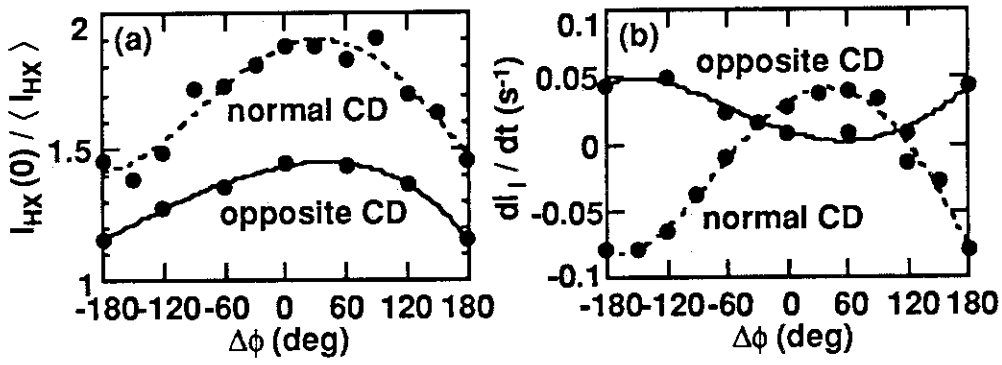

Fig. I.3.7-2. (a) Peakedness of a radial hard X-ray profile as a function of module phasing angle Δφ for normal and opposite current drives. (b) Changing rate of the internal inductance versus the phasing angle.

3.8 Development of fusion plasma analysis codes

The numerical codes have been systematically developed and updated to analyze experimental data and predict plasma performance. Efforts have been made through 1994 to evaluate the improved plasma performance more accurately and to make a detail analysis of physical mechanisms. A number of utility software have been also added their functions to facilitate a detail analysis. Furthermore, to provide against the replacement of an operating system to UNIX to be scheduled in the middle of 1996, it has been started that all codes are remodeled to meet such a new operating system.

3.8.1 Experimental data time slice monitoring software, SLICE

The "SLICE" code maps various kinds of data such as n_e, T_e, and T_i, onto the magnetic surfaces calculated by the MHD equilibrium code FBI/SELENE. Experimental data are treated as a function of volume averaged minor radius r in SLICE. The experimental data measured as line integrated values such as interferometer data for n_e, bolometer data for radiation loss, bremsstrahlung, etc. are transformed by Abel inversion and reduced to a profile data as a function of "r". The mapped data are fitted to a various functional forms. Complicated profile data, for example, when the internal transport barrier is formed can be described by two different fitting functions which covers the separated zone of the plasma adjacent each other. The fitted data are saved as 21 to 51 point data to the MAPDB database. SLICE can read such data from MAPDB and re-display and transform them. SLICE also creates run data of orbit following Monte-Carlo code, OFMC, and tokamak predictive and interpretation code system, TOPICS.

3.8.2 Tokamak prediction and interpretation code system, TOPICS

The 1-1/2 dimensional transport code system, TOPICS, for analyzing the tokamak performance and plasma characteristics has been updated according to the progress in JT-60 experiments. TOPICS code has two main routines, which make up both the steady-state and the time transient analysis code. SLICE provides a set of profile data (n_e, T_e, T_i, Z_{eff}, P_{rad}) at the specific time from the profile MAPDB database, which is used for the input data of steady-state TOPICS. Several sets of profile data at different times are combined and used for the input data of transient TOPICS. Physics models in TOPICS have been updated to meet the requirements for data analysis in the series of the 1995 experiments on JT-60. TOPICS are also used for studying the operational method in the self-ignition phase of the steady-state tokamak reactor.

3.8.3 Orbit-Following Monte-Carlo code, OFMC

The "OFMC" code follows particle orbits by using the Monte-Carlo method to analyze the slowing down process and confinement efficiency of high energy particles. The OFMC code is combined with the time transient code, TOPICS, so that the contribution to the equivalent fusion production by high energy particles can be evaluated with time-varying plasma parameters. At the

same time, the OFMC code was modified to meet the new advanced computer with parallel processors, which was introduced in the end of FY 1994. Concerning the OFMC code, its elapsed time could be effectively reduced to about 25% of the former calculations.

3.8.4 Analyzer for current drive consistent with MHD equilibrium, ACCOME

ACCOME has been developed to investigate, during steady state, the ohmic, neutral-beam-driven and bootstrap plasma currents, with consistent MHD equilibrium taking the effects of those plasma currents into account. The analysis of MHD stability regarding a resultant current profile can be made analytically using ACCOME. ACCOME also included a ray-tracing code which evaluates RF driven currents by electron cyclotron waves and fast waves.

3.8.5 Divertor simulation code, SOLDOR

To study the transport of heat and particles in SOL and the divertor plasma, a two-dimensional divertor code, SOLDOR, was developed. Fluid equations are discretized in space by using the finite volume method. The total variation diminishing schemes are used for the convective terms. The equations are solved time-dependently by using a full implicit scheme together with the Newton-Raphson method. The numerical scheme was successfully tested in slab geometry and the calculation results of the Braams code were reproduced. The code is extended to treat a part of edge region in the main plasma and the private region simultaneously.

3.8.6 Impurity transport Monte Carlo code, IMPMC

Using a two-dimensional impurity code based on Monte Carlo techniques (IMPMC), the carbon impurity behavior in JT-60 NB heated plasmas was successfully analyzed. Chemical sputtering model was newly incorporated into the IMPMC code to investigate the effects of carbon chemical sputtering in the high density divertor plasmas close to MARFE onset. It was found that in high density plasmas, chemical sputtering by neutral particles which strike the wall in the private region becomes dominant in impurity generation and enhances the radiation near the X-point [3.8-1]. This enhanced radiation power near the X-point is considered to trigger MARFE. Concerning low density plasmas, the impurity source profiles can be explained by deuterium ion physical sputtering and self-sputtering [3.8-2].

References

[3.8-1] Shimizu K. et al., "Modeling of impurity and Plasma Transport for Radiative Divertor", Proc. 15 th Int. Conf. on Plasma Physics and Controlled Nuclear Fusion Research, Seville, 1994, paper IAEA-CN60 / D-P-I-2.

[3.8-2] Shimizu K. et al., "Impurity transport modeling and simulation analysis of impurity behavior in JT-60U", J. Nucl. Mater. **220-222**, 410 (1995).

3.9 Development of the JT-60 super upgrade

3.9.1 Introduction

The main role of the JT-60 experiment is to provide the physics data needed for ITER EDA. This ITER physics R&D program will be completed at the end of ITER EDA. The tokamak fusion research basis in Japan should make progress continuously after the JT-60 experiment. According to the 3rd Phase Basic Program of Fusion Research and Development laid down by the Atomic Energy Commission of Japan, JAERI is in charge of establishing advanced new technology, which is essential for realizing of a DEMO reactor in addition to contributing the ITER project. For these objectives, the concept of an advanced steady-state tokamak, the JT-60 Super Upgrade, is now under investigation [3.9-1]. A conceptual design study of JT-60SU has been made by satisfying the following requirements: the JT-60SU has to be able to supplement the ITER project, to develop advanced new technology for a DEMO reactor, to utilize the full capabilities of the existing JT-60 facilities, and to ensure the flexibility regarding operation of the device. The size of the device, methods to control the steady-state plasma, and operational schemes are investigated based on physical and technological results from the JT-60 experiments.

3.9.2 Objective of JT-60SU

The objective of JT-60SU is to establish integrated basis of physics and technology for an advanced steady-state tokamak reactor. Main issues for this objective are as follows:

- Simultaneous achievement and sustainment of high-β_p, high-β_N, full non-inductive current drive, high confinement, and divertor heat and particle control.
- Long pulse operation with superconducting magnets, development of high heat conductivity materials for divertor plates and establishment of system integration
- Low activation materials to reduce activation, neutron/secondary γ-ray shielding, tritium processing and remote handling

To achieve these goals, advanced tokamak experiments are to be conducted in JT-60SU. These studies will also contribute to the extended burn of ITER and steady-state as the ultimate goal.

3.9.3 JT-60SU device

Based on the experimental results in JT-60U, the best integrated performance (simultaneous achievement of high confinement, large bootstrap current, high β limit, less probability of disruption and low heat load on the divertor plates) would be obtained at $q_{95} = 4\sim5$ ($q_{eff} = 5\sim6$). Therefore, the JT-60SU design aims at a high toroidal field (6 T) to enable high q operation ($q_{95} = 3.8$ at $I_p = 10$ MA). Superconducting toroidal and poloidal coils will be installed for 1 hour steady-state operation. We assume the ELMy H-mode to be the candidate for steady-state operation. As a current driver, the negative ion based neutral beam injection with an input power of 60 MW and a beam energy of 0.3 - 0.7 MeV will be used. Non-inductive discharge

with $I_p \leq 10$ MA at the volume average density of $\geq 0.5\times10^{20}$ m^{-3} can be expected under this system. At low current regime ($I_p = 5$ MA), a fully non-inductive discharge with a high bootstrap current fraction (> 60%) is possible at $n_e = 10^{20}$ m^{-3}. This operational regime is one of our targets for studying the advanced steady-state operation. Since profile control is essential for the advanced operation, various methods such as beam energy control and local profile control by an RF system are being considered. The JT-60SU will be assembled after dissembling of the existing JT-60U device in order to utilize all of the capabilities of the existing facilities. The basic design parameters and the cross section of the JT-60SU device are shown in Table I.3.9-1 and Fig. I.3.9-1, respectively.

References

[3.9-1] Ninomiya H., Aoyagi T., Azumi M. et al., "Conceptual Design of JT-60 Super Upgrade", in proc. 15th IAEA Conf. on Plasma Phys. Contr. Fusion, 1994 Seville, IAEA-CN-60/F-1-I-1.

Table I.3.9-1 Machine parameters of JT-60SU.

Plasma current I_p	10MA
Toroidal field B_t	6.0T
Major radius R_p	5.0m
minor radius a_p	1.5m
Elongation κ	1.8
Triangularity δ	0.4
Safety factor q_{95}	3.8
average density $<n_e>$	10^{20}m^{-3}
Neutral Beam Power P_{NB}	60MW
Poloidal β β_p	1.83
Confinement time τ_E	2.99s

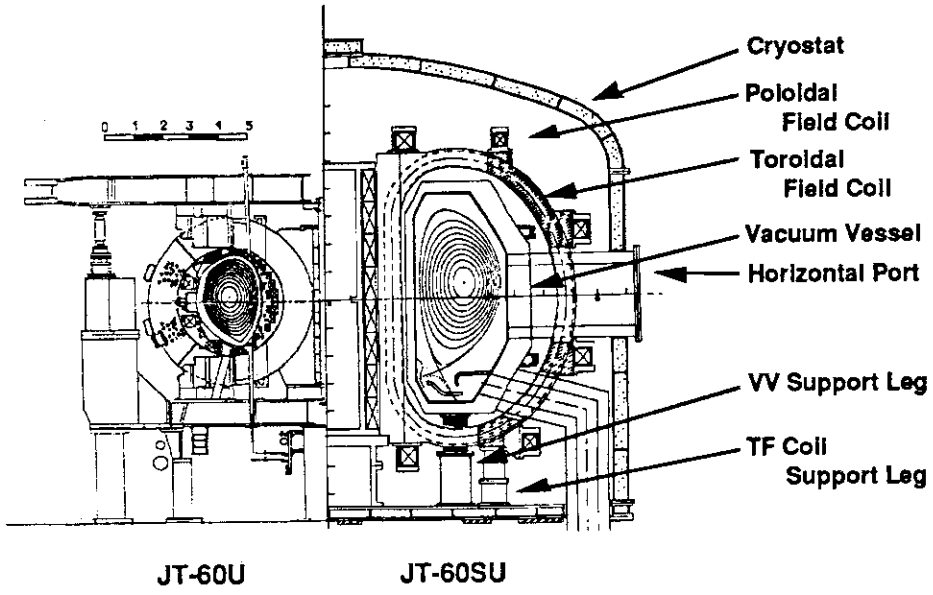

Fig. I.3.9-1. Cross-sectional view of JT-60SU in comparison with JT-60U.

4. Related Developments and Maintenance

4.1 Development of a tritium monitor using PIN diode

To evaluate tritium inventory at the first wall of JT-60, we had measured tritium in the sample tiles which were actually used in JT-60 by means of burning sample pieces of graphite tiles, converting the tritium into HTO and scintillation counting of the resultant water. This method, however, does not give quick enough results and destroys the sample tiles. To improve on these demerits, we have developed a tritium monitor using a PIN diode as the tritium sensor, which was first developed in Sandia National Laboratories[4.1-1]. It is possible to evaluate the tritium distribution promptly without the need to cut the sample tiles. Low noise charge-sensitive preamplifier and pulse shaping electronics are used for this tritium monitor, making it possible to detect tritium whose energy is down to 6 keV. Since this tritium sensor is very sensitive to light, cutting the light off is necessary to measure the tritium. The space between the sensor and the surface of the sample tile also affects the measurement. The tritium measured using a PIN diode is only the tritium which is in the surface thin layer (<approximately 1 μm) due to the absorption of the beta-rays, and hence, it is not clear whether this method does evaluate the total tritium content in the tiles or not. It is, therefore, necessary to compare the results of the tritium measurements with these two methods.

Reference

[4.1-1] Wampler W.R. et al., Nucl. Inst. and Methods in Physics Research A349(1994)473

4.2 New composite composed of boron carbide and carbon fiber with high thermal conductivity for the first wall

New composite, which has a content of 20~35 vol.% B_4C (80~65 % carbon fiber) has thermal conductivity of 250 W/m•K at room temperature which is a little less than that of the felt-type C/C, but has higher thermal conductivity at temperatures above 400°C than that of the felt-type C/C.

Retained amount of deuterium decreases with an increase in B_4C after saturation with deuterium ion and heating for the release of deuterium, i.e., a composite with 50 vol.% B_4C shows a retention rate halfway between graphite and B_4C. Erosion yield of a composite with B_4C of 35 to 50 vol.% at 800 K is around 60% lower than that of graphite. Electron beam irradiation for examining thermal shock resistance shows that a composite with 35 vol.% B_4C and networking structure of carbon fiber does not break even at high irradiation powers of 22~23 MW/m^2 which raises the surface peak temperature to around 2500°C. The weight loss by vaporization is very small and is nearly the same as that of the felt-type C/C at an irradiation power of 10~11 MW/m^2, when the surface peak temperature was around 2000°C.

This new composite has better controllable recycling properties for deuterium and better anti-erosion resistance against deuterium ion than that of the felt-type C/C, and has nearly the same thermal shock resistance as the felt-type C/C.

4.3 Development of a computer-aided software engineering tool for sequential control of discharges

Sequential control is an essential control function for intermittent and pulse discharge operations of a tokamak device, so that many subsystems may work with each other in correct order and/or synchronously. In the discharge control of JT-60, its central control system supervises its subsystem controllers with control commands such as messages and timing signals. The discharge sequential control function consists of the following three parts: (1) To perform the logical operation (AND, OR, etc.), which is driven by the changes in plant conditions, (2) to monitor these changes and to register them on a table, and (3) to manage job scheduling. During the development of a discharge sequential control program, block diagrams of the control functions are put in its design at first. Then, the logical operators and I/O's which are involved in the whole block diagrams are compiled and converted to a certain particular form. Since the block diagrams of the sequential control amounts to about 50 sheets for the high power discharge, great effort has been required in the development of this program.

To improve on the efficiency of such development, a computer-aided software engineering (CASE) tool has been developed on a UNIX workstation. This tool consists of the following two tools. (1) Editing tool, which can help us to create and/or modify the block diagrams of the sequential control function. The block diagrams shown on a workstation are automatically converted into execution forms of the sequential control logical operation. (2) The trace tool, which can help us to grasp the status of the actual discharge sequence. This CASE tool, an object-oriented programming tool, having graphical formulation, can greatly reduce any troubles in the development of the sequential control function commonly associated with pulse discharge in a tokamak fusion device.

4.4 DSP application to fast parallel processing in JT-60 plasma shape reproduction

Recently, the following experimental observations are recognized: (1) Triangularity of the plasma shape is one of the essential factors for plasma energy confinement performance. (2) The gap between the plasma surface and the antenna of the radio-frequency (RF) wave heating system determines the efficiency for a launching RF-wave into the plasma column. (3) Control of strike points of separatrix lines on the divertor plates is very important for protecting the plates and for producing desirable divertor plasma. In addition, it is also pointed out in the ITER engineering design activity (EDA) that full shape reproduction is one of the important issues for its plasma

equilibrium control. The requirements for more a sophisticated plasma position and shape real-time control adds more to the development of the parallel processing system.

4.5 Negative-ion-based neutral beam injection system

The construction of the JT-60 negative-ion-based neutral beam injection system (JT-60 N-NBI), for plasma heating and current drive experiment, has made progress and will be completed in spring 1996. The specifications are shown in Table I.4.4-1.

In March 1995, a part of the system; one of the negative ion sources, a beam line, a dc 500 kV power supply system inclusive of negative-ion generator power supply for the negative ion source, a control system and auxiliary systems, has been completed as can be seen in Fig. I.4.4-1. We have been operating it to verify the many technical issues such as the extraction of a large amount of negative ions and handling of dc high voltage ahead of the beam injection into JT-60. The verification test of JT-60 N-NBI has progressed aiming at D-beams of 22A with an energy of 500 keV.

Table I.4.4-1. Specifications of the JT-60N-NBI

Beam energy	500 keV
Negative ion beam current	44 A/ two sources
Beam pulse	10 sec
Neutral beam power	10 MW

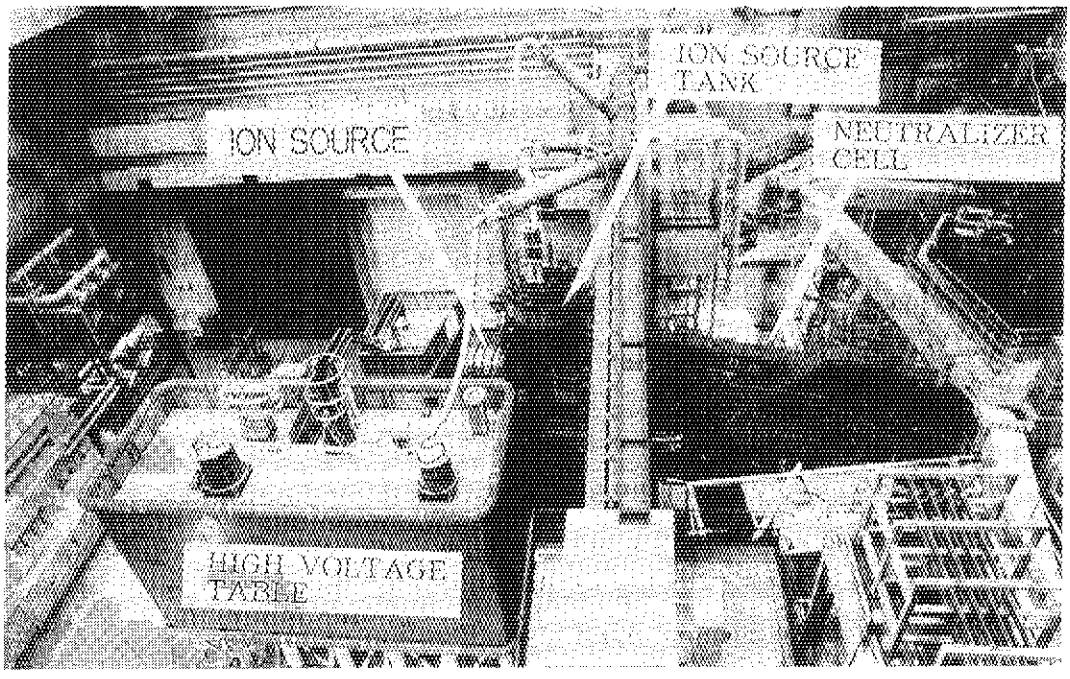

Fig. I.4.4-1. Negative-ion based NBI system for JT-60.

II. JFT-2M PROGRAM

1. Toroidal confinement experiments

1.1 Overview

The main progress on JFT-2M experiments in FY 1994 are summarized. There are two main efforts, one is the momentum transport study by applying an external helical field and by toroidal momentum input with NBI, and the other is a boundary plasma study with introducing an electric field in the scrape-off layer (SOL) by the divertor biasing. Design of the divertor modifications for the closed divertor study was carried out the divertor biasing capability still being maintained.

1.2 Experimental results

1.2.1 Toroidal momentum transfer into plasma by external rotating magnetic fields

The profile control of toroidal momentum is a promising method for improving the characteristics of plasma confinement. An experiment to control the toroidal momentum of plasma was carried out by using the external rotating helical magnetic field through phase synchronization with the magnetic island caused by the $j \times B$ force. The rotating magnetic field was generated by a set of eight saddle coils installed inside the vacuum vessel connected to two independent power supplies. The maximum frequency of the magnetic field was about 5 kHz and the amplitude of the magnetic field at that frequency was about 5 G. Magnetic probes were used to detect the synchronization of the motion of the magnetic island and the external magnetic field. The toroidal velocity of the plasma was measured by the charge exchange recombination spectroscopy (CXRS), which measured the toroidal velocity of fully ionized carbon .

The profile change of the toroidal rotation velocity was observed clearly when a 1.5 kHz external rotating magnetic field was applied to the plasma. The natural frequency of the m=2/n=1 islands was 3.0 kHz before the external magnetic field was applied. The rotation velocity at the plasma center changed from about 3 km/s in the opposite direction of plasma current to 6 km/s in the direction of the plasma current. The change at the q~2 surface was smaller being about 5 km/s. The direction of the velocity change was consistent with that of external rotating magnetic field.

We could demonstrate successfully on JFT-2M that (i) the rotating external magnetic field with m=2/n=1 helical component could interact with the intrinsic m=2/n=1 magnetic islands, (ii) toroidal momentum of the external rotating magnetic field could be transferred into the plasma and (iii) radial profile of toroidal momentum could be modified.

1.2.2 Toroidal momentum transport experiment by NBI

It is well known that the evaluated transport coefficients are larger than that of a theoretical estimated value, and the evaluation of the transport coefficients for the particles, momentum, and heat fluxes is still an important issue in the plasma transport study. Recently, the existence of a non-diffusive term for the electron heat flux (inward heat flux) was demonstrated in the off-axis electron cyclotron heating experiment in DIII-D.

In JFT-2M, the transport of toroidal momentum during the transient phase was analyzed, where the toroidal rotational velocity changes the sign due to the changing of the direction of the injected neutral beam. The profiles of toroidal rotation velocity v_ϕ and ion temperature T_i were measured by CXRS every 16.6 ms, using Carbon VI charge-exchange line emissions. Figure II.1.2-1 shows profiles of toroidal momentum ($m_i n_i v_\phi$) for discharges when the direction of the injected neutral beams changes from COUNTER to CO [Fig. II.1.2-1(a)] to the plasma current. The hydrogen beam energy was 32 keV and the injected power of CO and COUNTER were 0.49 MW and 0.56 MW, respectively. The toroidal momentum in the COUNTER injection steady-state phase was two to three times greater than that in the CO injection phase, although the injected NB power during CO injection was comparable to that during COUNTER injection. The radial flux of toroidal momentum was estimated from the time derivative of toroidal momentum and the toroidal force driven by NBI.

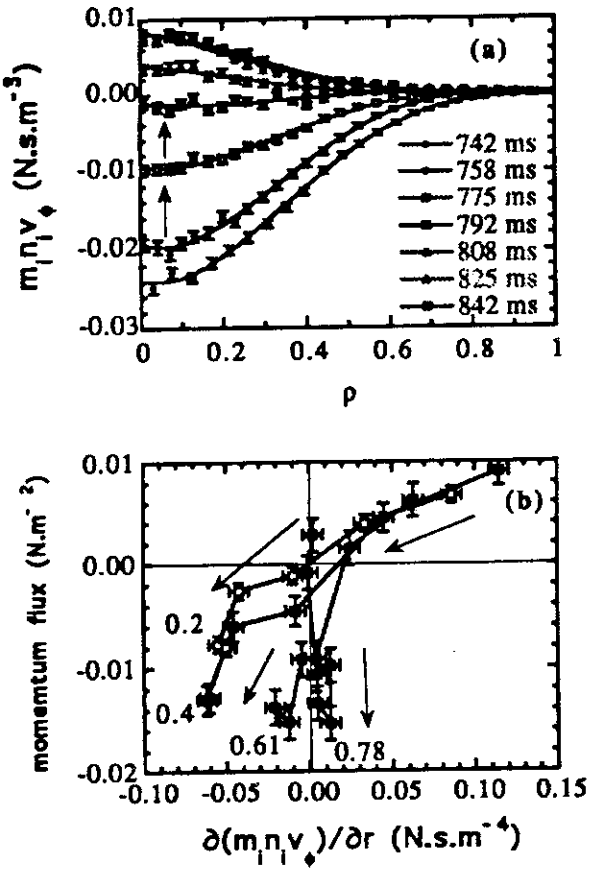

Fig. II.1.2-1. (a) Time evolution of toroidal momentum profile from COUNTER-NB (550-750 ms) to CO-NB (750-950ms), (b) radial fluxes of toroidal momentum vs. gradient of toroidal momentum for various minor radii.

The driven force by NBI was calculated by a Monte Carlo beam deposition code. Figure II.1.2-1(b) shows the radial fluxes of toroidal momentum as a function of the gradient of the toroidal momentum for the case of COUNTER to CO. This figure clearly shows the finite offset of the momentum flux at the zero gradient of toroidal momentum for ρ less than 0.6. This pinch term vanishes near the plasma axis. This spontaneous momentum flux was found to be negative (the counter direction) both for the CO and COUNTER injections. Also, it was observed as being 0.2 – 0.5 of the beam driven momentum flux in the core region.

To summarize the results, the analysis of the transport of the toroidal momentum in the transient phase suggests the existence of a non-diffusive term in the transport matrix. This term

results in a spontaneous source of toroidal momentum in the direction anti-parallel to the plasma current.

1.2.3 Turbulence suppression and transport reduction in the strong sheared flow region

The sheared flow is expected to reduce the fluctuation level and decrease energy and particle transport. It was clearly shown on JFT-2M that the reduction in density fluctuations depends on the electric field shear in the divertor biasing experiment and in the H-mode experiment.

The triple Langmuir probes, movable at the outer mid-plane, measured the time evolution of electron density, electron temperature and space potential. The negative divertor biasing (-60~-180 V) formed the negative electric field and the electric field shear in the SOL region, and a steep density profile was observed. Density fluctuations $\tilde{n}_e / n_e$ in the strong shear region were reduced according to the bias voltage from 70% with no biasing to 45% with -180 V biasing.

In the L-mode and H-mode with NBI, the density fluctuations just inside the separatrix were measured by the triple Langmuir probe with good spatial resolution of 2 mm and by a 50 GHz reflectometer. The density profile of the H-mode shows a clear steepness inside the separatrix compared with that of the L-mode as shown in Fig. II.1.2-2(a). Here, the best estimation of the separatrix location is -2 cm in the figure. The floating potential decreases also at d_S= -2.5 cm ~ -3.1 cm and becomes more negative in the H-mode case (Fig. II.1.2-2(b)), that means formation of a high electric field shear. The density fluctuation level is reduced significantly at the high electric field shear region formed in the H-mode (Fig. II.1.2-2(c)). These observations agree qualitatively with the predictions concerning the reduction of fluctuations in high electric field shear region by Zhang and Mahajan.

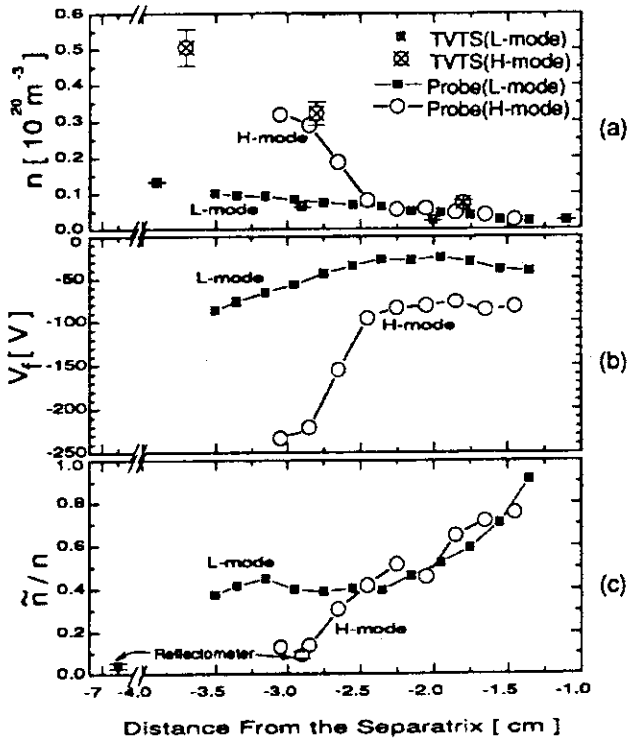

Fig. II.1.2-2. (a) Electron density,(b) floating potential ,(c) fluctuations of electron density as a function of the distance from the separatrix. The separatrix position is about -2 cm. The density fluctuations with the reflectometer are also plotted.

References

[1.2.1] Oasa K. et al., Proc.15th IAEA Conf. on Plasma Phys. and Cont. Nucl. Fusion Research A3/5-P-14.
[1.2.2] Ida K. et al., Phys. Rev. Letters **74**, 1990 (1995).
[1.2.3] Toyama H. et al., Proc.15th IAEA Conf. on Plasma Phys. and Cont. Nucl. Fusion Research A-4-II-3.

1.3 Modification to closed divertor

Regarding the engineering design of ITER, it is one of the key issues for solving whether or not dense-and-cold divertor plasma with remote radiative cooling, which drastically reduces the erosion of the divertor target plate, is compatible with high confinement. However, a simultaneous formation of the above both conditions is difficult or the operational density regime is very narrow with an open divertor configuration, since the high heat and particle fluxes, which are the necessary conditions for the formation of dense-and-cold divertor plasma, decrease drastically during the buildup phase of the H-mode. On the other hand, strong gas-puffing is necessary to form dense-and-cold divertor plasma, which deteriorates the confinement characteristics. Actually, it was only possible with the help of a pump limiter located near the divertor X-point with strong gas-puffing from the divertor region in a high density regime on JFT-2M with an open divertor configuration.

To improve particle controllability and extend the operational regime for the simultaneous realization of the above two conditions, the design of the closed divertor configuration in JFT-2M was completed. The new closed divertor has a cryo pump (1 m^3/s for D_2) and is capable of electrical biasing on both divertor and baffle plates made of stainless steel (Fig. II.1.3-1). The analysis of the closed divertor characteristics using a computer code (UEDA-code) is still being continued.

The main aims of this modification are to optimize fueling/exhaustion and obtain both an H-mode and dense-and-cold divertor plasma simultaneously in a wide operational regime not only in a high density regime by individual control of neutral particles in the divertor chamber and in the main plasma periphery.

Studies on fueling and exhaustion, particle control, neutral buildup scaling and SOL plasma behaviors will be carried. Divertor plasma characteristics are analyzed using the UEDA-code to optimize on divertor operation. The shape of the divertor will be changed step by step according to the code analysis. Results will be used for the design of the divertor modifications for JT-60.

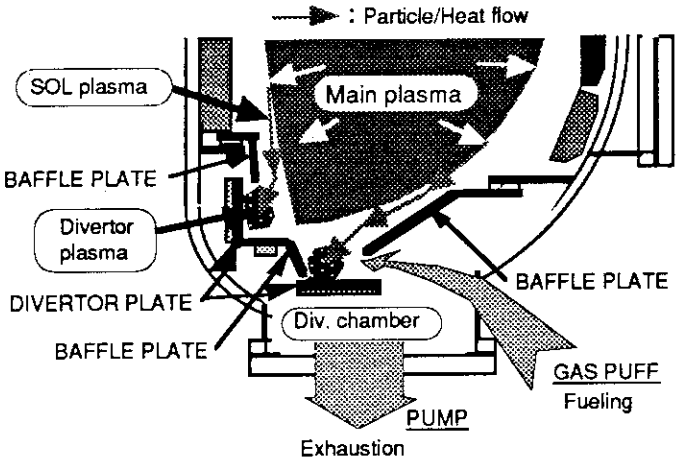

Fig. II.1.3-1. JFT-2M closed divertor configuration.

References

[1.3] Sengoku S. et al., in Bull. Amer. Phys. Soc. **27**, 1085 (1982).
Sengoku S. et al., in Proc. Europ. Conf. on Cont. Fusion and Plasma Phys., **13B**, 959 (1989).

2. Operation and Related Developments

2.1 Operation and Maintenance

The JFT-2M Tokamak has been operating for ITER physics R&D experiment. In this fiscal year, the period of operation has been 5 months from April to the middle of August. Each apparatus of the JFT-2M machine ran smoothly according to the experimental plan. During this half year, the old flywheel motor-generator(MG) of toroidal field coil was replaced by a new one which generated a magnetic field of 2.2 T. Operation records of JFT-2M during FY 1994 can be summarized as shown in Table II.2.2-1.

The main apparatuses such as the Tokamak machine and MG were operated at a minimum loss time by periodic inspections of the electricity of toroidal field coil, the first cooling system, the circuit breaker of power supply, etc. The loss time was mainly caused by troubles with the electric circuits in various components of the control system in the poloidal power supply. These had been operated for over ten years, so only a few parts have had to be replaced and some parts have to be periodically exchanged to keep up operation. Power supplies of the vacuum pump were improved so as to keep it going for an instant voltage drop. Electrostatic proves were strongly fixed to avoid it falling into the vacuum chamber due to the electromagnetic force induced as a result of disruption.

Table II. 2.2-1 Summary of operation records of JFT-2M during FY 1994

		FY 1993	FY 1994				
			Apr - Jun	Jul -Sep	Oct - Dec	Jan - Mar	total
MG	#1MG(hr.)	733	307	179	0	0	486
	#2MG(hr.)	731	305	179	0	0	484
JFT-2M	Shot number	2,935	1464	1196	0	0	1342
	TDC(hr.)	151	77	28	0	0	105
	Baking(times)	0	1	0	0	0	1
	Pellet(day)	4	6	3	0	0	9
NBI	Operation(day)	42	17	16	0	0	33
	A-line (times)	9,858	1468	5737	0	0	7205
	B-line (times)	10,264	1475	5770	0	0	7245
ECH	Operation(day)	28	17	0	0	0	17
	Injection(times)	90,264	22,711	0	0	0	22,711
FW	Operation(day)	0	20	3	0	0	23
	Injection(hr.)	0	158	21	0	0	179

Neutral beam injection system is contributing to experiments as the main heating machine except for the breaking of a filament in the ion source. Electron cyclotron heating system(ECH) was operated for 17 days. After 6 days of operation, the window of one gyrotron broke by breakdown during the adjustment of RF power around 30 - 40 kW. As the system consists of two gyrotrons, the system was operated by only one gyrotron during the residual period. The transmission line components of ECH were examined carefully to reduce the transmission loss and to decrease the breakdown phenomena. Rearrangement of components and adjustment of the wave-guide axis contributed to inject more power into the plasma. Fast wave system was also operated without any major problems.

2.2 Development of equipment and apparatus

In cooperation with the experimental Plasma Physics Laboratory, some developments regarding the Tokamak machine, heating system and power supply have been carried out as follows. The development of the Tokamak machine was centered around a closed divertor so as to improve the control method of particles and heat flux in the divertor region. The closed divertor was designed and installed for ITER physics R&D. For the purpose of searching for a potential material for the divertor plate in fusion reactor, stainless steel(SUS-316) was selected as a sample material for the divertor plate. The other components for the baffle plate and support structure was also fabricated using SUS-316. Furthermore, in order to enhance the particle flux control, the divertor was designed so as to be able to apply electric voltage between the baffle plate and vacuum vessel on the basis of the results of the divertor bias experiment of JFT-2M. A cryo-pump with a pumping speed of 1000 l/sec was installed in the divertor to increase the controllability of the pressure in the divertor. The pressure of divertor would be controlled by evacuation with the cryo-pump and gas puffing with gas valves. The results will be reflected in JT-60 divertor experiment carried out by ITER physics R&D.

Development of heating system was performed on ECH and FW system. It was investigated so as to increase ECH power from 0.4 to 1 MW. The increase in power is carried out in cooperation with GA technology in the U.S.A. The FW experiment on the capability of the antenna with back Faraday shield was carried out around 200 - 300 kW. In order to inject maximum power of 600 kW, a new antenna with same back Faraday shield was installed. Its width and mutual separation were made wider than the old antenna so as to increase electric -resisting voltage.

The DC generator was replaced by new one with an over all capacity of 51,300 kW which is the largest in the world. In the making of this generator, an insulation system for 2,700 V using H-class polyamide and polyimide materials was developed, because the insulation voltage of 1500 V was the maximum for a DC machine until this time. Accordingly, it has been possible to operate at a maximum toroidal field of 2.2 T in JFT-2M.

III. PLASMA THEORY AND COMPUTATIONS

1. Introduction

In FY 1994, extensive theoretical and computational work has been carried out on topics regarding Analyses of Confinement and Heating Processes; MHD Equilibrium and Stability Analyses; Analyses of Burning Plasma in Tokamaks. Especially a TAE mode study has been started because of its importance for future experiments. In addition, the development of effective algorithm for massive parallel computers has been started.

2. Analyses of confinement and heating processes

2.1 Self-organized critical gradient transport and shear flow effects on ion temperature gradient mode in toroidal plasmas [2.1-1, 2.1-2]

A theoretical and computational study of the ion temperature gradient and η_i instabilities in tokamak plasmas has been carried out. In toroidal geometry, the modes have a radially extended structure and their eigen frequencies are constant over many rational surfaces that are coupled through toroidicity. These nonlocal properties of the ITG modes impose strong constraint on the drift mode fluctuations and the associated transport, showing a self-organized characteristics. As any significant deviation away from the marginal stability causes rapid temperature relaxation and intermittent bursts, the modes hover near the marginality and exhibit strong kinetic characteristics.

As a result of these, the temperature relaxation is self-similar and nonlocal, leading to a radially increasing heat diffusivity. The nonlocal transport leads to the Bohm-like diffusion scaling. The heat input regulates the deviation of the temperature gradient away from the marginality. The transport scaling and properties obtained are globally consistent with experimental observations of the L-mode discharges. The radial mode structure can be disintegrated into smaller radial islands by the E×B poloidal shear flow, suggesting that the transport changes from Bohm-like to near gyro-Bohm. Poloidal momentum deposition couples with the turbulent energy and found to lead to a new strongly transport suppressed branch .

References

[2.1-1] Kishimoto Y., Tajima T., LeBrun M. J. et al. "Self-organized Critical Gradient Transport and Shear Flow Effects for Ion Temperature Gradient Mode in Toroidal Plasmas", Proc. 15th Int. Conf. on Plasma Physics and Controlled Nucl. Fusion on Research, IAEA-CN-60 / D-2-II3 Seville, Spain, 1994.

[2.1-2] Tajima T., Kishimoto Y., Horton W. and Dong J.Q., "Shear Flow Effects on Ion Thermal Transport in Tokamaks", IFSR #697, March 1995.

2.2 Particle simulation study of the toroidal ion temperature gradient mode in shear flow plasma and a comparison with theory

How the global structure and stability of the toroidal ion temperature gradient mode change with $E\times B$ shear flow has been studied using a 3-dimensional particle simulation code [2.2-1], where E is the radial electric field given by $E_r(r)=\alpha(r-a/2)$ (a: minor radius). It was found that with an increasing shear flow by changing α the change in growth rate and global mode width occur in close relation to that of poloidal asymmetry or tilting [2.2-2]. In a small shear limit, the poloidal asymmetry decreases or increases, depending on initial equilibrium profile and shear flow direction, making the mode more unstable or stable. In a large shear flow limit, however, it moves to the large values ($\theta \rightarrow 90°$ or $-90°$), making the growth rate and mode width nearly disappear, and thus, stabilizing almost completely the toroidal mode (cf. Fig. III.2.2-1). This simulation result has been compared with the two existing theories by Kim et al. [2.2-3] and by Connor et al. [2.2-4]. It is found that the simulation result can be explained much better by the theory by Kim et al.

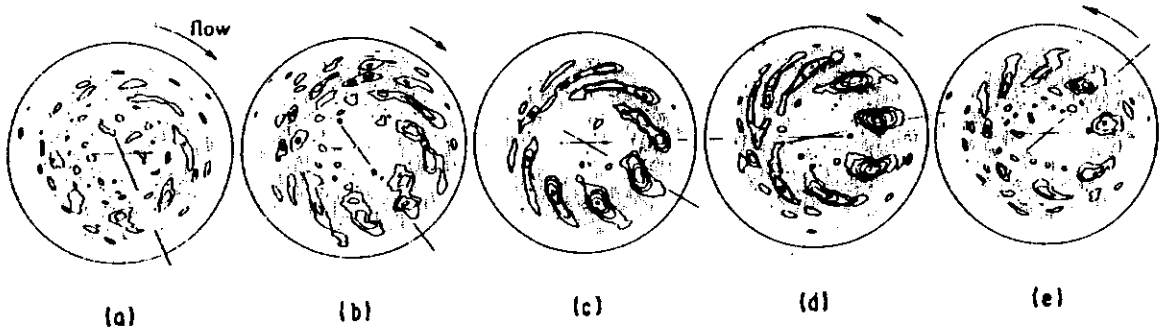

Fig. III.2.2-1. Potential contours in poloidal cross section in linear phase for a series of the strength of the shear flow, α=-6, -3, 0, 3, 6 for (a)-(e), respectively. (note the ion diamagnetic drift direction is counterclockwise of the same direction with $\alpha>0$)

References

[2.2-1] LeBrun M. J. et al., "Toroidal Effects on Drift Wave Turbulence", Phys. Fluids **B 5**, 752 (1993).
[2.2-2] Kishimoto Y., Tajima T., LeBrun M. J . et al. ,"Self-organized Critical Gradient Transport and Shear Flow Effects for Ion Temperature Gradient Mode in Toroidal Plasmas", Proc. 15th Int. Conf. on Plasma Physics and Controlled Nucl. Fusion on Research, IAEA-CN-60 / D-2-II3 Seville, Spain, 1994.
[2.2-3] Kim J. M. and Wakatani M., "Radial Structure of High-Mode-Number Toroidal Modes in General Equilibrium Profiles", Phys. Rev. Lett. **73**, 2200 (1994).
[2.2-4] Connor J. W., Taylor J. B. and Wilson H. R., "Shear Damping of Drift Waves in Toroidal Plasmas", Phys. Rev. Lett. **70**, 1803 (1993).

2.3 Differences in global mode-structure between toroidal Alfven eigenmode and drift-type mode

The problem of the global structure and stability of various toroidal modes, like the toroidal ion temperature gradient, trapped particles, or kinetic ballooning modes, and the toroidal Alfven eigenmode (TAE), in general equilibrium profile has been studied using the translational invariance argument. It was found that the global structure and stability of toroidal modes have a significant difference, depending on whether the eigenvalue is real or complex. For the modes with a real eigenvalue, like TAE, the radial width is of the order of equilibrium scale length and the eigenvalue has a discrete spectrum. Meanwhile, for the modes with a complex eigenvalue, like the

toroidal drift-type modes, the radial mode width becomes much smaller, of the order of $(\rho_i L)^{1/2}$ where ρ_i is the ion Larmor radius and L is the equilibrium scale length, and also the eigenvalue becomes to have a continuum spectrum.

3. MHD equilibrium and stability analyses

3.1 Eigenvalue method for computation of outer region matching data

A new method has been developed which computes the outer region matching data of the one-dimensional Newcomb equation [3.3-1]. In this method an eigenvalue problem is formulated for the Newcomb equation. Variational principles are derived for the problems to be solved and a finite element method is applied. Except for the case of marginal stability, the eigenvalue method is equivalent to the boundary value method. However, the eigenvalue method has the several advantages: it is a new method of ideal MHD stability analysis for which the marginally stable state can be identified, and it guarantees numerical stability in computing matching data close to marginal stability. We perform detailed numerical experiments for a model equation with analytical solutions and for the Newcomb equation in the m=1 mode theory. Numerical experiments show that the new method gives the matching data with numerical stability as well as high accuracy.

References

[3.1-1] Tokuda S., Watanabe T., "Computation of the Outer-Region Matching Data for a Plasma close to the Marginal Ideal MHD Stability", Proceedings of 1994-Workshop on MHD Computations-applied to the controlled thermonuclear fusion research based on MHD mathematical model-, The Institute of Statistical Mathematics Cooperative Research Report 72, 1995.

3.2 Optimization of MHD stability in Steady-State Tokamak Reactor: SSTR

[3.2-1]

Stabilities of high-β_p plasmas with a large bootstrap current have been investigated as a function of the pressure profile and current profile in SSTR. In this analysis, MHD equilibria are generated as to be consistent with the bootstrap current and the neutral beam driven current, and they are tested for ideal MHD stability, i.e., the low n kink mode and infinite-n ballooning mode. While fusion power gain Q increases with a broadening of the pressure profile due to the larger bootstrap current on the outer half radius, pressure broadening reduces internal inductance l_i, making plasma more MHD unstable. MHD stable plasma without wall stabilization, which has a high Troyon factor of 3.45 and a large Q of 30, is obtained by making a nearly parabolic pressure profile and controlling the q_{min} value to slightly above one (~ 1.1) by a beam driven current. These results indicate a way to optimize the current profile and the pressure profile for the steady-state reactor.

References

[3.2-1] Ozeki T., Azumi M., Kikuchi M. et al. "Optimization of MHD Stability in Steady-State Tokamak Reactor : SSTR ", Proc. 15th Int. Conf. on Plasma Physics and Controlled Nucl. Fusion on Research, IAEA-CN-60 / F-P-7 Seville, Spain, 1994.

3.3 Beta limit analysis of ITER plasma with q_0=1 [3.3-1, 3.3-2]

Stability analyses of n = 1 kink mode and high-n ballooning modes are made for the ITER L-mode and H-mode profiles (n: toroidal mode number). In case of $q_0 > 1$, the beta limit is determined by the stability of the high-n ballooning mode. On the other hand when $q_0 < 1$, the beta limit is determined by the stability of the m=1 internal kink mode and it is reduced to the value of less than the design value.

References

[3.3-1] Tokuda S., Ozeki T., "Stability Analysis of External Kink Mode for ITER L-mode Profile Plasmas", JAERI-Research 94-013.
[3.3-2] Tokuda S., Ozeki T., "Stability Analysis of ITER Plasmas with H-mode Profiles", JAERI-Research 94-030.

3.4 Stabilizing effect of local heating on tearing mode

It has been known that radially localized axisymmetric current perturbations can stabilize the resistive tearing modes by changing the equilibrium current profile near the mode rational surface. Local ECH heating also can stabilize by modifying the plasma resistivity of the tokamaks with small and middle size. We studied the efficiency and time response of these methods to stabilize the tearing mode and examine the possibility to apply them to a large tokamak such as ITER. Time response of localized current drive is limited by a skin time of δ_J^2 / η, here δ_J and η are the layer width of the driven current and plasma resistivity respectively and the necessary amount of the localized driven current to stabilize the tearing mode is of the order of $(r_s\Delta')(r_s/\delta_J)^2 I_{total}$ and stabilizing effect of radially localized current is enhanced by a large factor of $(r_s/\delta_J)^2$. Here r_s represents the radial position of resonant surface of the mode and Δ' is the jump of the radial derivative of the helically perturbed flux function. Thus, it is important to use a well localized current source to get high efficiency and quick response for stabilizing the tearing modes. In the case of localized heating, to make a very localized current perturbation, the induced temperature perturbation is reduced by the effect of the finite thermal conduction and the induced current also becomes small by a factor of $(\delta_h/r_s)^2$, where δ_h is the width of localized heating and there is no merit for strong localization of a heating source. In the case of high bootstrap current tokamak, perturbed current is proportional to the temperature gradient, not to perturbed temperature and heating position must be displaced by ~ δ_h inside of the rational surface.

4. Analyses of burning plasma in tokamaks

4.1 Relaxation of sawtooth stability criterion upon magnetic shear due to alpha particle pressure [4.1-1]

Sawtooth stabilization by local magnetic shear reduction has been studied for D-T plasmas which contain alpha particles. Magnetic shear critical to the onset of sawtooth has been evaluated by taking the alpha particle pressure into account. Critical magnetic shear has been found to be higher for lower densities and/or broader density profiles. The temperature increase due to alpha heating in the course of operation could possibly improve the stability margin for the shear, provided that the density and its peakedness are not too high. The higher density operation may be the better for sawtooth control, which would be realized for not too low and not too high values of critical shear.

References

[4.1-1] Yamagiwa M. et al, "Relaxation of Sawtooth Stability Criterion upon Magnetic Shear due to Alpha Particle Pressure", to be published in Nuclear Fusion.

4.2 TAE mode stability of steady-state plasma in JT-60U [4.2-1]

The stability of Toroidal Alfven Eigenmode (TAE) is presented for steady-state plasmas in the JT-60 Super Upgrade (JT-60SU). Studies were carried out by using the ACCOME code for calculating self-consistent MHD equilibria and by using the NOVA-K code for analyzing the TAE mode stability. Characteristics of the TAE mode stability is obtained for steady-state plasmas (3 MA/3 T) with a large bootstrap current and a 500 keV neutral beam (NB) current. Above the density value corresponding to $V_h / V_A \approx 1$, the TAE mode becomes unstable due to a large pressure gradient, ∇P_h, and a large beta of the hot particle, $\langle \beta_h \rangle$. As the density and temperature increase, the bootstrap current increases so that the NB power required for the current drive decreases. As a results, both ∇P_h and $\langle \beta_h \rangle$ decreases and the TAE modes are stabilized by ion Landau damping. In the high current plasma (10 MA) case, because ∇P_h is small due to high density and V_h / V_A is less than unity due to high toroidal field (6.25 T), the TAE mode is stable for low n to medium n (≤ 15).

References

[4.2-1] Ozeki T., Cheng C.Z., Nagashima K., "TAE mode Stability of Steady State Plasma in JT-60U", IAEA Task Force Meeting on Alpha Particles in Fusion Research, April 25-28, PPPL, USA.

IV. COOPERATIVE PROGRAM ON DIII-D (Doublet III) EXPERIMENT

1. Introduction

The primary goal of the DIII-D tokamak research program is to provide data needed for International Thermonuclear Experimental Reactor (ITER) and to develop a conceptual physics blueprint for a commercially attractive electrical demonstration plant (DEMO) that would open a path to fusion power commercialization. Specific DIII-D objectives include the steady-state sustainment of plasma current as well as demonstrating techniques for microwave heating, divertor heat removal, fuel exhaust and tokamak plasma control. The DIII-D program is addressing these objectives in an integrated fashion with high beta and good confinement.

2. Highlights of FY 1994 research results

2.1 Divertor radiation research

The major goals of the divertor and boundary physics studies are for controlling the impurities, efficient heat removal and to obtain an understanding of the strong role that the edge plasma plays in the global energy confinement of plasma. Gas puffing experiments demonstrated heat flux reduction in high confinement H-mode plasmas, as shown in Fig. IV.2.1-1. An about 1 s D_2 pulse was puffed at one toroidal location above the plasma midplane. After a delay of several hundred ms, the heat flux measured at the divertor plate with an IR camera dropped by a factor of 3; this reduction was maintained even after the puff was decreases. Effects on the energy confinement time is small. Tomographic reconstruction of the radiation pattern in the plasma shows a very localized radiation zone just outside the separatrix near the X-point. Before the D_2 puff, most of the radiation appears near the inner strike point. This is evidently a "natural" radiative divertor with carbon and deuterium radiation source.

As neon recycles from the carbon walls in DIII-D, only a short 100 ms puff at 15 Torr l s^{-1} was injected below the X-point. The heat flux at the divertor plate decreased immediately, while the average τ_E

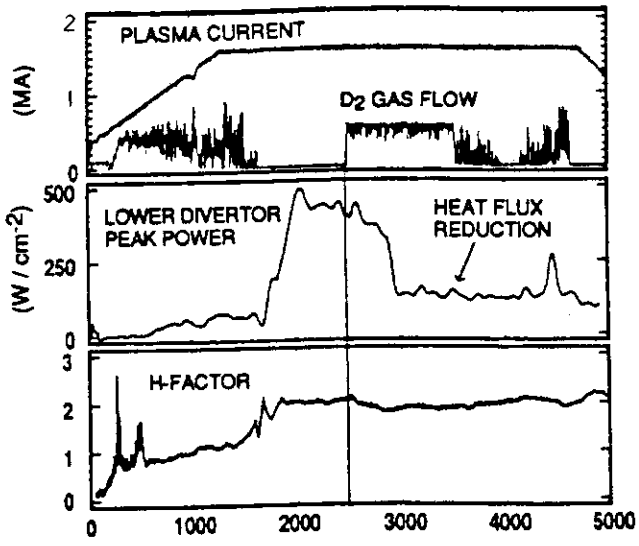

Fig. IV.2.1-1. Typical wave form for the D_2 puff discharge.

remained nearly constant. There was a large change in the ELM behavior, resulting in modulation of the stored energy. A core neon concentration of 2–3% was measured from charge exchange recombination emission. The resulting Z_{eff} was ~3.

2.2 Advanced tokamak research

The advanced tokamak studies initiated into new techniques for improvement of energy confinement, controlling particle fueling and increasing plasma beta. While nominal performance (H=2, β_N~3.5) is adequate for near term ignited plasma experiments, advanced tokamak performance can lead either to smaller, lower cost reactors at a given power output or higher power output for a given device size. Here H and bN are defined by $H = \tau_E / \tau_E^{ITER\text{-}89P}$ and $\beta_N=\beta_T/(I/aB)$ (%, MA, m, T), respectively. While enhanced confinement enables the reaching of high bootstrap current fractions needed for steady-state operation, the bootstrap current can pose challenges for plasma stability. The approach of DIII-D to the advanced tokamak is to increase the stability limit of these high confinement regimes without disturbing good confinement. The feasibility of an advanced physics approach to tokamak reactors has been demonstrated.

Reverse central shear is a better alignment of the total current with a large bootstrap current, requiring less total current drive, and less current drive on the axis. Reverse central shear was obtained by neutral beam heating during the plasma current ramp and it was maintained for $\tau_{DUR} > 2$ s. The initial experiments showed that good confinement was readily attained with strongly reversed central shear. As shown in Fig. IV.2.2-1, the high central ion temperature with internal transport barrier was produced and a very good DIII-D H-mode with H=3 was obtained. MHD activity was often observed when q_{min} was at a low order rational value; q_{min} ~ 2,3/2. Control of q_{min} was necessary to avoid the low n MHD activity, for example, by off axis current drive.

A new error field compensation coil (C-coil) was installed to reduce the existing n=1 error field. The C-coil has six segments which can control dynamically the toroidal phase of $\tilde{B}r$. The reduction in the n=1 error field allowed lower density operation without locked modes. Further optimization with the dynamic toroidal phase control will allow lower density operation.

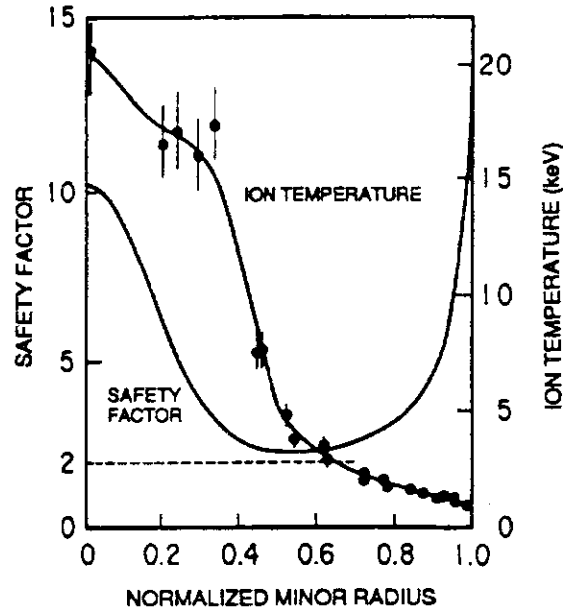

Fig. IV.2.2-1. q profile and ion temperature profile measured in the reverse-central-shear discharge.

Detailed analysis of recent high beta discharge demonstrated that the resistive vacuum vessel can provide stabilization of the low-n MHD modes. The experimental beta values, reaching up to β_T=12.6%, were more than 30% larger than the maximum stable beta calculated with no wall stabilization. Plasma rotation was essential for stabilization. When the plasma rotation slowed sufficiently, unstable modes with characteristics of the predicted "resistive wall" mode were observed. By slowing of the plasma rotation between the q=2 and q=3 surfaces by applying the nonaxisymmetric field, it could be determined that the rotation at the outer rational surface is the most important, and that the critical rotation frequency is of the order of $\Omega/2\pi$=1 kHz.

2.3 Tokamak physics studies

The major goal of the tokamak physics studies is to get an understanding of energy and particle transport in a reactor relevant plasma. Shear in toroidal rotation, which causes sheared E×B flow, was found to play a key role regarding confinement improvements of the VH-mode. Plasma evolves much more gradually from the H-mode into the VH-mode than in the case of the L-H transition. τ_E and its enhancement over JET/DIII-D scaling increase gradually until the so-called "spin-up" time at which time substantial shear in the toroidal rotation speed develops in the region $0.6 \leq \rho \leq 0.85$. While the ∇P_i and poloidal flow term are most prominent in forming the edge (ρ~0.9) E_r in the H-mode, the toroidal rotation dynamics are dominant in the VH-mode (ρ~0.7). VH-mode can be considered to arise from an increased radial penetration of the E×B shear layer.

The relative gyroradius scalings of the electron and ion thermal diffusivities were determined separately using a two-fluid transport analysis. For L-mode plasmas, the electron diffusivity scaled as $\chi \propto \rho_*^{1.0}$ (gyro-Bohm-like) while the ion diffusivity scaled as $\chi \propto \rho_*^{0}$ (worse than Bohm-like). The results were independent of the auxiliary heating method (radio frequency or neutral beam). Since the electron and ion fluids had different gyroradius scalings, the effective diffusivity and global confinement time scalings were found to vary from gyro-Bohm-like to Bohm-like depending on whether the electron or ion channel dominated the heat flux. This last property can explain the previously disparate results with dimensionally similar discharges on different fusion experiments that have been published. Experiments in the H-mode were also done with the expected values of beta, collisionality, safety factor, and plasma shape for thermonuclear ignition experiments. For these dimensionally similar discharges, both the electron and ion diffusivities scaled gyro-Bohm-like, $\chi_e, \chi_i \propto \rho_*^{1.0}$, as did the global thermal confinement time.

V. TECHNOLOGY DEVELOPMENT

1. Outline

Emphasis is being placed recently on the Research and Development (R&D) of nuclear fusion reactor technology regarding ITER-related areas, such as superconducting magnets, particle-injection heating, plasma facing components, radio-frequency (rf) heating, reactor structures, remote maintenance, brankets, tritium handling, etc.

During the development of DC toroidal field coils, a high performance Nb_3Al strand was developed. A trial fabrication of full-size conductors with 1152 strands was carried out having an length 3.5 m in length. This conductor was successfully tested up to 39 kA at 11.6 T and 7.1 K. In the development of pulsed poloidal field coils, R&D for mass-production of high-performance Nb_3Sn conductor was completed and fabrication of 9.6 tons Nb_3Sn strand for 13 T use was started for ITER. Construction of a new test facility called the "MeV-class Ion Source Test Facility (MTF)" was completed in May, 1994. Following the voltage holding test, beam acceleration was carried out. The negative H beam, produced in a "KAMABOKO"-shaped volume production type negative ion source, was successfully accelerated up to 580 keV with a drain current of 110 mA for 1 sec.

In the area of rf heating, a stable, high efficiency, high power generation was achieved in a gyrotron with beam energy recovery. By the application of an electron retarding potential, efficiency was enhanced from 30 to 50% at an output power of 610 kW for 50 msec and 400 kW for 4 sec at 110 GHz. Development of an ITER-relevant 170 GHz gyrotron was started.

Remarkable progress was made in the study of plasma facing components, both for JT-60U and for ITER. A divertor mock-up consisting of a flat-plate unidirectional CFC (carbon fiber reinforced carbon composite) armors brazed onto W/Cu composites successfully endured a heat load of 25 MW/m^2, 30 sec for more than 1000 thermal cycles.

As for the reactor structure of a tokamak machine, fabrication and testing of a full-scaled section model of double-walled vacuum vessel was completed. Fabricability of the HIPped (Hot Isostatic Pressing) first wall of the ITER shield blanket was investigated through the fabrication of test specimens and partial mockups.

A new tritium removal system using gas separation membranes was studied so as to develop a more compact and cost-effective system for a fusion reactor. In a scaled test loop using a gas separation membrane (polyimide) module, there was almost no difference in the recovery rate in case of H_2 gas and in case of tritium gas. A tritium package has been developed and the approvals for an actual tritium transportation was obtained from STA-Japan, Canada, and U.S.A. Using this package, about 20 grams of tritium was transported from Canada to Japan.

2. Fueling/pumping and vacuum technology

2.1 Development of railgun pellet accelerator

A two-stage type railgun accelerator has been studied for developing a repetitive and speed-controllable pellet accelerator for the current fusion investigations. The control of the pellet speed from low (1 km/s) to high (more than 5 km/s) is necessary so as to control the fuel particle profile and to regulate the fusion rate, etc. The railgun system under development consists of a pneumatic single-stage pipe-gun for the first stage and a railgun for the second stage acceleration. The YAG laser (0.9 J, 6 ns, 1064 nm) is used to produce a plasma armature in order to reduce the supplied voltage between rail-conductors to a few hundred volts.

This fiscal year, hydrogen pellet acceleration properties were investigated for a short rail (acceleration length=1 m) with augmented rail and long rail (acceleration length=2 m). The size of the hydrogen pellet produced in the pipe-gun is 3 mm in diameter and 4 - 7 mm in length. Materials of the rail are oxygen-free copper and ceramics. Figure V.2.1-1 shows the final speeds (u_{final}) of the pellets versus charged energy (E_{chg}) of the capacitors of the PFN power supply. The speeds are compared for three types of rails: short-length single-type rail, short-length augment-type rail and long-length single-type rail. The speeds increase according to the charged energy. The highest pellet speed obtained by using the long rail was 2.6 km/s with 1.7 kJ charged energy. It was found that the pellet acceleration efficiency depended on a wave-form of the current flowed in the rails. Also, the copper-made rails had almost no damage, in spite of being used for more than 100 operations under various conditions. The success rate of the pellet acceleration was almost 100%. In the cases of the augment-type rail the pellet speed obtained was higher than those in the long rail cases with the same charged energy. Therefore, a pellet speed of more than 3 km/s will be extrapolated by using a 2 m augment-type rail.

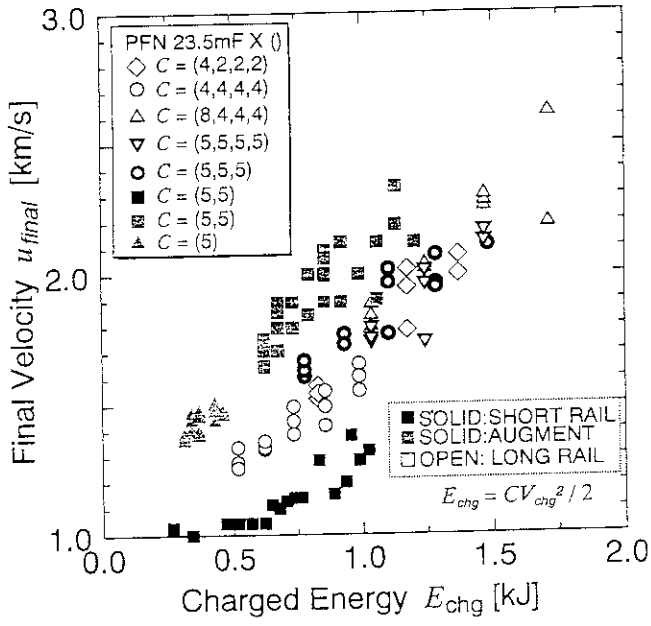

Fig.V.2.1-1 Final pellet speed versus charged energy $E_{chg}=CV_{chg}^2/2$, C is the capacity of the condenser, V_{chg} is the charging voltage. Solid symbols : short -length single-type rail, semi-solid symbols : short-length augment-type rail, open symbols : long-length single-type rail.

2.2 Progress in R&D of pumping

2.2.1 Fabrication and test of emergency bearings with tolerance to large lift forces

JAERI has proposed a large turbo-type mechanical pump for the ITER torus pumping system [2.2-1]. The mechanical pump is equipped with large rotors suspended by magnetic bearings. For an accident with a sudden pressure rise in the torus caused by a rupture in the coolant lines or windows, the pump rotors momentarily produce a large lifting force and eventually touch the stators. To protect the stators from touching the rotors caused by an accident, the mechanical pump is equipped with emergency bearings. This fiscal year, special emergency bearings with tolerance to a large lift force were fabricated and tested [2.2-2]. A copper alloy was selected for the retainers of the emergency bearings and the sudden venting test of the bearings was performed using a test pump. Figure V.2.2-1 shows that the pressure rise of 2.7 x 10^5 Pa/s produces a maximum lift of 6.9 x 10^3 N. The emergency bearings were able to withstood, in conclusion, 10 times that of the sudden venting tests. This result will be applied to the prototype pump for ITER.

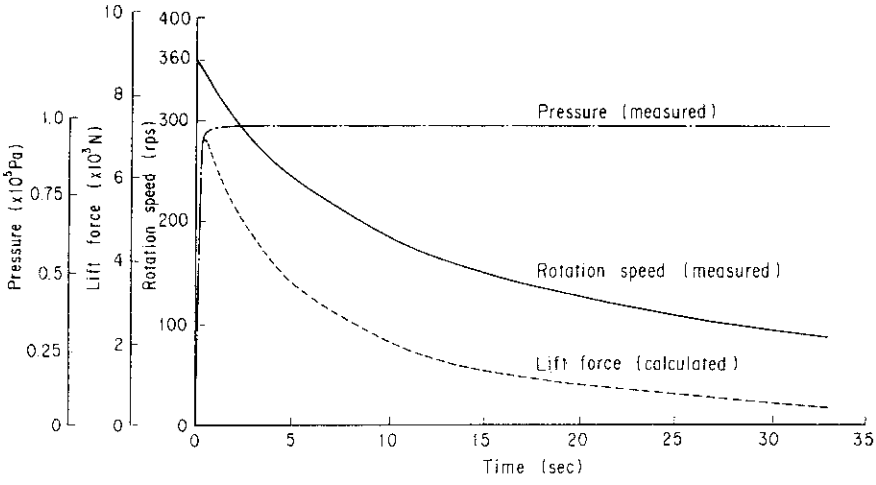

Fig.V.2.2-1 Inlet pressure, rotation speed of the rotor with lift force changing as a function of the venting time.

2.2.2 Performance test of a ceramic turbo-viscous pump

Following a 10000-cycle acceleration-deceleration test in the previous year, the prototype ceramic turbo-viscous pump was used for a test to evacuate a large vessel, 0.11 m^3 in volume, which was initially filled with atmospheric air. The air in the vessel was successfully pumped out by the new pump as shown in Fig. V.2.2-2. The rate of pressure decrease was relatively low in the high pressure region of 10^5 - 10^3 Pa, but it became sufficiently high below 10^3 Pa. The pressure reached 0.3 Pa during the first 10 min. These performances

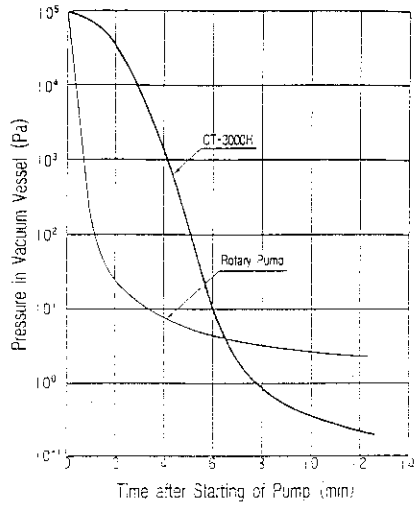

Fig.V2.2-2 Pump down curves for a large vacuum vessel of 0.11 m^3 in volume with the CT-3000H and 1.4 m^3/min(N_2) rotary pump.

might come from the pumping speed vs the pressure characteristics of the turbo-viscous pump.

2.3 Vacuum technology

2.3.1 Development of ceramic coating technology

In fusion devices, electrical insulation and conduction are required to maintain the electrical resistance and connection between in-vessel and out-of-vessel components. For this purpose, the plasma spraying method had been employed to coat the components with insulating (Al_2O_3) or conducting (Cr_3O_2) materials for several years.

On this basis of the previous investigations using small samples, the applicability of the plasma spraying method to large structural components were SUS316 and 100 x 1000 mm, respectively, and the coating conditions of the method are shown in Table V.2.3-1. From the experiment, it was found that Al_2O_3 was uniformly deposited on the components at a thickness of 200 μm without any cracks or scraping marks.

Table V.2.3-1 Coating condition of the plasma spray method.

Coating material	Al_2O_3
Environment	Atmosphere
Working gas	Ar + H_2
Distance from gun to substrate	120 mm
Coating speed	Traversing speed of 20 m/min

2.3.2 Influence of the fringing field length on the performance of the high-resolution quadrupole mass spectrometer

The fringing fields which arise on the inlet and outlet of the quadrupole field are recognized to affect the performance of the quadrupole mass spectrometer (QMS), because the traveling ions in the fringes receive the confused static and dynamic forces. To clarify the influence of the fringing field length on the separated $^4He/D_2$ peak shape of the high-resolution QMS, a special QMS which equips the movable ion source and quadrupole were fabricated and experimented using various fringe lengths [2.3-1]. The results showed that the resolution, sensitivity and peak disturbance were improved by decreasing the inlet and outlet fringe lengths. The calculated data supported the experimental results.

References

[2.2-1] Annual Report of Naka Fusion Research Establishment, JAERI-Review 94-011,56(1994).
[2.2-2] Hiroki S., Abe T., Okamoto M. et al., J. Vac. Soc. Jpn.38, 458 (1995). (in Japanese)
[2.3-1] Hiroki S., Abe T., Murakami Y., Int.J.Mass Spectrom. and Ion Processes, 136, 85 (1994).

3. Superconducting magnet development

3.1 Introduction

JAERI has been developing high-field and large superconducting magnets, cryogenic technologies and related test facilities under the Engineering Design Activity of the ITER Program.

ITER tasks shared by the Japanese Home Team were the development of a Central Solenoid (CS) Model Coil Outer Module (ID. 2.75 m, Bmax 13 T), a CS Insert Coil (ID. 1.45 m, Bmax 13 T) and a Nb_3Al Insert Coil (ID. 1.45 m Bmax 13 T) and development and construction of the test facilities (CSTF) for the CS Model Coil and Insert Coils. CSTF consists of a helium refrigerator (5 kW at 4.5 K, Name: Hellics), a vacuum tank (OD. 6.5 m, height 9.1 m) and pumps, high-power pulsed power supply (50 kA, 4.5 kV), DC power supplies (60 kA, 50 kA) and current control system, and data acquisition system.

Major highlights during the period of FY 1994 are as follows:

- R&D for mass-production of high-performance Nb_3Sn conductor was completed and fabrication of 9.6-ton Nb_3Sn strand for 13-T use was started.
- Cabling technology to make a 40-kA conductor from 1080 strands was developed.
- 13-T, 40-kA Nb_3Al conductor was fabricated and successfully tested in collaboration with the EU Home Team.
- Fabrication designs of CS Model Coil Insert Coils have been made.
- 50 and 60-kA DC power supplies were installed and successfully tested.
- Helium refrigerator and vacuum tank were fabricated and installed.

3.2 Central solenoid (CS) model coil

3.2.1 Development of Nb_3Sn strand

JAERI has been fabricating remaining 9.6-ton Nb_3Sn superconductor strands for the outer CS Model coil and CS Insert Coil. There are two different types of the Nb_3Sn strand fabricated this year, namely a strand using the bronze technique and one using the internal Sn technique. The merit of internal Sn technique is that it is easy to reduce the strand diameter to the objective value during fabrication because this type strand is composed of more ductile materials compared to the bronze type strand. On the other hand, it was difficult to reduce hysteresis losses (less than 300 mJ/cc),

Table V.3.2-1. Parameters of internal Sn and bronze technique Nb_3Sn strand.

Types of strand	Internal Sn	Bronze
• Critical current density at 12T (non Cu, 0.1 μV/cm)	578 A/mm2	645 A/mm2
• Hysteresis losses (non Cu,for±3 T cyclic field)	107mJ/cc	79.4mJ/cc
• Diameter	0.81 mm	0.81 mm
• Max. fabricated unit length	5.3 km	11.3 km
• Cu / non Cu ratio	1.5	1.5

because effective Nb_3Sn filament diameter was larger than the geometrical one due to the contact between the filaments. JAERI developed a low hysteresis and high critical current strand using the internal Sn technique. The major parameters are listed in Table V.3.2.1. The merit of bronze technique is that low hysteresis is available much easier than the internal Sn technique. On the other hand, to fabricate a long length strand was difficult because the raw materials for the bronze technique were more rigid and a reduction in the strand diameter was not easy. JAERI succeeded to fabricate a long length strand with low hysteresis losses and high critical current using the bronze technique. The parameters are also listed in Table V.3.2.1.

3.2.2 Development of a Nb_3Sn conductor

According to the task agreement between the Japanese home team and JCT, trial cabling was successfully carried out previous to the manufacture of the superconducting cable for the CS model coil. The superconducting cable for the outer module of the model coil consists of 720 superconducting strands and 360 pure copper strands whose diameter is 0.81 mm. The cable consists of six final sub-cables twisted around a central spiral channel as shown in Fig. V.3.2-1. Each sub-cable is built up in four successive cabling stages involving triplets, quadruplets and quintuplets. The final sub-cable is wrapped by the Inconel tape whose electric resistivity is large at the cryogenic temperature compared with stainless steel, in order to reduce the coupling losses between the sub-cables. The final cable is wrapped using a thin stainless steel tape (25 μm) to protect the strands during insertion into the conduit. A 100-m dummy copper cable (JA100D) and a 20-m superconducting cable (JA20SC) were fabricated and transported to Italy to attach the Inconel jacket. The JA100D and JA20SC will be used for trial windings and the layer-to-layer joint R&D, respectively. After these fabrications, a quality assurance procedure was established and a 1-km copper dummy cable was also successfully fabricated. We are ready to fabricate the superconducting cables for the SC model coil.

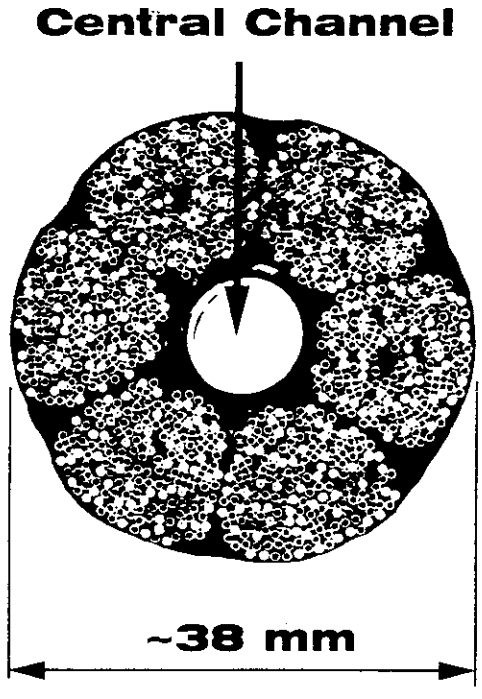

Fig. V. 3.2-1. Cross-section of 40-kA Nb_3Sn superconducting cable.

In the first trial cabling, the Inconel wrapping tape broke, because the tape was harder than the squeezing dies. The second trial was successfully performed by using forming rolls instead of dies for the squeezing process during the final stage.

3.2.3 Design of CS model coil [3.2-1]

As one of the most important R&D objectives regarding the ITER-EDA, the CS model coil program is now in progress. The CS model coil is fabricated with the same conductors and uses the same fabrication technique as the full-size CS coil of ITER to demonstrate the feasibility of the fabrication of a full-size CS coil. The coil, composed of 18 layers, is manufactured with a two-conductor-in-hand winding method and a wind-react-insulation-transfer technique, and assembled with structural support. The inner and outer winding diameters are 1.6 and 3.6 m, respectively. The total weight is 54.2 tons. The coil fabrication is carried out under cooperation between Japan and the US. Figure V.3.2.2 shows a view of the CS model coil. The coil can be operated up to 48 kA corresponding to 13 T generation, with 1 T/s and the stored energy is 668 MJ. Regarding the insulation design, a prepregnated glass-Kapton-glass tape with a thickness of 1.5 mm is used for turn-to-turn insulation, an epoxy impregnated glass-Kapton-glass tape impregnated with a thickness of 3 mm for layer-to-layer insulation and a epoxy impregnated glass-Kapton-glass tape with a thickness of 10 mm for ground insulation to withstand each design value of 10, 30 and 150 kV.

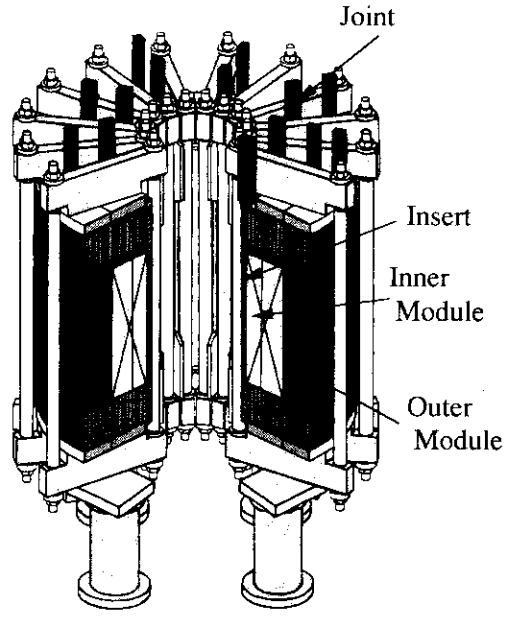

Fig. V.3.2-2. View of the CS model coil.

3.2.4 CS insert coil

The inner diameter of the CS insert coil is 1.5 m. The CS insert coil has one layer winding. The conductor of the CS insert coil is the same as that of the ITER-CS coil. The CS insert coil will be installed inside the CS model coil as shown in Fig. V.3.2.2. The conductor performance will be tested in the maximum magnetic flux density of 13 T at the test facility of JAERI. The purpose of the CS insert coil is a demonstration of the design for the ITER-CS conductor. The superconducting characteristics of the conductor, the critical current and the current sharing temperature is evaluated under conductor hoop strain. AC loss characteristics of the conductor is also evaluated in the pulsed magnetic field. The cyclic test of CS insert coil is planned to confirm that there is no damage in the superconducting strands during the pulsed operation. The CS coil in ITER is operated in the cyclic condition (total 5×10^5). The conductor is expected to show no damage during this cyclic operation. The stability margin of the CS conductor is also estimated under the same environment as that of the ITER-CS coil.

3.3 Development of Nb_3Al

3.3.1 Nb_3Al Strand

Nb_3Al is attractive because of its high potential superconducting performance. Moreover, less sensitivity in critical current performance to the strain of Nb_3Al than Nb_3Sn is excellent in the application to a fusion reactor. However, there exist difficulties regarding its commercial manufacture. JAERI has developed a manufacturing technique for the Nb_3Al strand. We were recently able to manufacture a high performance Nb_3Al strand, whose maximum critical current is 800A/mm^2 at 12 T. Also, we succeeded in drawing of a 7 km unit length strand. The technique of reaction at low temperatures, about 750 C°, and long heat reacting periods, about 100 hr, was developed through our research work. As a result of the improvements in the Nb_3Al strand manufacturing technique, it has become possible to fabricate a long length conductor for the coil of a fusion reactor, such as ITER, with the Nb_3Al strands. Table V.3.3-1 lists the main parameters of the Nb_3Al strand developed for the ITER TF conductor. Figure V.3.3-1 shows the cross-sectional view of the Nb_3Al strand.

Table V.3.3-1. Main parameters of Nb_3Al strands for the ITER conductor.

• Diameter	0.78 mm
• Cu/Non Cu ratio	1.75
• RRR	>100
• Critical current at 12 T	700 A/mm^2-Non-Cu
• Hysteresis loss at ±3T	<2 J/cc (⊥ field)
	<0.6 J/cc (// field)
• Surface	2 μm chromium plating

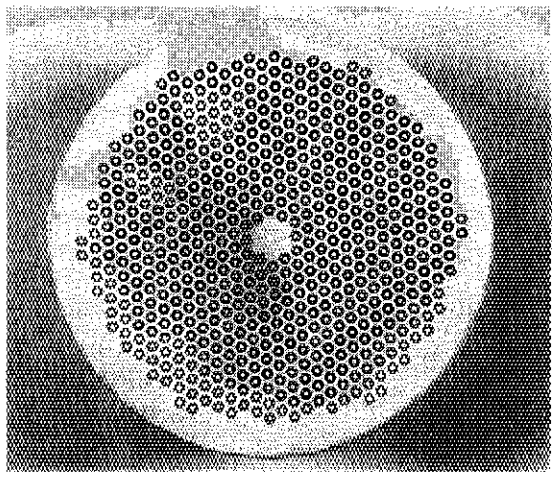

Fig. V.3.3-1 Cross-sectional view of Nb_3Al strand.

3.3.2 40-kA Nb_3Al conductor

To evaluate the Nb_3Al conductor behavior, a full-size cable-in-conduit conductor relevant to the ITER-TF coil was tested at the SULTAN facility at EPFL/CRPP in Switzerland. The sample consists of two different straight conductors with Ti and

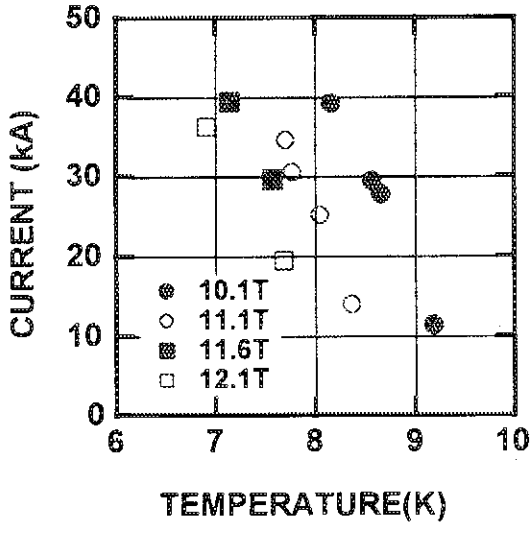

Fig. V.3.3-2. Results of Ic measurements of Nb_3Al.

stainless steel conduit, respectively. These conductors are connected electrically at both ends. The current flows through both conductors in series by using a superconductor transformer which can supplies current of up to 55 kA. Each of conductor consists of 1152 strands and a center cooling tube. Their outer and inner diameter, and overall length are 41.0 mm, 38.9 mm and about 3.5 m long, respectively. They were cooled with supercritical helium. Temperature can be set at the various values by adjusting ohmic heater current from 4.2 to about 9.5K. Critical current (Ic) measurements were performed at various levels of background magnetic filed and temperature while the sample current was ramped up until a normal zone appeared in the conductor. The criterion of Ic is 0.1μV/cm. Figure V.3.3-2 shows the results of Ic measurements of the Ti conductor at various fields and temperatures. Extrapolating the obtained results to the value at 13T and 4.2K, the expected critical current was shown to be more than 55 kA which satisfies performance required for the ITER-TF conductor.

3.4 CS model coil test facility (CSTF) [3.4-1]

JAERI is constructing the CS model coil test facility (CSTF) to demonstrate the performance of the CS model coil. Most components except two pairs of current leads and a computer system were installed during the period from April 1994 to March 1995. A view of the CSTF in the test building in February 1995 can be seen in Fig. V.3.4.1. Two pairs of current leads will be installed in July 1995 and whole facility including the computer system will be completed by March 1996. The progress of the major systems is described below.

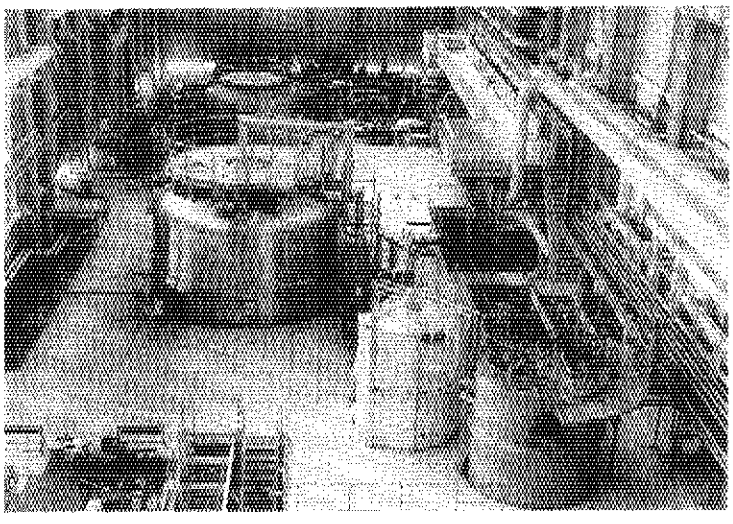

Fig. V.3.4-1. A view of CS model coil test facility (CSTF).

3.4.1 Cryogenic system (Hellics)

Construction of the cryogenic system is now in progress. The components of the cryogenic system, such as a cold box, helium compressor system, and turbo-expanders, were completed at the facilities and were installed at JAERI. Figure 3.4.2 shows a view of the newly developed cold box just before installation, which will have the refrigeration capacity of 5 kW at 4.5 K or liquefaction capacity of 800 l/h with the size of 3.2-m diameter and 7-m height. The newly developed helium compressor system is composed of three low pressure stage (0.101 to 0.9 MPa) compressors and one high pressure stage (0.9 to 1.9 MPa) compressor, which will be able

to produce helium mass flow rate of 750 g/s. Especially, the low pressure stage compressor will be the largest oil lubricated screw compressor in the world. Installation of the cryogenic system is now completed and performance test will be started from the beginning of April 1995.

3.4.2 Vacuum chamber and pump system

Vacuum chamber with the size of 6.6-m diameter and 9.1-m height and pump system with 4000 l/s diffusion pump were transported from the factory to JAERI Naka Establishment in July 1994. The installation and instrumentation works were completed in the middle of October 1994. Pre-performance test to demonstrate an evacuation power and performance of 80-K radiation shield system was carried out from October to November, 1994. A vacuum pressure of 1×10^{-5} Torr was achieved within 70 hours (design value: <150 hours) from start of evacuation. In addition, it was demonstrated that the 80-K radiation shield system had only a small liquid nitrogen consumption of 21.3 l/h (design value: <32.8 l/h). The final test to demonstrate cooling time of the 80-K radiation shield will be conducted after construction of a new liquid nitrogen supply system in May 1995. The vacuum chamber and pump system will be completed by July 1995.

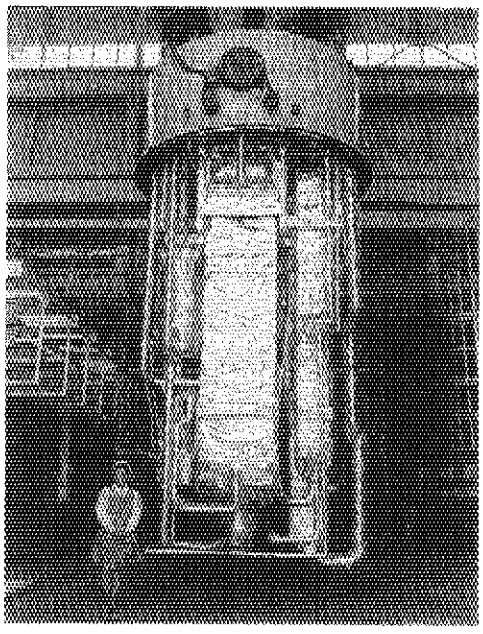

Fig. V.3.4-2. A view of newly developed cold box.

3.4.3 Power supply system

A new 50-kA, 15-V DC power supply was constructed, installed and successfully tested at its rated performance in June 1994. In addition, up-grading of existing 30-kA, 12-V DC power supply to the increased rated current of 60 kA was made and successfully completed by its performance test at 60 kA and 12 V. Components of the power supply system such as a 50-kA, 10-kV circuit breaker, a 1-GJ dump resistor, and 50-kA bus-lines were fabricated and have been installed. Performance test of the circuit breaker, the dump resistor and the bus-bar lines will be carried out jointly in June 1995.

References

[3.2-1] Ogata H., et al., 14th Magnet Technology Conference (1995), to be published in IEEE.
[3.4-1] Shimamoto S., et al., 14th Magnet Technology Conference (1995), to be published in IEEE.

4. Beam technology

4.1 Introduction

A negative-ion-based neutral beam injector (N-NBI) has the potential of current drive and plasma control for stable operation of tokamaks as well as the plasma heating at a high efficiency. Two active N-NBI programs are going on at JAERI. They are MeV test facility for R&D's of ITER NBI and N-NBI for JT-60. In FY 1994, the two major programs and other R&D's have made progressin the realization of N-NBI systems as the promising heating and current drive devices.

4.2 Negative ion beam technology

4.2.1 MeV test facility [4.2-1]

Construction of a MeV test facility was completed in May 1994. Since then the facility has been used for high energy beam acceleration tests of ampere class negative ions. Specifications of the facility are summarized in Table V.4.2-1. The MeV test facility is the only one in the world which can develop a high energy accelerator scalable to the ITER NBI. The ion source/accelerator installed in the MeV test facility is shown in Fig. V.4.2-1. The dimensions of the ion source/ accelerator is 2 m in diameter and 1.9 m in hight. The accelerator is a five stage electrostatic accelerator with insulator columns made of fiber reinforced plastic (FRP).

In a DC voltage holding test of the accelerator, the following phenomena could be observed: 1) Electric breakdown initiates at the triple junction formed at the contact point of the metal flange and the insulator in a vacuum; 2) The breakdown takes place along the insulator inner surface, which results in emission of hydrocarbon gas in the vacuum. For electric field relaxation at the triple junction, metal rings were installed on the flange. The voltage holding characteristic was drastically improved as a result of the rings. The accelerator was conditioned to hold a voltage of up to 600 kV.

After the voltage holding test, a beam acceleration test was carried out. The H^- ions were produced in a KAMABOKO shaped volume production type negative ion source, and extracted through nine apertures of 14 mm in diameter. The H^- ion beams of 0.11 A were successfully accelerated up to 580 keV for 1 s. Degradation of voltage holding characteristics was not observed with/without the beam at this level of the current and energy.

Table V. 4.2-1. Specifications of MeV test facility.

High Voltage Power Supply	Cockcroft-Walton Type DC Generator
Output Voltage	1 MV (200 kV x 5 stages)
Output Current	1 A
Pulse Duration, Duty Cycle	1 min, 1/60
Electric Power for Ion Production	100 kVA by Motor Generator

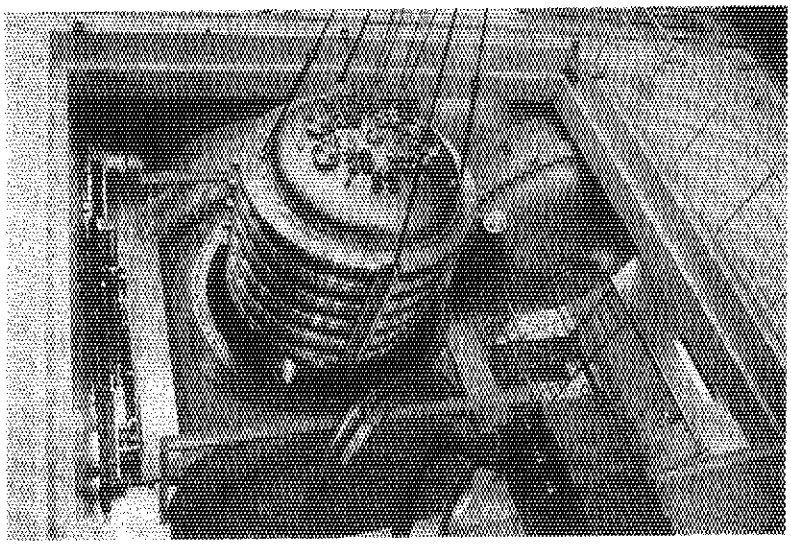

Fig. V.4.2-1. The MeV ion source/accelerator being installed in MeV test facility.

4.2.2 Large negative ion source for JT-60 N-NBI [4.2-2]

In parallel with the construction of JT-60 N-NBI, a preliminary test of the large negative ion source has been conducted since 1993 at a high current ion source test stand. A picture of the ion source mounted on the test stand can be seen in Fig. V.4.2-2. The ion source is required to produce 500 keV, 22 A, D^- ion beams for 10 s. To satisfy the high current requirements, negative ions are produced in a large semi-cylindrical (KAMABOKO) shaped ion source, of which dimensions are 64 cm in diameter and 122 cm in length. The ions are extracted through 1080 apertures (14 mm in diameter) drilled in a wide extraction area of 45 cm x 110 cm. The ion beams are accelerated through a three-stage electrostatic accelerator. The overall dimensions of the source including the accelerator is 2 m in diameter and 1.6 m in height.

In an H^- ion production test, an efficient and uniform negative ion production could be confirmed over a wide extraction area even at a low gas pressure of 0.2 Pa, which satisfies the design value (< 0.3 Pa). The ion source was also mounted and tested in the MeV test facility for voltage holding and ion acceleration tests. The voltage holding capability of up to 184 kV could be confirmed for a single column of the accelerator insulator. This is equivalent to applying 110 % of full voltage (i.e., 550 kV) for the accelerator composed of a stack of three insulators. As a combination test of both ion production and voltage holding, the beam test was carried out. The H^- ions of 0.2 A were extracted from a 12 cm x 12 cm area in the extractor and successfully accelerated up to 460 keV for 1 s. The ion source is ready to be mounted on JT-60 N-NBI.

4.2.3 400 keV negative ion source for simulation of the JT-60 N-NBI source acceleration [4.2-3]

400 keV negative ion source has the same three-stage electrostatic accelerator as the JT-60 source. The accelerator structure related to the beam optics (gap length, aperture diameter etc.) was made to be the same as the JT-60 source. Only the number of the grid apertures was reduced to 49 apertures to fit the power supply capability (400 keV, 1 A) of the test stand. The 400 keV

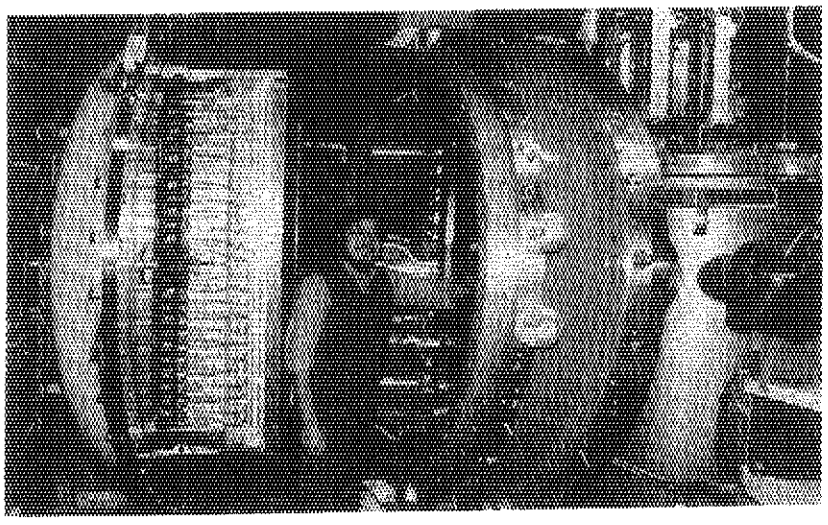

Fig. V.4.2-2. Large negative ion source for JT-60 N-NBI.

source has been utilized for simulation of high energy beam acceleration in the JT-60 source.

Heat loads in the accelerator grids were precisely measured. By reducing the gas pressure in the source, the heat load decreases linearly due to less stripping loss of the ions in the accelerator. Therefore it is important to produce negative ions efficiently at a lower pressure. At the pressure equal to zero, only 1 ~ 2 % of accelerator input power was dissipated in each grid due to direct interception of the beam and/or leakage electron from the extractor. As a result, the acceleration efficiency of the JT-60 source was estimated to be nearly 90% at the design pressure of 0.3 Pa.

Beam steering by aperture displacement was also examined with the 400 keV source for confirmation of beam focusing in the JT-60 source. At the perveance equivalent to full power operation of the JT-60 source, the beam steering characteristics by grounded grid displacement were in almost good agreement with the analysis used in the design of the JT-60 source. It was also confirmed that the beam did not hit the grid by the displacement range of the JT-60 source.

4.2.4 Design of ITER NBI [4.2-4]

After conceptual design of 50 MW, 1 MeV NBI system for ITER was completed in April 1994, a common reference design of ITER NBI was established under an agreement between European Union, Russian Federation, and Japan. A plan view of the common reference NB module installed in ITER torus hall is shown in Fig. V.4.2-3. In the following engineering design phase JAERI has been in charge of designing mainly in the three areas described below. 1) Ion source/accelerator: The ion source/accelerator has been designed on a basis of the JT-60U source and the R&D conducted at JAERI. The ion source/accelerator is composed of a KAMABOKO shaped large source and a five-stage electrostatic accelerator, which can deliver D^- ion beams of 1 MeV 30 A for 1000 s. 2) Neutronics/maintenance: Neutronics environment, neutronics response of the components, activation in the NB system have been studied using a two-dimensional computation. A possibility of hands-on maintenance for NB module was suggested based on the

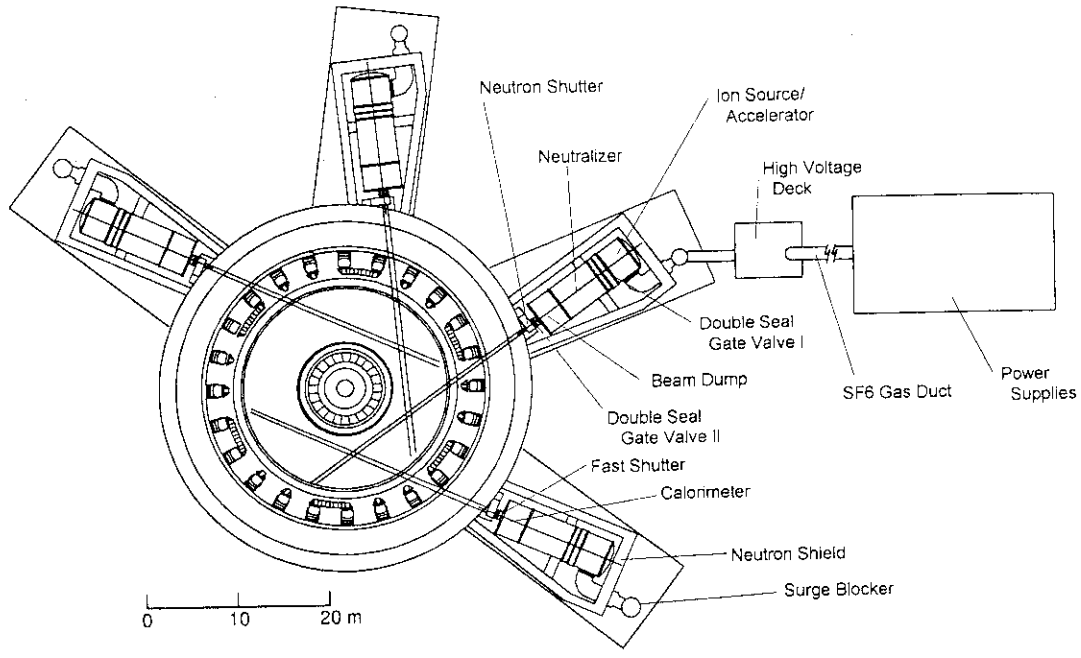

Fig. V.4.2-3. A plan view of ITER NBI installed in ITER torus hall.

neutronics study. 3) Magnetic shielding: The ITER stray magnetic field at the NB location is estimated to be a few kilo-gauss, while a permissible field in the beamline is below 1 gauss to prevent ion beam deflection. A three-layered passive type shield structure which can suppress the stray field below the permissible level was designed and is being optimized.

References

[4.2-1] Inoue T., Hanada M., Maeno S. et al., JAERI-Tech. 94-007 (1994).
[4.2-2] Okumura K., Hanada M., Inoue T. et al., 15th Symp. on Fusion Eng., Hyannis, Oct. 11 - 15 (1993).
[4.2-3] Miyamoto K., Hanada M., Inoue T. et al., 18th Symp. on Fusion Tech., Karlsruhe, Aug. 22 - 26 (1994).
[4.2-4] Okumura K., Hanada M., Inoue T. et al., JAERI-Tech. 95-018 (1995).

4.3 Application of high current positive ion beam technology

4.3.1 Super low energy ion source

In FY 1994, a super low energy ion source was utilized in irradiation tests of CFC materials to be used as plasma facing components, like first wall. The source can produce ampere class hydrogen positive ion beams of a low energy (100 ~ 300 eV) range. Such a high current, low energy ion beam is produced from the source uniquely designed as follows: 1) A strong electric field is formed between the grids with a small gap of 0.7 mm; 2) The ions are extracted through a large slit opening formed between a hundred of tungsten wires (0.5 mm in diameter) lined up on the grid surface with 0.5 mm interval in between. A new grid was developed instead of the wire arranged grid to simplify the structure. The slit openings are formed on the molybdenum film with a chemical etching process. In the end of the slit structure, spring mechanisms are also formed to secure the thermal expansion. Then it became possible to manufacture the grid of such a fine structure easily at a costthat was much less.

5. Rf heating technology

5.1 Introduction

Radio-frequency (rf) wave is a key tool for heating and current drive of the tokamak fusion reactor. Development of a high efficiency rf source for Electron Cyclotron Heating (ECH) and Lower Hybrid Current Drive (LHCD), and a high performance launching system for LHCD and Ion Cyclotron Heating (ICH) is the main effort of JAERI rf research. The greatest achievement in FY 1994 was the success in efficiency enhancement of up to 50 % at a frequency of 110 GHz high power gyrotron with a beam energy recovery system.

5.2 Developments of high power gyrotron and ECH components

The gyrotron is the key component of the ECH system. Under the task agreement of ITER/EDA, the gyrotron development is being continued at JAERI. The depressed collector was applied to the gyrotron for efficiency enhancement with beam energy recovery. The design and fabrication was completed in 1993 and an experiment to recover energy recovery was carried out in 1994. A view of this can be seen in Fig. V.5.2-1. The oscillation mode is the $TE_{22,2}$ whispering gallery mode. The power is converted to a Gaussian like beam mode and output quasi-optically through a sapphire window. The power supply system is composed of a main power supply and a beam accelerating one, the voltages being V_c and V_a, respectively. By the application of the positive potential to the body section, the electron retarding potential V_r ($=V_a-V_c$) arises between the body and the collector. The spent beam (the beam after the interaction of oscillation) is decelerated by the potential of V_r and its kinetic energy is recovered by the power supply system electrostatically, causing the efficiency enhancement. The total efficiency is expressed by $\eta_{tot} = P_{out}/(V_a I_c) = \eta_{out} (V_a/V_c)$, i.e., (V_a/V_c) is the efficiency enhancement factor. In Fig. V.5.2-2, V_r dependence of the output power, oscillation efficiency, total efficiency and body current are shown.

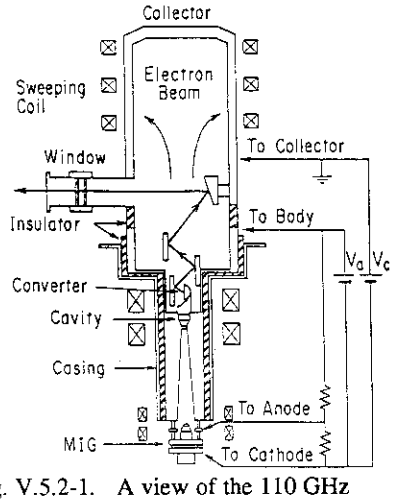

Fig. V.5.2-1. A view of the 110 GHz gyrotron with a depressed collector system.

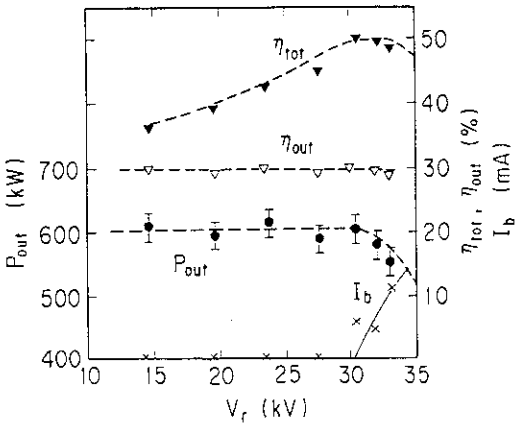

Fig. V.5.2-2. Electron retarding potential (V_r) vs output power (P_{out}), output and total efficiencies (η_{out}, η_{tot}) and body current (I_b).

Here, beam voltage is ~77 kV, the beam current is 26.5 A and the pulse duration is 50 msec. P_{out} maintains a constant value (~610 kW) up to V_r=30 kV, and the corresponding efficiencies are η_{out}=30 % and η_{tot}=50 %. Above V_r=30 kV, P_{out} decreases and the leakage current to the body section appears, which indicates the low energy component of the spent beam is trapped inside the gyrotron. The long pulse operation was performed at P_{out}=350 kW, V_r=34.3 kV, I_c=17 A, then the total efficiency becomes 48 %. Figure V.5.2-3 is a dependence of output energy on pulse duration. The output energy increases linearly with the pulse duration, i.e., a very stable oscillation can be attained. In conclusion, it could be shown that the depressed collector is quite suitable for high power and long pulse gyrotron, which bring about a large efficiency enhancement of the gyrotron and ECH system. Following the success of the depressed collector gyrotron, the development of a 170 GHz gyrotron, with ITER relevant frequency, was started. The experiment of the 170 GHz gyrotron will start in 1995.

High power experiments of a cryogenic cooled window were carried out. The sapphire disk is cooled by a refrigerator to 13 K. With the rf injection of 400 kW for 1 sec at 110 GHz, no arcing could be observed on the sapphire.

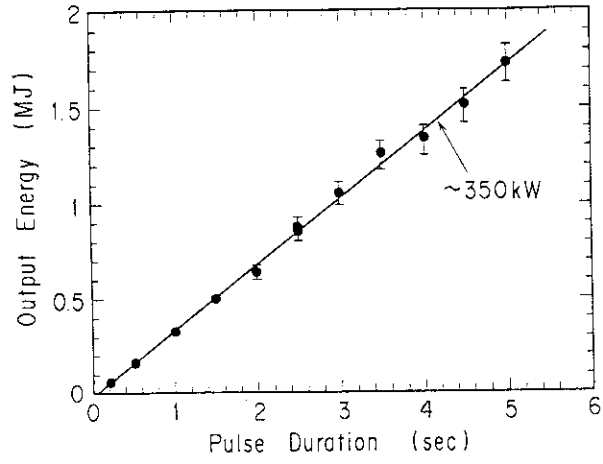

Fig. V.5.2-3. Output energy vs pulse duration.

5.3 Development of ICRF and LHRF launchers [5.3-1]

ICRF antenna is being developed as an attractive additional heating method for a fusion reactor. The Faraday shield is the most critical part of ICRF antenna due to significant heat load in the ITER design. The back Faraday shield concept has been proposed for avoiding heat load and improving antenna coupling [1]. The first test of the back Faraday shield installed in an FWCD antenna for JFT-2M was carried out in 1995. Good coupling results of this antenna could be obtained in divertor plasma. Next, a new antenna optimized for electron heating was developed to confirm the fast wave excitation by the antenna with the back Faraday shield. Fast wave direct electron heating experiments using this antenna are planned for 1995.

To establish design base for an LHRF launcher for a steady-state tokamak machine, the cooperative activities between JAERI and CEA-Cadarache were initiated to obtain the outgassing database from an LH antenna module under high rf power and long pulse operation. JAERI poloidal power divider, the 3x6 multijunction module and CEA mode converter were tested at the

lower hybrid test bed of CEA-Cadarache which included a frequency of 3.7 GHz with a CW 500 kW klystron. JAERI components were made from dispersion strengthened copper which had high-mechanical properties even at high temperatures up to 500°C and under neutron irradiation and high-thermal conductivity for heat removal. All components showed good power capability such as 300 kW-5400 sec and 420 kW-100 sec with and without water cooling, respectively. These power capabilities show that all components are stable during a steady-state operation. It was found that a low outgassing flux of ~ 10^{-6} Pa m^3 / sec at 250°C could be obtained, which shows that a large pumping system is not required to evacuate the pressure in the LH antenna for a steady-state tokamak machine.

Reference

[5.3-1] M. Saigusa et al., JAERI-Conf 94-001, 49 (1994).

5.4 Millimeter wave free electron laser [5.4-1]

To get a better understanding of the effects of beam space charge on FEL performance, extensive simulation data for 60% of the real experiments carried out at our laboratory during the last three years have been compiled, and the behaviors of particle orbits in the phase space relative to the rf field were studied.

Although an ordinary Hamiltonian analysis cannot rigorously be applied to the Raman FEL due to its dissipative character, it was found that the orbits in the phase space became chaotic as the beam intensity increased. It is of interest that exponential rf growth still occurs even when beam orbit behavior becomes chaotic.

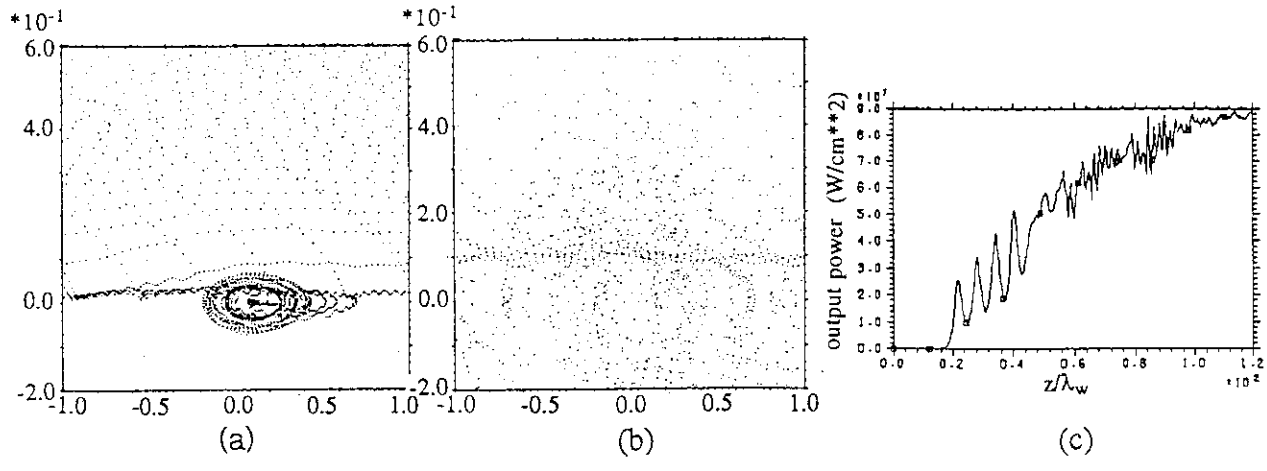

Fig. V.5.4-1. (a),(b) Orbits in ψ-$d\psi/dt$ plane with tapering. Abscissa is π to $-\pi$. Ordinate is $d\psi/dz/k_w$. Beam intensity I = (a) 10A, (b) 1000A. (c) Evolution of rf power along the wiggler with tapering, where λ_w is the wiggler period.

Reference

[5.4-1] Kawasaki S., Ishizuka H., Shiho M., et al., Nucl. Instr. Meth. in Phys. Res. A358 (1995) 114-117.

6. Tritium technology

Studies on tritium technology were performed continuously in the Tritium Process Laboratory (TPL) and some new activities were initiated. Regarding the study of tritium processing technology, the joint operation at Tritium Systems Test Assembly (TSTA) in LANL under US-Japan collaboration was completed on June 10. This collaboration entered into a new phase. The major activities this year were demonstration and testing of non-steady operation of fusion fuel processing system and breeding blanket interface. Also, the decommissioning of JAERI Fuel Cleanup Unit (JFCU) has been carried out. In the study of tritium safety technology, the experimental work using graphite was performed in concern with a study on tritium-material interaction. Safe operation of the TPL tritium facility, itself, is on-sight valuable experience that proves the ability of the safe handling of tritium. The annual environmental dose from TPL was less than 5×10^{9}Bq/year that is an extremely low release to the environment. Then, about 20 g of tritium were transported from Canada using the new tritium transport package developed in TPL.

6.1 Research activity under US-Japan collaboration

The non-steady operation was tested with the TSTA loop to satisfy realistic fusion devices such as ITER. Examples of non-steady operations tested in recent experiments are the initiation of simulated torus exhaust processing, changing isotope separation system (ISS) operations from stand-alone (direct recycle) operations to integration with fuel purification, changing JFCU operations from stand-alone to integration with ISS, and off-loading of purified tritium to container. Fuel processing for a simulated non-steady tokamak in an integrated closed loop was carried out successfully. In the experiment, JFCU showed various configurations suitable for ITER-like operations, and processed tritiated impurities without generating water while obtaining an overall decontamination factor of 7×10^{4}. This application of JFCU leads the development of improved FCU continued in TPL.

A Breeding Blanket Interface (BBI) study was performed to evaluate the recovery of tritium from a purge gas stream simulating tritium recovery from a ceramic breeding blanket. FCU has been used for the practical-scale tests of cryogenic molecular sieve beds (CMSB) for separating low-concentration hydrogen isotopes from helium. JFCU was used for tritium recovery from regenerated gas of CMSB (He and hydrogen isotopes) in FCU. HT gas recovered was sent to ISS to separate the tritium from hydrogen. This series of tests demonstrated that the components of the TSTA processing loop (FCU, JFCU and ISS) provide an excellent test bed for showing the interfacing of a breeding blanket tritium recovery stream with the plasma exhaust gas processing loop.

Since June 10, the collaboration entered into a new phase to emphasize the tritium safety technology. Major activity at TSTA is the decommissioning of JFCU, decontamination studies using materials from JFCU, and Tritium Plasma Experiment (TPE). The decommissioning of JFCU is being carried out in accordance with the schedule.

6.2 Development of tritium processing technology in TPL

The study of FCU that purifies and recovers tritium from a gaseous mixture in fusion fuel processing systems focused on the improvement toward a more flexible and versatile function to much better serve entire fusion fuel system. Also, modification of the original FCU concept for meeting of ITER requirements, minimization of inventory and avoidance of potential hazards related to an oxidizer catalyst was attempted. Some variations and extensions of a FCU system based on the combination of palladium diffuser and a vapor electrolysis cell were studied. A component study was also performed without the use of tritium. Processing of He-CH_4, H_2, H_2O mixtures in a simple closed loop consists of a palladium diffuser, platinum catalyst bed and an electrolysis cell was studied for plasma exhaust processing without handling condensed water. The electrolysis cell made of zirconia ceramic membrane with platinum electrode converted CH_4 to CO_2 and vapor with high efficiency and decomposed H_2O to H_2, simultaneously. This application of the cell eliminates the use of a catalyst and handling of pure oxygen gas. It is suggested that in the design of plasma exhaust processing, versatile use of the system for practical fuel processing needs is possible without sacrificing simplicity, which improves on the entire fuel cycle design.

The most probable candidate of ISS in the fusion fuel cycle is the cryogenic distillation. It is best suited to the needs in the separation system which treats a large amount of hydrogen isotopes in the fusion reactors. Especially, the cryogenic distillation column having a feedback stream can separates an H and T mixture into H and T by a single column. Design data were obtained for this column, and demonstration tests were also carried out. This year, the control method of this column has been studied in detail. It has been shown by simulation studies that the control system of this column gives us a set of successful results for the stability of the system. A new simulation based on a mass transfer model has been carried out to predict the HETP value which is one of the key parameters for the design of the cryogenic distillation columns. The thermal diffusion is an attractive process for the separation system which treats a small amount of hydrogen isotopes. It has been found in experimental studies that the separation factor can remarkably be increased by cooling the column wall with liquid nitrogen.

With respect to BBI development, tritium behavior in the breeding blanket is still not completely clear. A study on the tritium behavior at the surface of ceramic breeder material was started. CMSB is one of the most probable BBI process candidates, and it is expected to be applicable for recovery of tritium from the exhaust gas by graw discharge cleanup (GDC)

operation in the ITER-EDA design. In the design, it is required to assume concentration of hydrogen isotopes (Q_2) and impurity (such as CH_4) as 1% and 0.3%, respectively. This year emphasis was focused on the impurity effect on the recovery of tritium in the helium purge stream. An example of breakthrough curves obtained can be seen in Fig. V.6.2-1. The adsorption isotherms of hydrogen isotopes and impurity mixture were proposed [6.2-1].

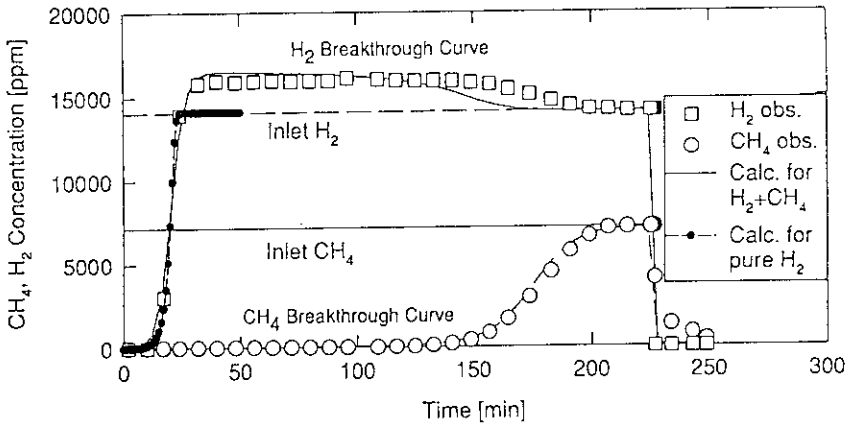

Fig. V.6.2-1. Influence of CH_4 presence H_2 breakthrough.
(RUN29: Total Flow Rate=1SLM, C_{CH4}=7178ppm, C_{H2}=14111ppm).

Reference

[6.2-1] Enoeda M., Kawamura Y. et al., Fusion Technol., 664, 26 (1994).

6.3 Development of tritium safety technology

To enhance the tritium safety technology for public acceptance of the D-T fusion reactor, R&D activities have been focused on (1) a compact tritium removal system, (2) the tritium accounting, (3) the tritium-material interaction and waste handling, and (4) a design of a caisson for studying tritium confinement and behavior in room, etc.

A new tritium removal system using gas separation membranes has been studied to develop a more compact and cost-effective system. To obtain parameters which are directly scalable to the ITER Atmospheric Detritiation System, the basic tritium recovery performances were investigated with a scaled polyimide membrane module loop. The function of H_2 recovery from air was about 97% at 293 K, flow rate ratio of permeated/feed (CUT) = 0.1, and feed & permeated side pressures = 2580 & 80torr. HT recovery function was almost the same as H_2 recovery, even though the total hydrogen concentration was a few ppm in the feed of module. H_2O recovery performance was better than the H_2 recovery. These recovery functions were effectively improved decreasing the pressure ratio of permeated/feed [6.3-1].

To establish the "in-bed" tritium accounting technology to apply to the ITER tritium storage beds, a scaled ZrCo bed was fabricated with a gas flowing calorimetric system. The steady-state temperature rise of He gas stream flowing through a secondary coil line fixed in the ZrCo tritide was measured and correlated with power input by a heater to simulate tritium decay

heat or with actual tritium storage. The target accountability is to measure ± 1g (0.32 W) of tritium for 100 g storage. The results show a good accounting function in which the temperature increases of He stream of 4.7 and 96.8° were measured under power input of 0.32 and 8.0 W, respectively [6.3-2].

To establish a technological basis for real-time process gas monitoring for tritium accountancy and process system control in glove boxes and/or isolated rooms, development of a real-time, *in-situ* and remote analyzing system of hydrogen isotopes and impurities has been started by application of laser Raman spectroscopy. Using hydrogen isotope gases as samples, it has been confirmed that remote analysis of the process gases with a very short measurement time will be possible with the same detection limit as a gas-chromatograph.

For prediction of tritium behavior in plasma facing components, investigations of hydrogen isotope permeation, retention and release in plasma facing and heat sink materials have been carried out. Implantation driven permeation (IDP) behavior of deuterium through pure vanadium (V) and V-5Cr-5Ti was investigated. The experimental conditions were incident ion flux = 3.8×10^{18}~$1.2\times10^{19}D^+/m^2s$, target temperature = 473~673K and incident D^+ion energy = 500~2000eV. The steady-state IDP flux through pure V was 1/100~1/700 of incident flux under these experimental conditions. IDP flux through V-5Cr-5Ti was about 1/10 of that through V.

For the decommissioning and decontamination of plasma facing components, the characteristics of tritium implanted in graphite should be clarified. Measurements of the amount of tritium retained in graphite was carried out [6.3-3]. The graphite sample exposed to D/T plasma in the D/T gas flow was combusted in dry air. Total amount of (D+T) retained in the graphite was obtained from the measurement of tritiated water generated by combustion of the sample. The amount of deuterium retained in graphite was proportional to half power of total incident fluence as shown in Fig. V.6.3-1. This tendency implies that deuterium retained in graphite was related to a sort of diffusion process.

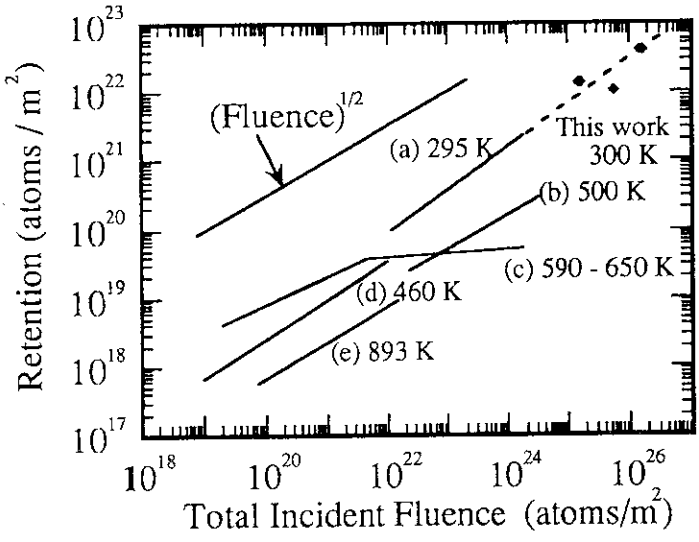

Fig. V. 6.3-1. Hydrogen retention in graphite;
(a) protium and tritium on pyrolytic graphite, Hucks et al.,
(b,c) protium and tritium on pyrolytic graphite, Youle et al.,
(d,e) deuterium on ETP10, Tanabe et al.

The system design of a new caisson (10 m^3) has been proceeded as a test stand for

overall demonstration of tritium confinement and for the study of in-room tritium behavior, etc. The safety analysis was also carried out under the basic experimental conditions, such as 37 TBq (1000 Ci) of tritium introduced in a caisson.

References

[6.3-1] Hayashi T., Yamada M, Suzuki T., et al., Gas separation performance of a hollow-filament type polyimide membrane module for a compact tritium removal system, 5th Topical Meeting on Tritium Technol. in Fis., Fus. and Isotopic Applications, Belgirate, Italy, May, 1995.
To be published in Fus. Technol.
[6.3-2] Hayashi T., Yamada M, Susuki T. et al., Tritium accounting characteristics of "In-Bed" gas flowing calorimetry, ibid.
[6.3-3] Yaita Y., O'hira S. and Okuno K., ibid.

6.4 Operation of tritium safety system in TPL

The safety system at TPL has been in tritium service since 1988 without any off-normal tritium release. The Glove Box Gas Purification System (GPS) has been operated for 7,400 hr. The Effluent Tritium Removal System (ERS) processed about 2.7×10^{12}Bq of tritium this year. Also, the Air Cleanup System (ACS) was operated for cleaning up 16,600m^3 of air during the maintenance work. Especially, bpth two root blowers of GPS were replaced with the electromagnetic suspension bearing type. Therefore, the possibility of oil leakage, which existed in the bearing seal case, for processing was almost eliminated in GPS. Fig. V.6.4-1 shows the monthly environmental tritium record from the stack of TPL this year. Total tritium release was less than 5×10^{9}Bq due to the very safe tritium handling operation at TPL.

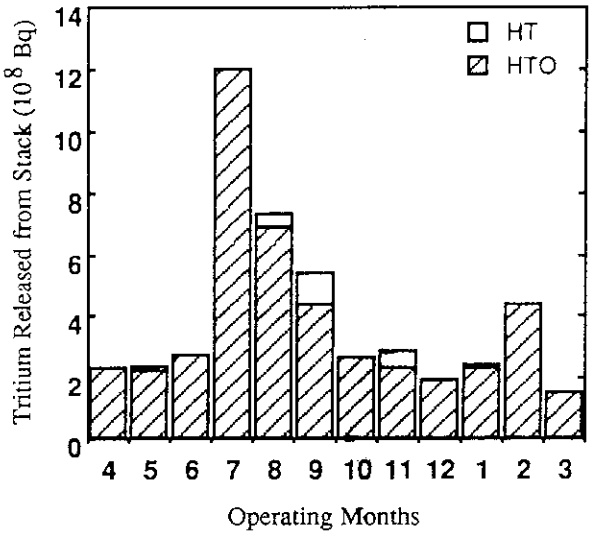

Fig. V.6.4-1. Monthly release of tritium from TPL in FY 1994.

6.5 Tritium transportation using an international transport package

A new tritium transport package (TPL-92Y-450K) has been developed and approvals for actual tritium transportation have been obtained from STA-Japan, Canada, and the U.S. Using this package, about 20 g of tritium was transported from Canada. Tritium gas was loaded into a ZrCo capsule after tritium analysis at AECL Chalk River Lab. in Canada. This capsule was assembled to a transport package with pre-shipment inspections, such as assembling, leak-tightness, radiation/contamination level, etc. Finally, the package was tied down in a special container and transported to TPL.

7. Development of plasma facing components

JAERI has been actively researching and developing plasma facing components (PFCs) for ITER and JT-60. The roles of PFCs such as divertor plates and a first wall are to remove the thermal loads from a fusion plasma and to protect in-vessel components against the high thermal loads. PFCs are subjected to a high heat flux and a particle flux. In particular, the divertor plates are considered to be subjected to a severe heat flux of around 5 MW/m^2 in the EDA phase of ITER.

7.1 R&Ds on divertor components for ITER

Divertor plates of ITER are required to satisfy with the following design specifications:

1) The surface materials of the divertor plate should be covered with low-Z (low atomic number) materials to minimize any impurity from getting into the plasma;
2) The divertor plates are required to endure a steady-state heat flux of 5 MW/m^2;
3) The divertor plates are required to endure a transient heat flux of 20 MW/m^2 at a duration of 10 sec during the power excursion event;
4) The thickness of the armor tiles should be more than 10 mm to sustain the sufficient lifetime against erosion caused by the plasma disruptions and sputtering; and
5) The maximum surface temperature of the armor tiles should be kept at around 1000°C.

To remove the steady-state heat flux and the transient heat flux described above, the heat removal performance of the divertor plates have to be kept as good as possible. Therefore, the carbon based materials, such as CFC (carbon fiber reinforced carbon composite) materials, has been selected and tested as armor tiles for the divertor plates from the viewpoint of the high thermal conductivity and low atomic number. In addition, the bonding technique between the armor tiles and the metal substrate should be thoroughly investigated to keep a good thermal performance of the divertor components. JAERI has tested the divertor structure which has a metallurgically bonded interface. This year, we have manufactured and tested 1-m long saddle-type divertor module with a fully rigid support structure. Figure 7.1-1 shows the schematic of the divertor module. This divertor module has saddle-shaped cross-section: the number of the armor tiles are 36 in all. The armor tiles are made of a unidirectional CFC material which has thermal conductivity of around 600 W/m/K at room temperature. The cooling tube is known as swirl tube: it is made of OFHC copper. The heat sink as a rigid support structure is also made of OFHC copper. In the experiment, the divertor module was cyclically heated by an electron beam at a surface heat flux of 25 MW/m^2: the heating duration was 10 sec. The flow velocity of the coolant was 15 m/s (axial flow velocity) at a pressure of 1.25 MPa. After 1,270 thermal cycles, coolant leakage occurred in the cooling tube between the armor blocks. As a result of a SEM observation for the broken part of the cooling tube, we found the crack spread due to fatigue of the material caused by the cyclic thermal stress and the stress concentration at the cooling tube (See Fig. 7.1-

2). However, the thermal performance of the divertor module was sustained through the thermal cycles: the maximum surface temperature of the armor tiles was around 1,700 °C through the experiment. Stronger copper based material such as DS-Cu (Dispersion strengthened copper) or Cu-Cr-Zr, should be selected as a cooling tube material.

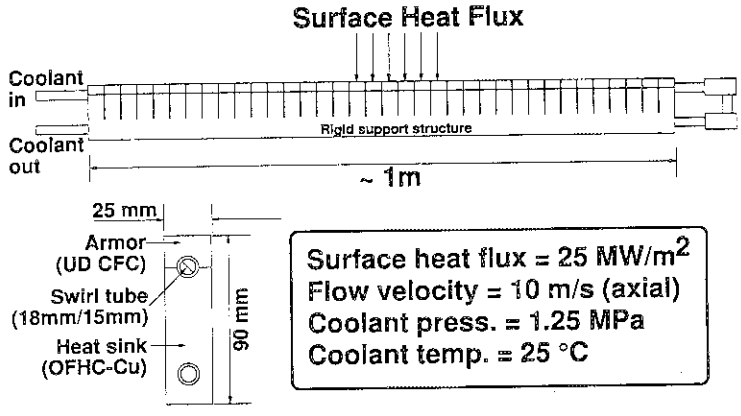

Fig. 7.1-1. Schematic of the module and test conditions.

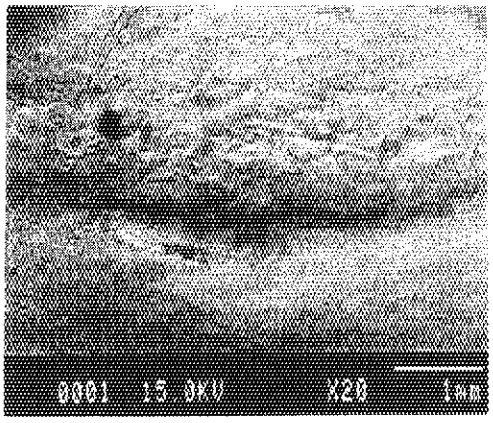

Fig. 7.1-2. Photograph of the broken part of the cooling tube.

7.2 R&D on heat removal technology [7.2-1]

Plasma facing components for fusion devices, in particular, the divertor plates, are subjected to high heat loads with heating on one side. From the manufacturing viewpoint, the simple process gives less expensive and more reliability. Therefore, we have developed a miled tube, namely, screw tube, and critical heat flux experiments have been carried out to verify its performance. As a result, the very high critical heat flux of 35 MW/m^2, which is the same level with the swirl tube, could be obtained with the new screw tube.

Reference

[7.2-1] Araki M., Sato K., Suzuki S., et al., "Critical heat flux experiment on the screw tube under one-sided heating conditions", Fusion Technology (to be published).

7.3 Erosion of plasma facing materials by plasma particle and heat [7.3-1], [7.3-2]

Since the surface of the PFCs is exposed to plasma, the materials of PFCs are eroded by particle flux during the normal operation and by high heat flux during the off-normal operation such as plasma disruptions. Therefore, it is necessary to evaluate the erosion of the plasma facing materials and to develop new materials, that can stand these loads from a fusion plasma, for development of long life-time PFcs.

7.3.1 Sputtering erosion

Sputtering performance tests of CFCs, which were candidate materials for the ITER divertor plates, have been performed at a particle flux of 10^{21} ion/m^2/s and at an energy of 50 - 100 eV. As a result, the preferential sputtering of the matrix parts to the fibers was found on some the CFCs. For the reduction of the sputtering yields of the matrix parts, B_4C doped CFCs, which have a high thermal conductivity of ~160 W/m/k, have been newly developed.

7.3.2 Disruption erosion

High heat flux experiments of the newly developed B_4C doped CFCs have been carried out under heat flux of 800~2000 MW/m^2 at durations of 2~5 ms at JEBIS. As a result, the erosion of B_4C doped CFCs was almost the same with the non-doped CFC uo to 5% B_4C contents(see Fig. 7.3-1). Thermal shock tests of CVD-W, which has very fine grain sise, have been also performed under a heat flux of 1000~2000 MW/m^2 and for a duration of 2 ms at JEBIS. The temperature of the samples during the heating ranged from R.T.~1000°C. As a result, the erosion of CVD-W at 1000°C was about three times smaller than that of monocrystal W at 1000°C.

References

[7.3-1] Nakamura K., Akiba M., Suzuki S., et al., "Erosion of CFC and W at high temperature under high heat loads", J. of Nucl. Mat.,212-215, (1994) 1201-1205

[7.3-2] Nakamura K., Nagase A., Dairaku M., et al., "Sputtering yields of carbon based materials under high particle flux with low energy", J. of Nucl. Mat. (to be published)

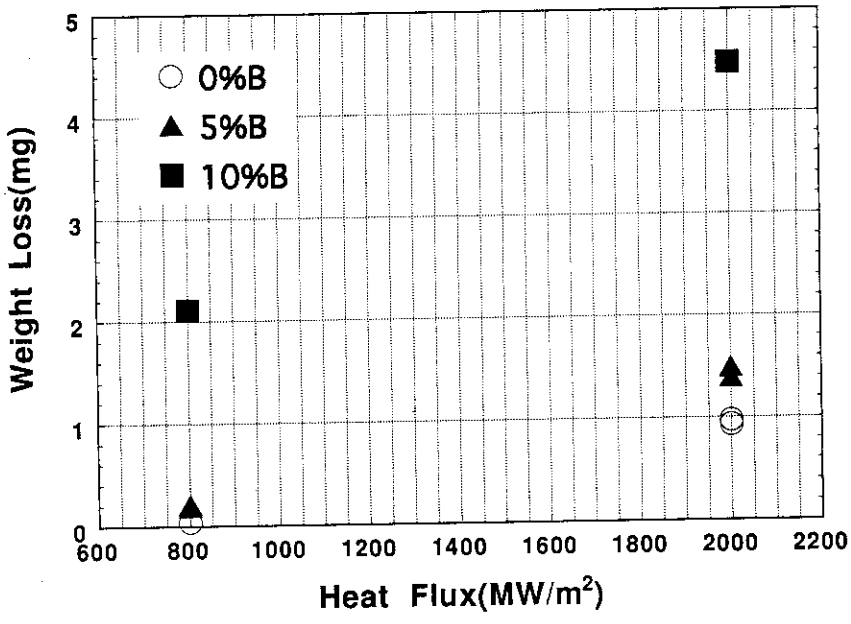

Fig. 7.3-1. Weight loss of B_4C doped CFCs under high heat flux.

8. Reactor structure development

8.1 Introduction

The ITER reactor core structure is basically composed of a vacuum vessel, shielding/breeding blankets, divertors and a cryostat for the superconducting magnet system. These components are massive and large, and should be able to withstand severe loads of neutron irradiation, electromagnetic forces and heat loads. Also, each component must be compatible with full-remote maintenance/exchange. Therefore, the major issues needing development here are the manufacturing technology for large components and remote assembling/disassembling technology. In this fiscal year, R&D efforts have been focused on the development of a double-walled vacuum vessel, fail-safe first wall, FGM insulation joints, rail transporter for in-vessel maintenance, bore tools for YAG laser and radiation hard components.

8.2 Reactor structure development

8.2.1 Vacuum vessel double-walled section model fabrication and testing

The ITER vacuum vessel is a large double-wall structure and divided into 24 sectors for the in-progress design of ITER EDA. The space between the outer and inner skin is filled with SS balls to provide a neutron shield for the TF coil. The major functions of the vacuum vessel are: 1) to provide a high quality vacuum for the plasma; 2) to give one-turn resistance with a blanket structure; 3) to allow for mechanical support of dead weight and EM loads for the in-vessel components; 4) neutron and biological shielding; and 5) to provide a first safety barrier for tritium confinement. Due to its large size, tight manufacturing tolerances, and large thermal and mechanical loads, fabrication and testing of the prototype vacuum vessel are essential to demonstrate its feasibility. This year, fabrication and testing of a full-scaled section model of the double-walled vacuum vessel were carried out. As a result, the fabrication procedures including major technical information on forming and welding have been verified due to the double-walled section model fabrication. In addition, the verification of the double-walled structure has been confirmed by non-destructive inspections, helium leak tests and proof pressure tests.

8.2.2 Double-walled structure for fail-safe

The first wall facing the plasma has the possibility of unexpected damages due to high surface heat flux and particle loads during normal and non-normal operations. Also, it is subjected to large electromagnetic loads induced by plasma disruptions. As a result of these high potential risks, the first wall needs to be replaced in case of failure, while a blanket module is classified into a semi-permanent component which is expected to survive anticipated load conditions through its lifetime. A concept of the first wall panel mechanically separated and separately cooled from the massive blanket module has been developed so as to ease the replacement. The replaceable FW

panel has also advantages in minimizing the amount of radwaste, to reduce thermal stresses of the massive blanket module and to enable higher temperature operation of the FW than the blanket module. In addition, a reliable double-walled quilting structure can be employed for the FW panels with fail-safe features. This year, fabrication of the quilting-type double-walled panel as shown in Fig.V.8.2-1 and its basic thermal and mechanical characteristics could be achieved. As a result, the basic feasibility of this double-walled panel was able to be demonstrated.

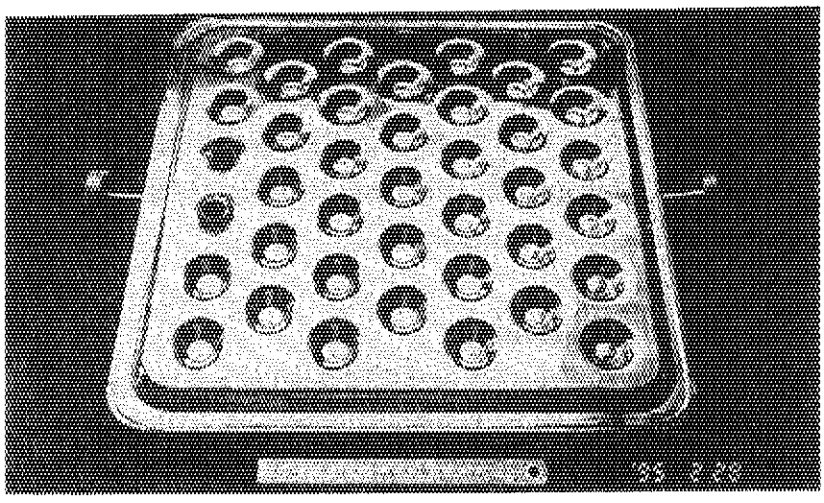

Fig.V.8.2-1. Fabrication of the quilting-type double-walled panel.

8.2.3 Functionally gradient material for electric insulation

In ITER, coupling of eddy currents induced by plasma disruption and a magnetic field causes severe magnetic forces to have an effect on the structural components or cooling pipes. To reduce these magnetic forces, it is essential to provide high resistance for the components and cooling pipes. However, conventional methods for insulation breakage such as mechanical joints and brazing of ceramic/metal interfaces are less reliable for a high vacuum/pressure environment required in a fusion reactor. The concept of insulation joints based on Functionally Gradient Material (FGM) has been developed since FGM is a continuously graded ceramic/metal compound structure and provides high reliability as there is no mechanical joints and brazed interfaces. This year, a FGM joint, which is 74 mm in outer diameter with a thickness of 8 mm and 100 mm in length, has been successfully fabricated by sintering with pure ceramics at the center, type 430 stainless steel at both ends, and graded region between them as shown in Fig.V.8.2-2.

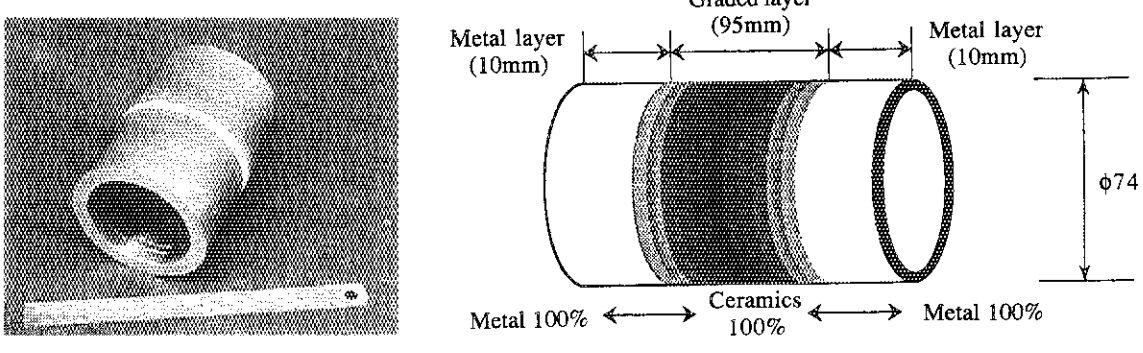

Fig.V.8.2-2. FGM sample of type 430 stainless steel.

8.3 Remote maintenance development

8.3.1 Full-scale in-vessel manipulator and rail deploying/storing system

The rail-mounted vehicle maintenance system was selected for the scheduled maintenance components such as plasma facing components. This system, the rail is extended into the vacuum vessel sequentially and supported by four arms from the respective 90-degree horizontal ports so as to provide stable and reliable operation.[8.3-1] This year, a prototypical rail deploying/storing system has been fabricated and the performance tests such as payload capacity, position control and rail deployment/storage have been conducted as shown Fig.V.8.3-1. As a result, it could be confirmed that the rail transporter with joints for locking/unlocking can be successfully deployed using a teaching playback control. In addition, the mechanical stiffness of the rail and joints satisfied the handling capability of more than 1 ton as the payload.

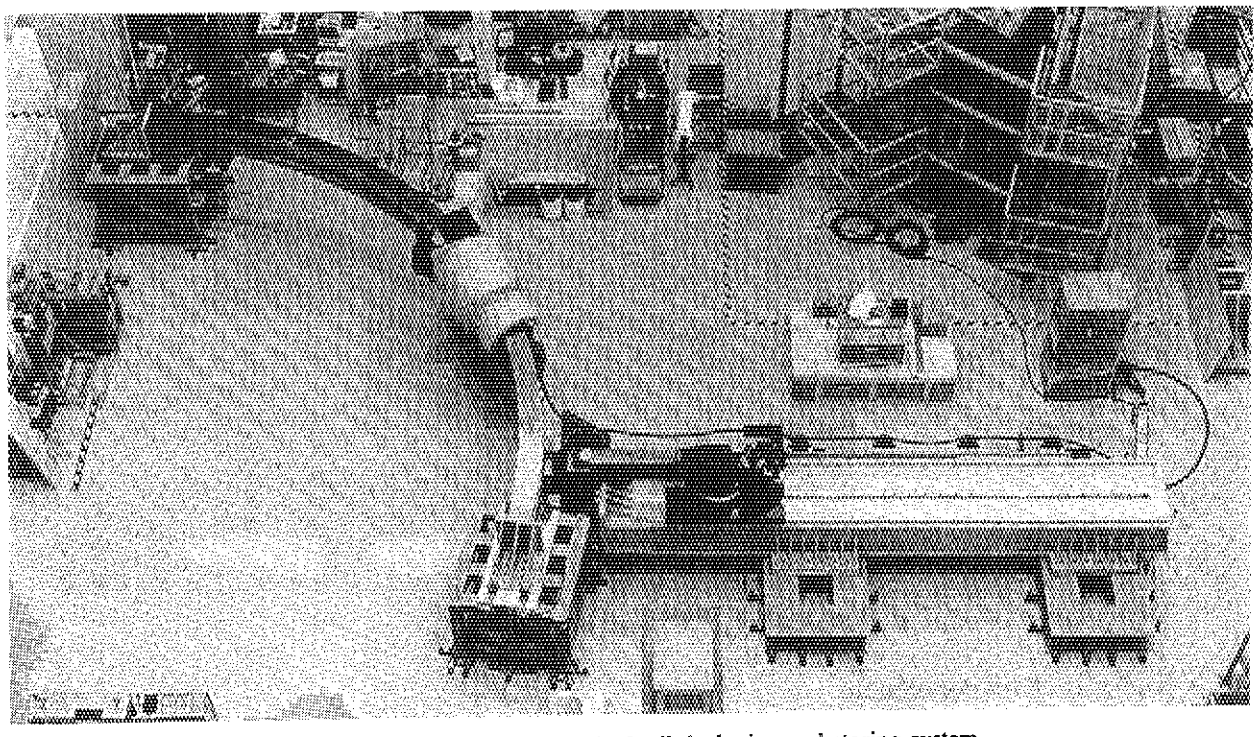

Fig.V.8.3-1. Full-scaled model of rail deploying and storing system.

8.3.2 YAG laser bore tooling

In the design of the fusion experimental reactor, the blanket/first wall module is categorized into the scheduled maintenance which includes a complete change from shielding to breeding. In the current modular type blanket, a branch pipe has to be cut and welded when a module is replaced. Since the branch pipe is connected to the cooling manifold which is routed onto the surface of the backwall up to the upper vertical port with several bends, the bore tools should be flexible to move inside the manifold and reach the branch pipe for welding and cutting. The YAG laser system based on laser beam transmission using a flexible optical fiber inside the pipe has been selected since the pipe welding/cutting by the internal access can be available even for the

pipes with bending and branching sections. This year, a YAG laser type processing head has been successfully fabricated as shown in Fig.V.8.3-2 and the applicability to the blanket branch pipe welding/cutting was able to be demonstrated. In particular, this system can be moved inside a 100-A pipe with a minimum curvature of 400 mm and the welding/cutting nozzle with telescopic mechanism can be extended into a branch pipe with a diameter of 50 mm for welding/cutting. In addition, this system is designed to have 5 axial freedom so as to position the welding/cutting nozzle within the required accuracy for welding/cutting. The centering mechanisms and position sensors are also used for positioning and fixing of the processing head. In addition to these tool developments, welding/cutting/rewelding experiments using a YAG laser have been performed to clarify the optimum welding and cutting conditions including the effects of gaps, process speed, laser power and assist gas on the weldability and reweldability.

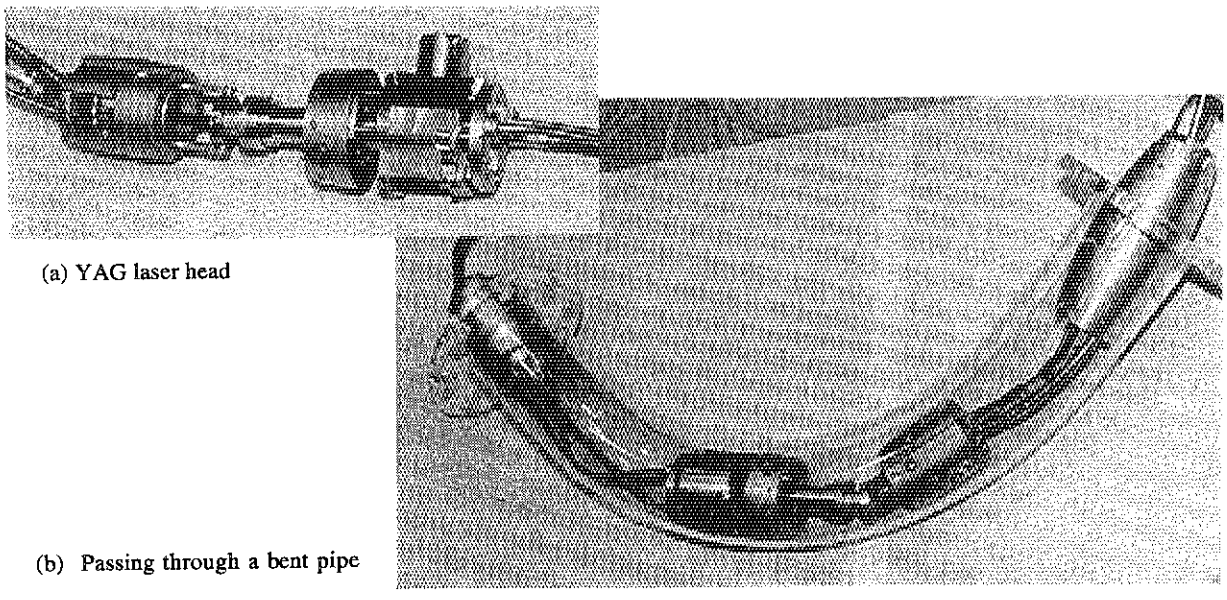

(a) YAG laser head

(b) Passing through a bent pipe

Fig.V.8.3-2. YAG laser bore tooling.

8.3.3 Radiation hard component

In fusion experimental reactors such as ITER, remote handling equipment has to be able to withstand radiation conditions of more than 10^6 R/h. For this purpose, irradiation tests on a number of critical components for the remote handling system have been extensively conducted under similar radiation conditions. As a result, radiation-hard-component development has been progressed and it has been demonstrated that critical elements such as motors, lubricants, optical lens and mirrors, and force sensors can be available for more than 10^9 R.

Reference

[8.3-1] Kondoh M., Shibanuma K., Kakudate S. et al, Design and Development of Remote Maintenance System for ITER-CDA In-vessel Components, JAERI-M 93-066 (1993).

9. Blanket technology

9.1 Introduction

The blanket is a component which protects vacuum vessel and the super conducting magnet from radiation, generates tritium as the fuel gas for thermonuclear reaction, and changes the kinetic energy of neutrons to thermal energy, and is one of the key components for energy-producing Fusion reactors.

This year, R&D efforts have been focused on the development of an ITER shielding blanket structure and an out-of-reactor testing of ITER breeding blanket. In addition, elementary R&D for a DEMO blanket has been started. Design work has been developed regerding the ITER shielding blanket and test program development.

9.2 Development of a shielding blanket

9.2.1 Fabrication of an HIPped first wall structure [9.2-1]

The first wall design of the ITER shield blanket is composed of Cu-alloy (typically, dispersion strengthened copper alloy, DSCu) and austenitic stainless steel (316SS) embedding 316SS rectangular tubes. The solid Hot Isostatic Pressing (HIP) bonding method has been proposed for first wall fabrication. Fabrication of the HIPped first wall has been investigated through the fabrication of test specimens and partial mockups, and preliminary analyses have been carried out for thermo-mechanical tests with mockups planned for next year.

Through the trial fabrication of the test specimens, it was found that a bonding temperature of 1050°C was optimal for simultaneous HIP bonding of DSCu/316SS and 316SS/316SS. In addition, insertion of a 316SS liner between the rectangular tubes and the DSCu plate were found to be effective in preventing DSCu from intruding into the gaps between the rectangular tubes, which might cause crack initiation.

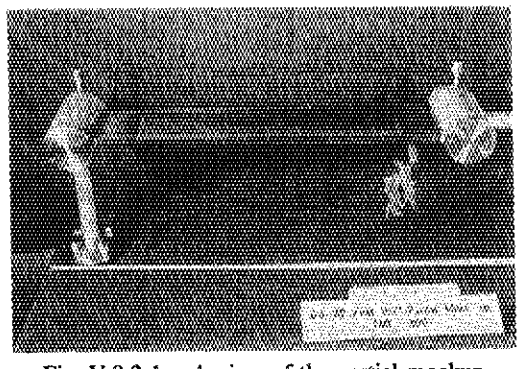

Fig. V.9.2-1. A view of the partial mockup of HIPped first wall.

Based on the above results, two partial mockups of the HIPped first wall structure were fabricated; 600-mm-long with 12 cooling channels (Fig. V.9.2-1) and 200-mm-long with eight cooling channels.

Through the fabrication of these partial mockups, practical fabrication data could be obtained, and feasibility of the fabrication technology was successfully demonstrated. The fabricated partial mockups are to be thermo-mechanically tested at a particle beam irradiation facility to examine their potential performance, and preliminary thermal with thermo-mechanical analyses being carried out.

9.2.2 Mechanical properties of HIP bonded materials [9.2-2]

To obtain mechanical and metallurgical properties for joints made by the above HIP process, mechanical tests were conducted using test specimens of 316SS-DSCu made by the HIP process under the conditions of 1050 °C, 150 MPa and 2 hr.

A view of the tensile test specimen can be seem in Fig. V.9.2-2. Tensile and fatigue tests showed final fracture was observed in the base metal of DSCu with a few exceptions. Fatigue data is shown in Fig. V.9.2-3. Tensile and fatigue strengths were nearly equal to those of the base metal of DSCu, though total elongation was very low compared with that of DSCu at 400°C. The Charpy impact values were 30 - 60% of those of the base metal of DSCu. Also, it can be concluded that the HIP bonded joints of DSCu and 316SS also showed a similar tendency with a few exceptions.

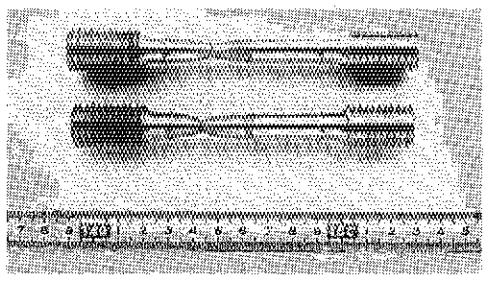

Fig. V.9.2-2. A view of a test specimen of HIP bonded 316SS-DSCu after a tensile test.

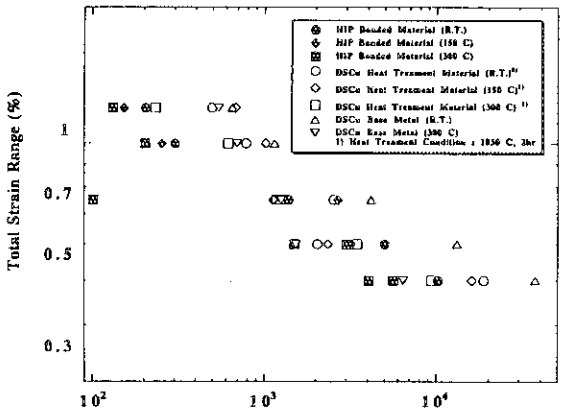

Fig. V.9.2-3. Fatigue data of HIP bonded 316SS-DSCu.

References

[9.2-1] Sato S., Takatsu H., Hashimoto T., et al. Fabrication of HIPped First Wall Structure for Fusion Experimental Reactor and Preliminary Analyses for Its Thermo-mechanical Test, to appear in 16th SOFE, Champaign (1995).

[9.2-2] Sato S., Takatsu H., Hashimoto T., et al. Mechanical Properties of HIP Bonded Materials for Fusion Experimental Reactor Blanket, to appear in 7th ICFRM, Obninsk (1995).

9.3 Out-of-reactor test of breeding blanket

9.3.1 Hydraulic test of first wall cooling channel

A hydraulic test of the first wall cooling channels with a rectangular cross-section has been started. Several tens of toroidal cooling channels are embedded in the first wall, and an evaluation of flow characteristics through parallel channels is a main issue from the viewpoint of thermo-hydraulic design of the blanket. Flow characteristics of one cooling channel was evaluated as a preliminary test.

The test stand is composed of inlet/outlet main manifolds, inlet/outlet headers, one cooling channel with rectangular cross-section, connection tubes between the manifold and the header. Pressure drops for straight, bending and expanding/reducing parts were measured. As a result of this test, contributions of these pressure drops to total pressure drop were approximately 30% for the straight part, 10 % for the bending part and 60% for the expanding/reducing parts. The

pressure drop for the straight part agreed well with the Blasius equation within an error of 20%. On the other hand, the pressure drop at inlet/outlet region of cooling channel from/to the header showed was five times larger than that calculated based on the ideal streamline, where the streamline is significantly influenced by complicated expanding/reducing geometry.

9.3.2 Thermo-hydraulic test of small-scaled pebble-packed layered blanket module

A small-scale test mockup was fabricated to conduct the thermo-hydraulic test of pebble-packed layered breeding blanket. An over all view of this test mockup is shown in Fig. V.9.3-1. This test mockup consists of the cylindrical vessel, the electrical heater simulating the nuclear heating installed at the center of the vessel, the inner vessel packing the breeding pebble of Li_2O and the outer vessel packing the multiplying pebble of Be installed surrounding the electrical heater. The preliminary test has been started by using the blanket loop test facility consisting of water and helium gas loops.

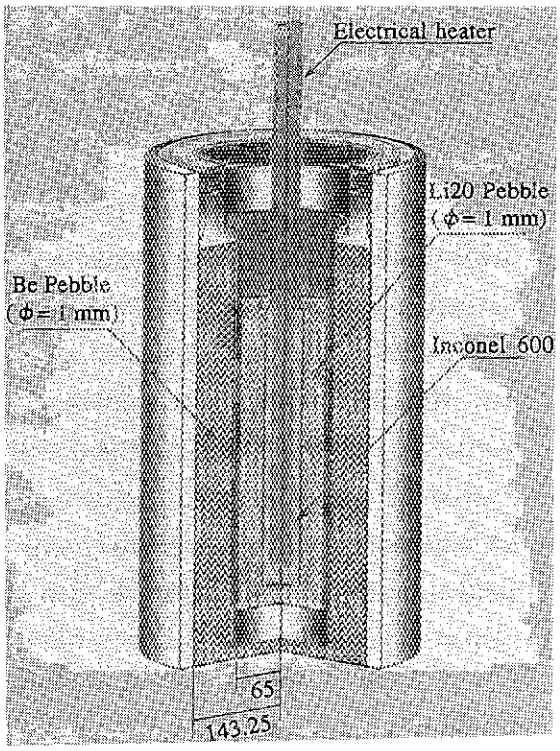

Fig. V.9.3-1. The birds-eye view of small-scaled pebble layered blanket module.

9.4 Development of DEMO blanket [9.4-1]

Expansion of the bonding of F82H, a reduced activation ferritic steel developed by JAERI for the DEMO blanket, has been tried to examine the fabricability of this type of ferritic steel to the DEMO blanket structure. To examine the characteristics and soundness of the joints, metallurgical examination and mechanical tests have been conducted. Through this study, it was shown that sufficient bonding was obtained under the conditions of 950 - 1,050°C, 5 MPa and the holding time of 1 hr, though Charpy impact values were approximately 60% of the base metal. Normalization and tempering of the diffusion bonded joints are necessary to obtain the mechanical properties of the joint similar to that of the base metal.

References

[9.4-1] Kurasawa T., Takatsu H., Sato S., et al. Diffusion Bonding of Reduced Activation Ferritic Steel F82H for DEMO Blanket Application, to appear in 7th ICFRM, Obninsk (1995).

9.5 ITER blanket design

9.5.1 Shielding blanket design [9.5-1] [9.5-2] [9.5-3] [9.5-4]

The design of ITER shielding blanket has been developed taking into account the integrated features of thermo-mechanical performance, fabricability, maintainability, initial assembly and so

forth. A modular box structure with a separate back plate is proposed, and the support legs of the module are welded to the back plate to maintain enough mechanical integrity against the large electromagnetic loads during a disruption. The first wall proposed has coolant channels embedded within its wall, which is to be fabricated by HIP bonding. Electromagnetic and structural analyses show that there is a possible structural solution without the toroidal electrical connection of the first wall. Thermo-mechanical analyses indicate that thermal stress and stress due to coolant pressure are well within the design limits. The design study of ITER "convertible" blanket was conducted, and it was found that the "convertible" concept has a number of technically critical problems.

9.5.2 Shielding design

Shielding analyses for radiation streaming through 20 mm width gap between adjacent blanket modules have been conducted using 2-D SN and 3-D Monte-Carlo codes so as to evaluate nuclear responses of the blanket, the vacuum vessel and the toroidal field coil. With the reactor configuration of ITER designed at present, nuclear responses of the vacuum vessel and the toroidal field coil satisfy the shielding design criteria, while helium production rates of the module support leg affixed to the back plate and the branch pipe connected from the module to manifold exceed the criteria in case of neutron fluence of 1 - 3 MWa/m^2, i.e., at the end of EPP. Therefore, an additional shielding structure is required in EPP. In addition, a shielding analysis for a toroidal field coil around ICRF port has been also carried out using the 3-D Monte-Carlo code. Nuclear responses of the toroidal field coil fully satisfy the shielding design criteria.

9.5.3 Test program development and design of test module [9.5-5] [9.5-6]

Test programs for water-cooled and helium-cooled DEMO blankets have been developed. Neutronics, scoping, performance, reliability enhancement and segment demonstration tests have been proposed to be performed in a series. Comprehensive tests of the ITER driver blanket during BPP are also proposed, typical test modules for water-cooled and helium-cooled ceramic breeder blankets have been designed including their installation into the ITER test port. The composition and space requirements of their cooling and tritium recovery systems have also been studied.

References

[9.5-1] Sato S., Takatsu H., Kurasawa T., et al. Conceptual Design of Shielding Blanket, JAERI-tech 95-019 (1995).
[9.5-2] Kitamura K., Takatsu H., Koizumi K., et al. Feasibility Study of First Wall Electrical Connector, JAERI-tech 95-032 (1995).
[9.5-3] Furuya K., Takatsu H., Kurasawa T., et al. Convertible Shielding to Ceramic Breeding Blanket, JAERI-tech 95-031 (1995).
[9.5-4] Furuya K., Takatsu H., Hashimoto T., et al. Transient Thermal and Stress Analyses of the ITER Shielding Blanket/First Wall under off-normal Condition, to be published as JAERI-tech (1995).
[9.5-5] Kurasawa T., Takatsu H., Sato S., et al. Test Program Development for ITER Blanket Design, JAERI-tech 95-021 (1995).
[9.5-6] Nakahira M., Takatsu H., Kurasawa T., et al. Integration of Test Modules in the Main Blanket and Vacuum Vessel Design, JAERI-tech 95-035 (1995).

VI. INTERNATIONAL THERMONUCLEAR EXPERIMENTAL REACTOR (ITER)

1. Introduction

Following the approval of the Outline Design by the ITER Council, the four Parties signed Protocol 2 in March 1994 implementing the 2nd phase of EDA.

It was recognized that the Outline Design had been successful in its attempt to maximize physics and engineering performance while minimizing cost and complexities. However, in order to determine the optimum way to achieve a further reduction in cost, a sensitivity study was conducted by the Director and JCT in close collaboration with the four Home Teams. The study was carried out over a period of about five months and TAC reviewed the results at its 5th Meeting.

In July 1994, there were minor changes in the JCT Organization. The Special Review Group (SRG) was established in December 1994 to review the ITER site requirements, and the first meeting was held in February 1995 at Naka.

The Director, Dr. R. Aymar, held a large meeting to conduct a comprehensive review of the Outline Design in October 1994 with wide participation from the Home Teams. The results and recommendations of the meeting were reflected or incorporated in the design. The draft of the Interim Design Report will be prepared in June 1995.

The Design Description Documents that provide the design requirements for the future detailed design were presented in February 1995.

The JCT member builds up to 150 including 34 Japanese members as of March 1995.

2. Sensitivity Study and Progress in the Engineering Design

The sensitivity study was conducted by the Director and JCT in close collaboration with the four Home Teams in order to determine the optimum way to achieve a reduction in the cost of ITER while minimizing the impact on its performance. To examine the sensitivity of plasma performance and machine cost to variations of the major machine parameters, the JCT/HT participants selected five "common study points" to be compared with the reference outline design parameters. The purpose of this study will be to determine the relative importance of different design parameters, within small differences in the variations, in determining the overall cost.

The study has revealed that the construction cost of ITER decreased by 5 - 10% as the reactor size decreases by 5 - 10%. Table VI.2-1 summarizes the common design variants and the resultant relative costs.

By using the results of the sensitivity study, it was possible to realize small reductions (<10%) in the cost estimate either because of the improved database in key areas (helium transport and exhaust, size-scaling of H-mode confinement) or because of an explicit decision to increase the risk of insufficient margines regarding confinements.

Table VI.2-1. Common Study Points

	Reference OD	(a)	(b)	(d)	(e)	(f)
R (m)	8.1	7.89	7.67	7.65	7.5	7.1
a(m)	3.0	3.0	2.67	2.64	2.78	2.63
A	2.7	2.63	2.87	2.9	2.7	2.7
B(T)	5.72	5.23	5.88	5.92	5.2	4.54
I(MA)	24	22.8	20.3	21.9	23.3	20.5
k(95%)	1.55	1.55	1.55	1.65	1.7	1.7
Relative cost	1	0.96	0.93	0.95	0.95	0.96

(a) -15% in coil currents (2 layers off from TF and CS), -7% in plasma current
(b) -5% in R, -12.5% in current
(d) -5% in R, +5% in k, -8.5% in current
(e) +10% in k, -5% in R, - 3% in current
(f) +10% in k, -10% in R, -12.5% in current

The Japanese Home Team performed the ITER design based on task agreements, in the field of vacuum vessel, first wall and blanket, initial assembly, power supply and plasma control, plant system, and so on. At the comprehensive design review meeting in October, the Japanese Home Team proposed a new design for magnet, vacuum vessel, blanket, etc., that had been elaborated through the investigation of technical and manufacturing feasibility . Almost all of the proposals were accepted as a reference design.

As for the safety assessment of ITER, the general safety principles for the design and safety assessment of fusion reactors including ITER were worked out and reported to JCT as a Japanese first draft.

3. Progress in the Engineering R&Ds

Negotiations on sharing of R&D and design tasks have been progressed and the amount of the credit allocated to each home team reached 442 kIUA, 30% of which was assigned to Japan. Table VI.3-1 summarizes the ITER Technology R&D and the Japanese share. Japan will take responsibilities in the construction of a CS model coil test facility, development of a CS model coil, manufacturing and testing of a full-scale 1/20 sector of the vacuum vessel, and the demonstration of the vehicle type remote maintenance system for blanket module replacement.

4. Future Plan

The Interim Design Report will be prepared for presentation at the 8th ITER Council to be held in July 1995. Major milestones of EDA can be seen in Fig. VI.4-1.

Fig. VI.4-1 ITER EDA Milestones

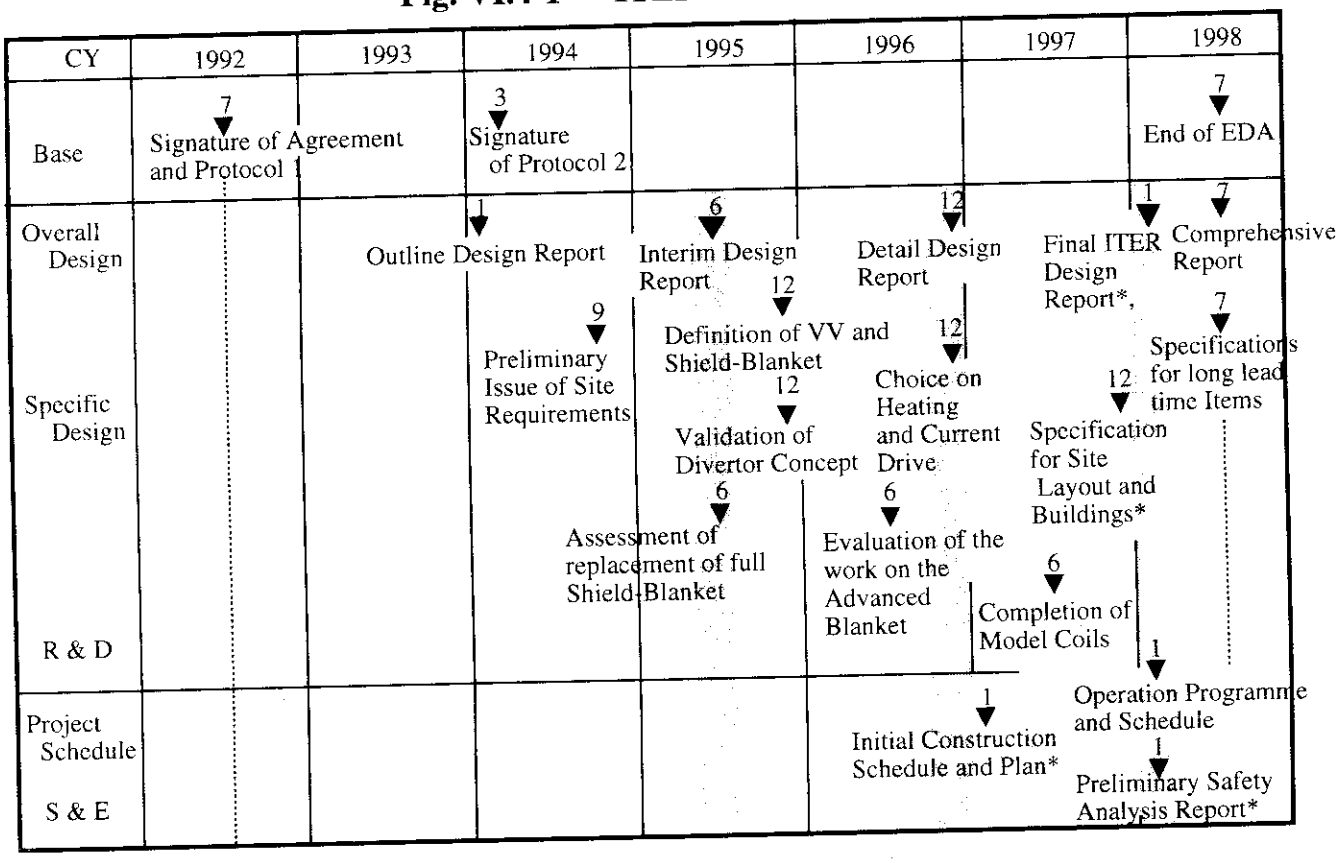

VII. FUSION REACTOR DESIGN

1. Introduction

In FY 1995, improvement of fusion power reactor concept DREAM was performed focusing on the reactor internals and safety. Concerning fusion safety, safety code developments, and experiments of LOVA and ICE in fusion devices including ITER were carried out.

2. Fusion reactor design

Fusion Power Reactor Concept DREAM was improved from the viewpoint of maintenance, thermal efficiency and safety. A part of the reactor configuration of DREAM is shown in Fig. VII.2-1. To enhance easiness regarding maintenance, a divertor cassette system which can be drawn horizontally independently of the blanket module was adopted. The blanket was partitioned into 12 modules in the toroidal direction. Each module can be drawn horizontally for maintenance. The blanket module is composed of 3 layers, that is, a replaceable blanket, shield I, and shield II, which allow the first two layers to be operated at high temperature of 900 °C and last layers operated at 400 °C. Fuel breeding is done in a replaceable blanket. This year, 10 MPa single helium cooling was investigated and found to be superior to the 5 MPa helium-SiC particles suspension flow. The series combination of the blanket and divertor cooling system provides a thermal efficiency of 42.3%. The concept of a 500 MW gas turbine unit was investigated. As a regards the effect of low activation material, silicon carbide was studied concerning radioactivity and radiation heat. The excellent behavior was founded for maintenance and safety.

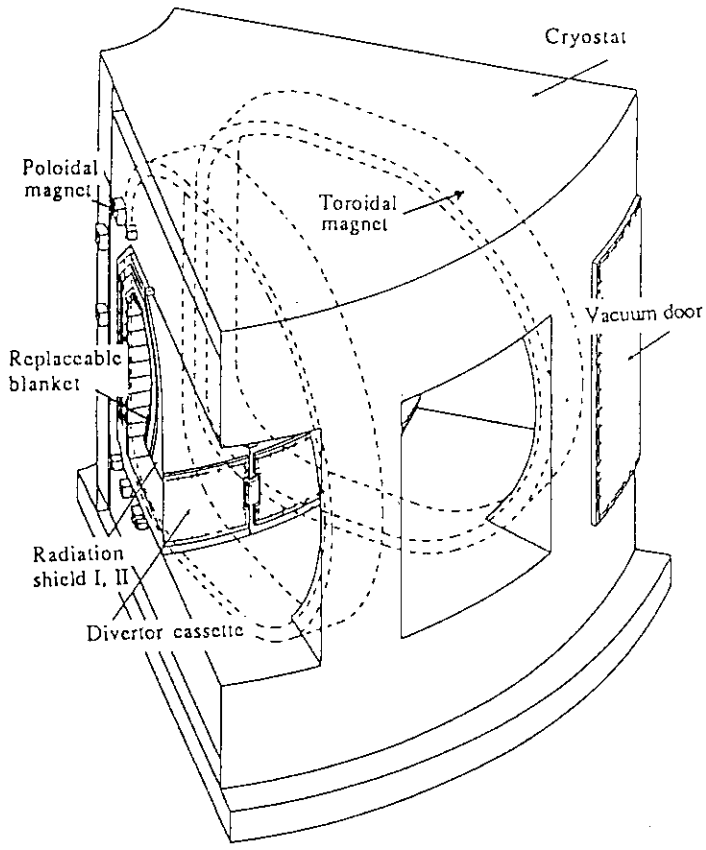

Fig. VII.2-1. Reactor configuration of DREAM.

3. Fusion safety

Research on loss of vacuum accident (LOVA) and ingress of coolant events (ICE), concluded to be environmentally most influential events from the view point of safety analysis was performed. Preliminary experiments on LOVA were carried out. The relation between breach size and location, and replacement flow was obtained. ICE small-scale experimental equipment has been designed and is now under construction. A schematic flow diagram of the ICE experimental apparatus is shown in Fig. VII.3-1. The size of cylindrical vacuum vessel is 900 mm in diameter and 600 mm in height. Data from these experiments are expected to contribute to verification of the safety analyses codes and ITER safety considerations. ICE analysis of experimental apparatus was done using the TRAC-BF1 code. The predictions of ICE vessel pressure and temperature were carried out and safety of experimental equipment was verified.

A survey on tokamak dust source term in vacuum vessels of JT60, JET and so on was performed. In addition, the methodology for dust removal was investigated and an electric precipitator was selected which seems to be promising for removal of dust from a tokamak under various operational states. Requirements for a dust removal system were preliminarily determined. A laboratory principle test of the electric precipitator was performed using simulated dust in a vacuum environment.

Concerning comprehensive safety evaluation methodology, the code was applied to the problem of plasma transient events and thermal hydraulics of plasma facing components during over-power event. The condition in which over-power transient of plasma was terminated passively was clarified.

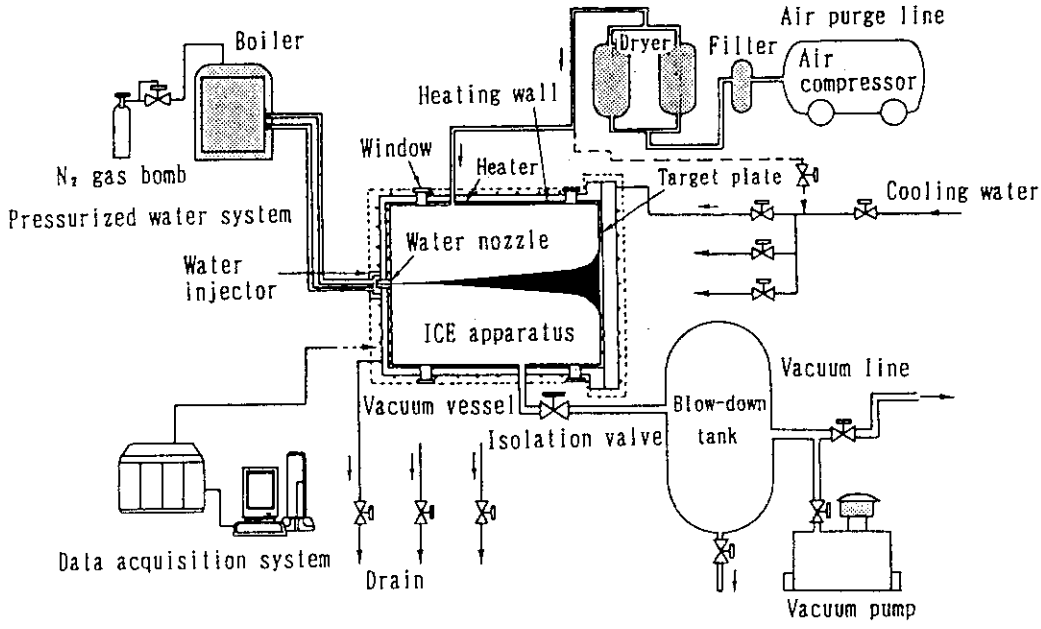

Fig.VII.3-1. A flow diagram of the ICE apparatus.

APPENDICES

A.1 Publication List (April 1994 – March 1995)

A.1.1 List of JAERI reports (Fusion Facility)

1) Aikawa H., JAERI-Research 94-037, "A Transport Model of Ohmically Heated Tokamaks – 'Profile Consistency" Revisited –' (1994).
2) Akino N., Hoonoki T., et al., JAERI-Tech 94-031, "Helium Gas Evaluation with a Cryo-sorption Pump Using an Argon Condensed Layer" (1994) (in Japanese).
3) Araki M., Ogawa M., Kunugi T., et al., JAERI-Tech 95-022, "Heat transfer experiments on the cooling tubes for divertor plates under one-sided heating conditions" (1995).
4) Hashimoto T., Takatsu H., Sato S., et al., JAERI-Tech 94-009, "Development and Trial Manufacturing 1/2-scale Partial Mock-up of Blanket Box Structure for Fusion Experimental Reactor" (1994).
5) Hiratsuka H., Miyo Y., Koike T., et al., JAERI-Tech 94-037, "Development of Piezoelectric Actuator Gas Injection Valve for JT-60U" (1994) (in Japanese).
6) Inoue T., Hanada M., Maeno S., et al., JAERI-Tech. 94-007, "Design Study of Prototype Accelerator and MeV Test Facility for Demonstration of 1 MeV, 1 A Negative Ion Beam Production" (1994).
7) Kanamori N., Kakudate S., Oka K., et al., JAERI-Tech 94-012, "Critical Element Development of Double Seal Door for Tritium Containment" (1994).
8) Kawano Y., Nagashima A., Hatae T., et al., JAERI-Research 95-023, "Development of Dual CO_2 Laser Interferometer for Large Tokamak" (1995).
9) Koizumi N, Takahashi Y, Tsuji, H., JAERI-M 94-017, "Implicit Time-dependent Finite Different Algorithm for Quench Simulation" (1994).
10) Kusama Y., Afanassiev V. I., Petrov S. Y., et al., JAERI-Research 94-036, "Direct Measurement of MeV-Range Atomic Hydrogen Using a Charge-Exchange Neutral Particle Analyzer in ICRF-Heated JT-60U Plasmas" (1994).
11) Murakami Y., Fujieda H., Tsunematu T., JAERI-M 94-080, "Parametric Analysis and Operational Performance of EDA-ITER" (1994).
12) Miya N., JAERI-Tech 95-028, "Radiological Safety of DT Experiments at TFTR" (1995).
13) Nakahira M., Tada E., Kanamori N., et al., JAERI-Tech 95-008, "Tokamak Assembly and Tooling" (1995).
14) Nakamura K., Ishikawa H., Ando T., et al., JAERI-M 94-046, "High heat flux experiments on B_4C-converted carbon based materials for plasma facing materials of JT-60U" (1994).
15) Nishio S., Abe T., Kawamura M., et al., JAERI-Tech 94-006, "Development of Integrated Insulation Joint for Cooling pipe in Tokamak Reactor" (1994).
16) Obara K., Kakudate S., Oka K., et al., JAERI-Tech 94-003, "Irradiation Tests of Critical Components for Remote Handling in Gamma Radiation Environment" (1994).
17) Oka K., Kakudate S., Nakahira M., et al., JAERI-Tech 94-022, "Critical Element Study on Autonomous Position Control of Articulated-arm Type Manipulator" (1994).
18) Oka K., Kakudate S., Nakahira M., et al., JAERI-Tech 94-033, "Critical Element Development of Standard Components for Pipe Welding/cutting by CO_2 Laser" (1994).
19) Okumura K., Hanada M., Inoue T., et al., JAERI-Tech. 95-018, "Design Study on a 1 MeV, 12.5 MW Neutral Beam Injector Module for ITER" (1995).
20) Sato M., Isei N., Ishida S., JAERI-M 94-082, "Design of Grating Filter for Grating Polychromator on Measurement of Electron Temperature Profile from Electron Cyclotron Emission" (1994).
21) Sato M., Nemoto M., Sakaki H., et al., JAERI-Tech 95-026, "Development of Control and Data Acquisition Software for Alpha Particle Apparatus" (1995).
22) Sato S., Takatsu H., Kurasawa T., et al., JAERI-Tech 95-019, "Conceptual Design of ITER Shielding Blanket" (1995).
23) Senda I., Nishio S., Tsunematsu T., et al., JAERI-Tech 94-018, "The plasma position control of ITER EDA plasma" (1994).
24) Shibui M., Nakahira M., Tada E., et al., JAERI-M 94-073, "Heat Removal Capability of Divertor Coaxial Tube Assembly" (1994).
25) Shibui M., Nakahira M., Tada E., et al., JAERI-M 94-074, "Fail-safe First Wall for Preclusion of Little Leakage" (1994).
26) Shirai H., JAERI-Research 94-001, "Transport Studies of Tokamak Plasmas in JT-60 Device" (1994).
27) Taguchi K., Kakudate S., Kanamori N., et al., JAERI-Tech 94-002, "Critical Element development of Standard Pipe Connector for Remote Handling" (1994).

28) Tokuda S., Ozeki T., JAERI-Research 94-013, "Stability Analysis of External Kink Mode for ITER L-mode Profile Plasmas" (1994).
29) Tokuda S., Ozeki T., JAERI-Research 94-030, "Stability Analysis of ITER Plasmas with H-mode Profiles" (1994).
30) Tokuda S., JAERI-Research 94-033, "Effect of Edge Bootstrap Current on Ideal MHD Stability" (1994).
31) Zimin S., Maki K., Takatsu H., et al., JAERI-Tech 94-015, "Shielding Analysis of the ITER/EDA NBI Duct" (1994).
32) Zimin S., Sato S., Hashimoto T., et al., JAERI-Tech 94-026, "Peaking Factors of Nuclear Heating due to Void Ducts in the 80% SS - 20% H_2O Shielding Blanket of Fusion Experimental Reactors" (1994).

A.1.2 List of papers published in journals

1) Akiba M., Madarame H., "Effects of plasma disruption on structural and plasma facing materials", J. Nucl. Mater., **212-215**, 90 (1994).
2) Akiba M., Madarame H., "Effects of plasma disruptions on structural and plasma facing materials", Fusion Eng. Des., **24**, 431 (1994).
3) Akiba M., Ohkubo K., Okuno K., et al., "Report on 18th Symposium on Fusion Technology", J. Plasma Fusion Res., **70**, 1127 (1994) (in Japanese).
4) Alen S. L., Brown M. D., Byers J. A., et al., "Nonlinear Absorption of High Power Free-Electron-Laser-Generated Microwaves at Electron Cyclotron Resonance Heating Frequencies in the MTX Tokamak", Phys. Rev. Lett., **72**, 1348 (1994).
5) Amemiya H., Uehara K., "Ion Temperature Measuring Probe in a Strongly Magnetized Plasma ", Rev. Sci. Instrum., **65**, 2607 (1994).
6) Ando S., Ninomiya A., Ishigohoka T., et al., "An Experimental Study on Current Unbalance in High Current Capacity Superconducting AC/Pulse Conductor", Trans. Inst. Electr. Eng. Jpn., **115-A**, 233 (1995) (in Japanese).
7) Ando T., Isono T., Tsuji H., et al., "Development of 10kA-Class High-Tc Superconducting Bus Line", IEEE Trans. Appl. Superconductivity, **5**, 817 (1995).
8) Ando T., Nishi M., Kato T., et al., "Measurement of Quench Back Behavior on the Normal Zone Propagation Velocity in a CICC", Cryogenics, **34**, 599 (1994).
9) Ando T., Sugimoto M., Tsuji H., et al., "The Applicability of the React-and-Wind Technique to the ITER-TF Coil with a Nb3Al Conductor ", Cryogenics, **34**, 509 (1994).
10) Annaratone B. M., Shoji T., Maeda H., et al., "Fluid Velocity and Electromagnetic Forces Measured by a Rotating Langmuir Probe in the Scrape-off Layer of JFT-2M", Nucl. Fusion, **34**, 1453 (1994).
11) Aoyagi T., et al., "Modifications to VME-bus system on Thyristor Controllers of the JT-60U Power Supplies", Trans. Inst. Electr. Eng. Jpn., **115-D**, 13 (1995) (in Japanese).
12) Araki M., Sasaki M., Kim S. W., et al., "Thermal response experiments of SiC/C and TiC/C functionally gradient materials as plasma facing materials for fusion application", J. Nucl. Mater., **212-215**, 1329 (1994).
13) Ayai N., Yamada Y., Koizumi N., et al., "Development of Nb3Al Multifilamentary Superconductors", IEEE Trans. Appl. Superconductivity, **5**, 893 (1995).
14) Conn R. W., Najmabadi F., Seki Y., et al., "Conferences and Symposia Fusion Reactor Design and Technology", Nucl. Fusion, **34**, 747 (1994).
15) Enoeda M., Okuno K., Nishikawa M., et al., "Recovery of Tritium by Cryogenic Molecular Sieve Bed in Breeding Blanket Condition", Fusion Technol., **26**, 664 (1994).
16) Fuchs G., Miura Y., Mori M., "Soft X-ray Tomography on Tokamaks Using Flux Coordinates", Plasma Phys. Control. Fusion, **36**, 307 (1994).
17) Fujita T., Tobita K., "Results of DT Experiments", J. Plasma Fusion Res., **71**, 214 (1995) (in Japanese).
18) Fukuda T., "Status of the Millimeter- and Submillimeter-Wave Plasma Diagnostics Interferometry and Cyclotron Radiation Diagnostics", J. Plasma Fusion Res., **71**, 127 (1995) (in Japanese).
19) Hamada K., Nishida K., Kato T., et al., "Final Design of a Cryogenic System for the ITER CS Model Coil", Cryogenics, **34**, 65 (1994).
20) Hayashi T., Suzuki T., Okuno K., "Long-Term Measurement of Helium-3 Release Behavior from Zirconium-Cobalt Tritide", J. Nucl. Mater., **212-215**, 1431 (1994).
21) Hiroki S., Abe T., Iguchi M., et al., "Fabrication and test of an induction motor for the turbomolecular pump using a ceramic-insulated wire", J. Vac. Soc. Jpn., **38**, 291 (1995) (in Japanese).
22) Hiroki S., Abe T., Murakami Y., "Detection of a 10^{-4} helium peak in a deuterium atmosphere using a modified high-resolution quadrupole mass spectrometer", Rev. Sci. Instrum., **65**, 1912 (1994).

23) Hiroki S., Abe T., Murakami Y., et al., "Development of a high-resolution quadrupole mass spectrometer capable of detecting ^{3}He and ^{4}He in a hydrogen isotope atmosphere", J. Vac. Sci. Technol., **A12**, 2711 (1994).

24) Hiroki S., Abe T., Murakami Y., "Influence of the fringing field length on the separated $^4He/D_2$ peak shape of a high-resolution quadrupole mass spectrometer", Int. J. Mass Spectrometry and Ion Processes, **136**, 85 (1994).

25) Hiroki S., Kaneko K., Abe T., et al., "Influence of a fringing field on the sensitivity of the quadrupole mass spectrometer", J. Vac. Soc. Jpn., **38**, 74 (1995) (in Japanese).

26) Hoek M., Nishitani T., et al., "Neutron Yield Measurements by Use of Foil Activation at JT-60U", Rev. Sci. Instrum., **66**, 885 (1995).

27) Honda T., Uda T., Seki Y., et al., "Comprehensive Safety Analysis Code System for Nuclear Fusion Reactors I; Model and Analyses of Overpower Events for the International Thermonuclear Experimental Reactor", Fusion Technol., **25**, 451 (1994).

28) Honda T., Maki K., Seki Y.,"Comprehensive Safety Analysis Code System for Nuclear Fusion Reactors II: Thermal Analyses during Plasma Disruptions for International Thermonuclear Experimental Reactor", Fusion Technol., **26**, 1288 (1994).

29) Ida K., Miura Y., Itoh S.-I., et al., "Physics Mechanism to Determine the Radial Electric Field and its Radial Structure in a Torus Plasma", J. Plasma Fusion Res., **70**, 514 (1994) (in Japanese).

30) Ida S., Miura Y., Matsuda T., et al., "Evidence for a Toroidal-Momentum-Transport Nondiffusive Term from the JFT-2M Tokamak", Phys. Rev. Lett., **74** , 1990 (1995).

31) Ide S., Naito O., Kondoh T., et al., "Enhancement of Absorption of Lower Hybrid Wave by Filling the Spectral Gap", Phys. Rev. Lett., **73**, 2312 (1994).

32) Ikeda Y., Naito O., Seki M., et al., "Simple Multijunction Launcher with Oversized Waveguides for Lower Hybrid Current Drive on JT-60U", Fusion Eng. Des., **24**, 287 (1994).

33) Ikeda Y., Naito O., Ushigusa K., et al., "Wave Accessibility Effects on Lower Hybrid Current Drive in JT-60U", Nucl. Fusion, **34** , 871 (1994).

34) Inoue T., Hanada M., S. Maeno, et al., "Recent Progress on High Power Negative Ion Sources at JAERI", Plasma Devices and Operations, **3**, 211 (1994).

35) Ioki K., Johnson G., Shimizu K., et al., "Design of the ITER Vacuum Vessel", Fusion Eng. Des., **24** (1994).

36) Isei N., et al., "Development of 180 GHz Heterodyne Radiometer for Electron Cyclotron Emission Measurements in JT-60U", Rev. Sci. Instrum., **66**, 412 (1995).

37) Isono T., Yasukawa Y., Hosono F., et al., "Development and Testing of 40-kA, 13-T Nb3Sn Cable-in-Conduit Conductors for a Fusion Reactor", IEEE Trans. Appl. Superconductivity, **5**, 909 (1995).

38) Isono T., Yoshida K., Takahashi Y., et al., "Development of Full-Scale Conductors for the ITER Central Solenoid Scaleable Model COILS", IEEE Trans. Magn., **30**, 2046 (1994).

39) Ito Y., Kanazawa N., Arakawa T., et al., "Electron Cyclotron Resonance Discharge of Sublimation Gas of Decaborane and its Application to Preparation of Boron Thin Films", Jpn. J. Appl. Phys. **33**, 4251 (1994).

40) Ito Y., Saidoh M., Arakawa T., et al., "Electron Cyclotron Resonance Discharge of Sublimation Gas of Decaborane and Its Application to Preparation of Boron Thin Films", Jpn. J. Appl. Phys., **33**, 4251 (1994).

41) Iwabuchi A., Arai H., Sugimoto M., et al., "Frictional Properties of Ceramics, MOS2 Coated Films and Polyethylene Fiber Reinforced Plastics at 4.2K in Liquid Helium", Cryogenics, **35**, 35 (1995).

42) Kamada Y., Ushigusa K., Naito O., et al., "Non-inductively Current Driven H Mode with High-β_N and High-β_p Values in JT-60U", Nucl. Fusion, **34**, 1605 (1994).

43) Kasugai A., Sakamoto K., Tsuneoka M., et al., "High power and long pulse gyrotron development in JAERI", Fusion Eng. Des., **26**, 281 (1994).

44) Kawashima H., Hasegawa M., Fuchs G., et al., "Measurement of Anisotropic Soft X-Ray Emission during Radio-Frequency Current Drive in the JFT-2M Tokamak", Jpn. J. Appl. Phys., **33**, 3590 (1994).

45) Kawashima H., Nagashima K., Tamai H., "Study of Runaway Electron Transport in Edge Stochastic Magnetic Field in the JFT-2M Tokamak", J. Plasma Fusion Res., **70**, 868 (1994).

46) Kikuchi M., "Basic Design of Fusion Reactor", Kikai no Kenkyu, **47**, 111 (1995) (in Japanese).

47) Kikuchi M., Seki Y., Motojima O., "Design of Commercial Magnetic Fusion Reactors" J. Plasma Fusion Res., **70**, 591 (1994) (in Japanese).

48) Kim J. Y., Kishimoto Y., Horton W., et al., "Kinetic Resonance Damping Rate of the Toroidal Ion Temperature Gradient Mode", Phys. Plasmas, **1**, 927 (1994).

49) Kimura H., Saigusa M., Moriyama S., et al., "Excitation of High n Toroidicity-Induced Alfvén Eigenmodes and Associated Plasma Dynamical Behaviour in the JT-60U ICRF Experiments", Phys. Lett. A, **199**, 86 (1995).

50) Kimura T., "VME and Network Applications to the JT-60U Control System", Nucl. Instrum. Methods. Phys. Res. A **352**, 125 (1994)

51) Kobori T., Horiguchi K., Shindo Y., et al., "Fracture Toughness Assessment for JN 1 Austenitic Stainless Steel Rolled Plate at Liquid Helium Temperature", J. Cryogenic Soc. Jpn., **29**, 46 (1994) (in Japanese).

52) Koide Y., Kikuchi M., Mori M., et al., "Internal Transport Barrier on q=3 Surface and Poloidal Plasma Spin-up in JT-60U High-β_p Discharges", Phys. Rev. Lett., **72** 3662 (1994).

53) Koizumi N., Okuno K., Takahashi Y., et al., "Experimental results on instability caused by non-uniform current distribution in the 30 kA NbTi Demo Poloidal Coil (DPC-U) conductor ", Cryogenics, **34**, 155 (1994).

54) Koizumi N., Okuno K., Takahashi Y., et al., "Stabilized Operation of 30kA NbTi DEMO Poloidal Coil (DPC-U) with Uniform Current Distribution in Conductors ", Cryogenics, **34**, 1015 (1994).

55) Koizumi K., Shibui.M., Nakahira.M., et al., "Design of Separated First Wall for Fusion Experimental Reactor", Fusion Eng. Des., **27**, 388 (1995).

56) Kondoh T., Ikeda Y., Ushigusa K., "Large Current Drive Experiments Using Simplified Multijunction Lower Hybrid Wave Launcher in JT-60U", J. At. Energy Soc. Jpn., **37**, 124 (1005) (in Japanese).

57) Konishi S., Nagasaki T., Hayashi T., et al., "Improvements in ZrCo Based Tritium Storage Media", Fusion Technol., **26**, 668 (1994).

58) Konoshima S., Toi K., "Improvement of the Energy Confinement in the Toroidal Plasma Experiment", J. Plasma Fusion Res., **71**, 109 (1995) (in Japanese).

59) Kurasawa.T., Takatsu.H., Sato.S., et al., "Ceramic Breeder Blanket Development for Fusion Experimental Reactor in JAERI", Fusion Eng. Des., **27**, 449 (1995).

60) Kuriyama M., Akino N., Araki M., "High Energy Negative Ion Based NBI System for JT-60U", Fusion Eng. Des., **26**, 445 (1995).

61) Kusama K., et al., "Charge-Exchange Neutral Particle Measurement in MeV Energy Range on JT-60U", Rev. Sci. Instrum., **66**, 339 (1995).

62) Linke J., Akiba M., Araki M., et al., "Evaluation of cooling concepts and specimen geometries for high heat flux tests on neutron irradiated divertor elements", Fusion Eng. Des., **28**, 72 (1995).

63) Maebara S., Ikeda Y., Seki M., et al., "Design of a 5 GHz window in a lower hybrid r.f. system", Fusion Eng. Des., **26**, 343 (1994).

64) Maki K., Takatsu H., Sato S., et al., "Biological Shield around the Neutral Beam Injector Ducts in the ITER Conceptual Design", Fusion Eng. Des., **24**,315 (1994).

65) Matsuda S., "ITER", Kikai no Kenkyu, **47**, 115 (1994) (in Japanese).

66) Matsuda T., et al., "New Data Acquisition System for the JFT-2M Tokamak", Rev. Sci. Instrum., **66**, 515 (1995).

67) Mitchell N., Bruzzone P., Nishi M., et al., "Strand Production and Benchmark Testing for the ITER Model Coils", IEEE Trans. Appl. Superconductivity, **5**, 905 (1995).

68) Miya K., Mutoh Y., Takatsu H.,"Structural Design Criteria", Kikai no Kenkyu, **47** (1994) (in Japanese).

69) Miya N., Nishitani T., Takeuchi H., "One-Dimensional Activation Analysis of Vacuum Vessel of JT-60U with Deuterium Gas Discharges", J. Nucl. Sci. Technol., **31**, 398 (1994).

70) Miya N., "Radiological Safety of DT Experiments", J. Plasma Fusion Res., **71**, 241 (1995) (in Japanese).

71) Miya N., "Recent Results of JT-60U and Safety Analysis in D-D Discharge", Genshiryoku Kogyo, **40**, 36 (1994) (in Japanese).

72) Miyo Y., Ogiwara N., Saidoh M., "Suppression of Outgassing from Spindt-type Cold-Cathode by Heat Treatment", J. Vac. Soc. Jpn., **38**, 274 (1995) (in Japanese).

73) Mizuno M., Akiba M., Akino N., et al., "Design of a 500 keV Negative-Ion-Based NBI System for JT-60U", Plasma Devices and Operations, **3**, 199 (1994).

74) Mohri K., Sato S., Kawaguchi I., et al., "Development of Blanket Box Structure Fabrication Technology", Fusion Eng. Des., **27**, 438 (1995).

75) Mori M., Ishida S., Ando T., et al., "Achievement of High Fusion Triple Product in the JT-60U High-β_p H-mode", Nucl. Fusion, **34** , 1045 (1994).

76) Nakajima H., Sasaki T., Ando T., et al., "Effects of Cyclic Pulsed Operation on the Coil Performance in the Nb3Sn Demo Poloidal Coil (DPC-EX)", IEEE Trans. Magn., **30**, 2535 (1994).

77) Nakajima H., Tsuji H., "Development and Prospects of Material Technology in Superconducting Coils for Fusion Reactor", J. Plasma Fusion Res., **70**, 733 (1994) (in Japanese).

78) Nakamura K., Akiba M., Suzuki S., et al., "Erosion of CFC and W at high temperature under high heat loads", J. Nucl. Mater., **212-215**, 1201 (1994).

79) Nakamura K., Ando T., Akiba M., et al., "Feasibility Tests on B_4C-converted Carbon with Various Film Thicknesses for JT-60U Application", Fusion Eng. Des., **24**, 431 (1994).

80) Nakamura K., Ando T., Akiba M., et al., "Feasibility tests on B_4C converted carbon with various film thicknesses for JT-60U application", Fusion Eng. Des., **24**, 431 (1994).

81) Nishi M., Armstrong J. R., Koizumi N., et al., "Effect of Strand Diameter on the Stability of the Cable-in-Conduit Conductor", IEEE Trans. Magn., **30**, 2527 (1994).

82) Nishi M., Yamamoto K., Sasaki T., et al., "Effect of the Void Fraction on the Property of the Nb3Sn Cable in Conduit Conductor ", Adv. Cryogenic Eng., **40**, 853 (1994).
83) Nishi M., Yoshida K., Ando T., et al., "Nb3Sn Superconducting Strand Development in Japan for ITER", Cryogenics, **34**, 505 (1994).
84) Nishio S., Murakami Y., Aoki I., et al., "The concept of drastically easy maintenance (DREAM) Tokamak Reactor", Fusion Eng. Des., **25**, 289 (1994).
85) Nishitani T., Asakura N., "Present Status and Issues in Burning Plasma", J. Plasma Fusion Res., **70**, 581 (1994) (in Japanese).
86) Nishitani T., Ishida S., Kikuchi M., et al., "Attainment of High Fusion Reactivity Under High Bootstrap Current Fraction in JT-60U", Nucl. Fusion, **34**, 1069 (1994).
87) Nishitani T., Shimada R., "DT Experiments on TFTR", J. Plasma Fusion Res., **71**, 212 (1995) (in Japanese).
88) Ogiwara N., Jimbou R., Saidoh M., et al., "The Reaction of H_2O, O_2 , and Energetic O_2^+ on Boron Carbide", J. Nucl. Mater., **212-215**, 1260 (1994).
89) Ohara Y., Hanada M., Inoue T., et al., "Development of High Power Negative-Ion Sources for Fusion Research at JAERI", Rev. Sci. Instrum., **65**, No. 4, (1994).
90) Ohara Y., Imai T., "Heating and Current Drive", Kikai no Kenkyu, **47**, 125 (1995) (in Japanese).
91) Ohara Y., "Progress of Neutral Beam R&D for Plasma Heating and Current Drive at JAERI", Fusion Eng. Des., **26**, 415 (1995).
92) Osborne T. H., Burrell K. H., Carlstrom T. N., et al., "Confinement and Stability of VH Mode Discharges in the DIIIV-D Tokamak", Nucl. Fusion, **35** , 23 (1995).
93) Saigusa M., et al., "Investigation of High-n TAE Modes Excited by Minority-ion Cyclotron Heating in JT-60U", Plasma Phys. Control. Fusion, **37**, 295 (1995).
94) Saigusa M., Fujii T., Kimura H., et al., "Electrical Design and Test of ICRF Antenna for JT-60U", Fusion Eng. Des., **24**, 47 (1994).
95) Saigusa M., Moriyama S., Fujii T., et al., "High coupling performance of JT-60U ICRF Antenna", Nucl. Fusion **34**, 275 (1994).
96) Sakamoto K., Tsuneoka M., Kasugai A., et al., "Major improvement of gyrotron efficiency with beam energy recovery", Phys. Rev. Lett., **26**, 3532 (1994).
97) Seki Y., "Fusion Reactor Design and Technology Program in Japan", Fusion Eng. Des., **25**, 49 (1994).
98) Senda I.,"The sheath formation in the presence of a hot plasma flow", Phys. Plasmas **2**, 6 (1995).
99) Sherman R. H., Taylor D. J., Yamanishi T., et al., "The role of Sidestream Recycle in Hydrogen Separation and Column Cascade Design", Fusion Eng. Des., **28**, 397 (1995).
100) Shibata K., Maki K., Otsuka M., et al., "The Conceptual Design of the Double-pin Type Blanket with Hollow Ceramic Breeder Pellets for Fusion Experimental Reactors", Fusion Eng. Des., **24**, 403 (1994).
101) Shimada M., "Advanced Divertor", Kikai no Kenkyu, **47**, 195 (1995) (in Japanese).
102) Shimakawa S., Sagawa H., Kuroda T., et al., "Estimation on Tritium Production and Inventory in Beryllium", Fusion Eng. Des., **24** (1994).
103) Shimomura Y., "Overview of International Thermonuclear Experimental Reactor (ITER) engineering design activities", Phys. Plasmas, **1**, 1612 (1994).
104) Shirai H., Hirayama T., Koide Y., et al., "Ion Temperature Profile Simulation of JT-60 and TFTR Plasmas with Ion Temperature Gradient Mode Transport Models", Nucl. Fusion, **34**, 703 (1994).
105) Shirai H., "Transport of DT Plasmas", J. Plasma Fusion Res., **71**, 223 (1995) (in Japanese).
106) Sugaya S., Kawasaki H., Seki Y., et al., "Development of Nuclear Thermal Coupled Calculation Code System", Fusion Eng. Des., **27**, 263 (1995).
107) Sugimoto M., Isono T., Koizumi N., et al., "Test Results of the FER/ITER Conductors in the FENIX Test Facility ", IEEE Trans. Magn., **30**, 2042 (1994).
108) Sugimoto M., Sasaki T., Nishi M., et al., "Experimental Results of 10kA Nb3Al Coil", IEEE Trans. Appl. Superconductivity, **5**, 897 (1995).
109) Suzuki S., Akiba M., Araki M., et al., "High heat flux experiments of saddle type divertor module", J. Nucl. Mater., **212-215**, 1365 (1994).
110) Takahashi Y., Sugimoto M., Isono T., et al., "Experimental Results of 40-kA Nb3Al Cable-in-conduit Conductor for Fusion Machines", IEEE Trans. Magn., **30**, 2531 (1994).
111) Takatsu H., "Blanket", Kikai no Kenkyu **47**, 136 (1995) (in Japanese).
112) Tanaka M., Ueda N., Suzuki Y., et al., "Numerical Simulation of Carbon Impurities in JT-60U Experiment", Contrib. Plasma. Phys., **34**, 460 (1994).
113) Thomsen K., Campbell D. J., Cordy J. G., et al., "ITER H-mode Confinement Database Update", Nucl. Fusion, **34** , 131 (1994).
114) Tobita K., et al., "Infrared TV Measurement of Fast Ion Loss on JT-60U", Rev. Sci. Instrum., **66**, 594 (1995).

115) Tobita K., Tani K., Nishitani T., et al., "Fast Ion Losses due to Toroidal Field Ripple in JT-60U", Nucl. Fusion, **34**, 1097 (1994).
116) Tsunematsu T., "Confinement of Plasma", Kikai no Kenkyu, **47** (1994) (in Japanese).
117) Tsuneoka M., Fujita H., Nagashima T., et al., "Power supply control and protection system for long pulse and high power gyrotron", J. Plasma Fusion Res., **70**, 992 (1994) (in Japanese).
118) Tsuneoka M., Sakamoto K., Kasugai A., et al., "Development of high efficiency and high power mm-wave system with CPD gyrotron", Trans. Inst. Electr. Eng. Jpn., **B-114**, 1179 (1994) (in Japanese).
119) Uda T., Ogawa M., Seki Y., et al., "Experiments on the High Temperature Graphite and Steam Reaction under LOCA condition", Fusion Eng. Des., **29**, 238 (1995).
120) Ueda N., Suzuki Y., Tanaka M., et al., "Review of the Present Status of Consistent Scrape-off Layer Modeling by Codes", Contrib. Plasma. Phys., **34**, 350 (1994).
121) Uriu Y., Ninomiya A., Takahashi Y., et al., "Monitoring of Superconducting Magnet System Using Fuzzy Theorem", IEEE Trans. Appl. Superconductivity, **5**, 469 (1995).
122) Ushigusa K., "Steady State Operation of Takamak 1 –Progress in Current Drive Experiments–", J. Plasma Fusion Res., **70**, 850 (1994) (in Japanese).
123) Willms R. S., Konishi S., Okuno K., "Use of Magnesium for Recovering Hydrogen Isotopes from Tritiated Water", Fusion Technol., **26**, 659 (1994).
124) Willms R. S., Taylor D. J., Enoeda M., et al., "Practical-Scale Tests of Cryogenic Molecular Sieve for Separating Low-Concentration Hydrogen Isotopes from Helium", Fusion Eng. Des., **28**, 386 (1995).
125) Yagi M., Horton W., "Reduced Braginskii Equations", Phys. Plasmas, **1**, 2135 (1994).
126) Yamai H., Konishi S., Yamanishi T., et al.., "Measurement of Capacity Coefficient of Inclined Liquid Phase Catalytic Exchange Column for Tritiated Processing", Fusion Technol., **26**, 654 (1994).
127) Yamaki T., Gotoh Y., Ando T., et al., "Thermal Desorption Spectroscopy of Boron / Carbon Films after keV Deuterium Irradiation", J. Nucl. Mater., **217**, 154 (1994).
128) Yamanishi T., Enoeda M., Okuno K., "Experimental Study for Characteristics of Cryogenic Distillation Column Having Feedback Stream with H-D-T System", J. Nucl. Sci. Technol., **31**, 937 (1994).
129) Yamanishi T., Okuno K., "Mass Transfer in Cryogenic Distillation Column Separating Hydrogen Isotope", J. Nucl. Sci. Technol., **31**, 562 (1994).
130) Yamawaki M.,Nakamura H., Noda N., et al., "Recent topics on interaction between fusion fuel and materials", J. At. Energy Soc. Jpn., **36**, 35 (1994) (in Japanese).
131) Yamazaki S., Miura H., Seki Y., et al., "Design Study of Helium-Solid Suspension Cooled Blanket and Divertor for a Tokamak Power Reactor", Fusion Eng. Des., **25**, 227 (1995).
132) Yamazaki S., Shimada M., "Technological Significances to Reduce the Material Problems –Feasibility of Heat Flux Reduction–", J. Plasma Fusion Res., **70**, 746 (1994) (in Japanese).
133) Yoshida H., Naito O., Yamashita O., et al., "Beam Combiner for Transient Phenomena Measurement in the JT-60 Thomson Scattering Diagnostic", Rev. Sci. Instrum., **66**, 143 (1995).
134) Yoshino R., "Multivariable Non-interacting Control of Plasma Configuration in JT-60U", Fusion Eng. Des., **24**, 375 (1994).
135) Yoshino R., Neyatani Y., Isei N., et al., "Operational Scenarios to Avoid Disruptions in JT-60U", J. Plasma Fusion Res., **70**, 1081 (1994).
136) Zimin S., "A Simplified methodology to Estimate the Displacement Damage in both a Copper Stabilizer of TF Coils and Steel Components of a Fusion Reactor", Fusion Eng. Des., **24**, 327 (1994).
137) Zimin S., Mori S., Takatsu H.,"Impact of material configuration behind first wall on He formation in in-vessel components of fusion reactor", J. Nucl. Sci. Technol., **31**, 629 (1994).

A.1.3 List of papers published in conference proceedings

1) Amemiya S., Masuda T., Ando T., et al., "Hydrogen Isotopes Retention and Impurity Deposition of Carbon Based Components Used in JT-60U", Proc. 11th Int. Conf. on Plasma-Surface Interaction in Controlled Fusion Devices, Mito, 1994, J. Nucl. Mater., **220-222**, 443 (1995).
2) Anderson J. L. and Okuno K., "Tritium Handling and Processing Experience at TSTA", Third Inter. Symp. on Fusion Nucl. Tech., Los Angeles, California, USA (1994).
3) Ando T., Masaki K., Kodama K., et al., "Performance of B_4C-converted Carbon Fiber Composites in High Power Neutral Beam Heated Divertor Discharges in JT-60U", Proc. 11th Int. Conf. on Plasma-Surface Interaction in Controlled Fusion Devices, Mito, 1994, J. Nucl. Mater., **220-222**, 380 (1995).
4) Araki M., Watson R. D., Marshall T. D., et al., "Effect of subcooling on the critical heat flux under one-sided heating conditions", Proc. of 18th Symp. Fusion Technology (1994) Karlsruhe.
5) Asakura N., Hosogane N., Itami K., et al., "Heat and Particle Transport in the Divertor and Remote Radiative Cooling on JT-60U", Proc. 15th Int. Conf. on Plasma Physics and Controlled Nuclear Fusion Research, Seville, 1994, A-4-I-3.

6) Asakura N., Itami K., Hosogane N., et al., "Field Reversal Effects on Particle and Heat Fluxes in Divertor on JT-60U", Proc. 11th Int. Conf. on Plasma-Surface Interaction in Controlled Fusion Devices, Mito, 1994, J. Nucl. Mater., **220-222**, 395 (1995).

7) Bosia G., Makowski M., Nagashima T., et al., "Physics Issues and Design Aspects of ITER Ion and Electron Cyclotron Systems," Proc.21th EPS Conf,on Controlled Fusion and Plasma Physics Montpellier, France, C102, [1994].

8) Chang C., Tani K., K. Hamamatsu, et al., "Radial Banana-Transitional Transport of Alpha Particles Driven by ICRH in a Tokamak Fusion Reactor", Proc. 21st EPS Conf. on Controlled Fusion and Plasma Physics Part II, 996 (1994).

9) Enoeda M., Okuno K., Nishikawa M., et al., "Recovery of Tritium by Cryogenic Molecular Sieve Bed in Breeding Blanket Condition", ANS 11th Topical Meeting on the Tech. of Fusion Energy, New Oleans, Lousiana, USA (1994).

10) Falter H. D., Akiba M., Araki M., et al., "Comparison between actively cooled divertor dump plates with Beryllium and CFC armour", Proc. of 18th Symp. Fusion Technology (1994) Karlsruhe.

11) Fukuda T., Kikuchi M., Koide Y., "H-mode Properties of JT-60U Discharges in DIfferent Collisionality Regimes", Proc. 4th H-mode Workshop, Plasma Phys. Control. Fusion, **36**, A87 (1994).

12) Fukuda T. and the JT-60 Team, "Steady State Improved Confinement Studies in the JT-60U Tokamak", Phys. Plasmas, **2**, 2249 (1995).

13) Fujii T., Saigusa H., Kimura H., et al., "Performance of toroidally wide-separation loop antennae for JT-60U ICRF experiments ", in Proceedings of 5th International Toki Conf. on Plasma Physics and Controlled Nuclear Fusion, Japan **26** (1995) 377.

14) Gohor Y., Antipenkov A., Cardella A., et al., "ITER nuclear engineeriing- first wall, blanket, shield design, and R&D program," 15th International Conf.on Plasma Phyics and Controlled Nuclear Fusion Research Sevilla,Spain Sep.26-Oct.1, [1994].

15) Gonihce M., Seki M., et al., "Outgassing Studies of Lower Hybrid Antenna Module During CW High RF Power Injection", Proc. 18th Symposium on Fusion Technology, Karlsruhe, 1994.

16) Hanada M., Dairaku M., Inoue T., et al., "A 1 MeV, 1 A Negative Ion Accelerator Test Facility", 18th Symposium on Fusion Technology, Karlsruhe, Aug. 22 - 26 (1994).

17) Hayashi T. and Okuno K., "Developement of Compact Tritium Confinement System Using Gas Separation Membrane", The 2nd Japan/China Symp. on Materials for Advanced Energy Systems and Fission and Fusion Engineering, University of Tokyo, Tokyo, Japan.

18) Hayashi T., Yamada M., Konishi S., et al., "Tritium Evacuation Performance of a Large Oil-Free Reciprocating Pump", Third Inter. Symp. on Fusion Nucl. Tech., Los Angeles, USA.

19) Higashijima S., Sugie T., Kubo H., et al., "Impurity and Particle Recycling Reduction by Boronization in JT-60U", Proc. 11th Int. Conf. on Plasma-Surface Interaction in Controlled Fusion Devices, Mito, 1994, J. Nucl. Mater., **220-222**, 375 (1995).

20) Hirohata Y., Okita M., Hino T., et al., "Gas desorption properties of carbon fiber composite/copper brazed material used for divertor", Proc. of 11th Int. Conf. PSI, (1994) Mito.

21) Ho, S.K., Cambi G., Seki Y., et al., "Progress in the Development of Methodology for Fusion Safety Systems Studies",10th Topical Meeting on the Technology of Fusion Energy, New Orleans, June (1994).

22) Hoshino K., Aikawa H., Asahi Y., et al., "Disruption Control by ECH in the JFT-2M Tokamak", Proc. 15th Int. Conf. on Plasma Physics and Controlled Nuclear Fusion Research, Seville, 1994, A-5-II-3.

23) Hosogane N., Shimada M., Shimizu K., et al., "Measurement of Gaseous Impurities in JT-60U", Proc. 11th Int. Conf. on Plasma-Surface Interaction in Controlled Fusion Devices, Mito, 1994, J. Nucl. Mater., **220-222**, 415 (1995).

24) Hosogane N., Itami K., Asakura N., et al., "Radiative Divertor in JT-60U", Proc. 11th Int. Conf. on Plasma-Surface Interaction in Controlled Fusion Devices, Mito, 1994, J. Nucl. Mater., **220-222**, 420 (1995).

25) Ida K., Miura Y., Itoh K., et al., "Thickness of E×B Velocity Shear at the Plasma Edge in the JFT-2M H-mode", Proc. 4th H-mode Workshop, Plasma Phys. Control. Fusion, **36**, A279 (1994).

26) Ide S., Naito O., Kondoh T., et al., "Non-Inductive Current Drive Experiments for Profile Control in JT-60U", Proc. 15th Int. Conf. on Plasma Physics and Controlled Nuclear Fusion Research, Seville, 1994, A-5-I-4.

27) Ikeda Y., Naito O., Kondoh T., et al., "High Power Lower Hybrid Current Drive Experiments in JT-60U", Proc. 15th Int. Conf. on Plasma Physics and Controlled Nuclear Fusion Research, Seville, 1994, A-3-I-1.

28) Inoue T., Hanada M., Kuriyama M., et al., "Development of High Power Negative ion Source and Accelerators for Neutral Beam Heating and Current Drive Systems", 15th International Conference on Plasma Physics and Controlled Nuclear Fusion Research, F-2-II-2, Seville Spain, Sept. 26 - Oct. 1 (1994).

29) Ioki K., Johnson G., Shimizu K., et al., "ITER Vacuum Vessel Design and Electromagnetic Analysis on In-vessel Components," 18th Symp.on Fusion Technol.,Karlsruhe, [1994].

30) Ishida S., Nishitani T., Mori M., et al., "Confinement and Beta Limit in JT-60U High-β_p Regime", Proc. 21st EPS Conf. on Controlled Fusion and Plasma Physics Part I, 98 (1994).
31) Ishidzuka H., Kawasaki A., Watanabe A., et al., "Formation and diagnostics of electron beam for micro FELs", 16th Int. FEL Conf. Stanford Univ. 1994.
32) Itami K., Asakura N., Tsuji S., et al., "Heat and Particle transport in the Boundary Plasmas during H-mode in JT-60U", Proc. 4th H-mode Workshop, Plasma Phys. Control. Fusion, **36**, A177 (1994).
33) Itami K., Hosogane N., Asakura N., et al., "Characteristics of Heat Flux and Particle Flux to the Divertor in H-mode of JT-60U", iProc. 11th Int. Conf. on Plasma-Surface Interaction in Controlled Fusion Devices, Mito, 1994, J. Nucl. Mater., **220-222**, 203 (1995).
34) Itoh K., Yagi M., et al., "Theory of Anomalous Transport in Toroidal Plasmas", Proc. 6th Int. Toki Conf. on Plasma Physics and Controlled Nuclear Fusion, Toki, 1994, Transactions of Fusion Technology **27**, 52 (1995).
35) Itoh S.-I., Itoh K., Fukuyama A., et al., "A theory of Anomalous Transport in H-mode Plasmas", Proc. 4th H-mode Workshop, Plasma Phys. Control. Fusion, **36**, A261 (1994).
36) Jimbou R., Ogiwara N., Saidoh M., et al., "Surface Compositional Change of B_4C under D_2^+ Implantation in High and Low Vacua and Its Effect on Hydrogen Retention", Proc. 11th Int. Conf. on Plasma-Surface Interaction in Controlled Fusion Devices, Mito, 1994, J. Nucl. Mater., **220-222**, 869. (1995)
37) Kakudate S., Tada E., Oka K., et al. "Mockup Test of Rail-mounted Vehicle type Maintenance System for Fusion Experimental Reactor", 18th Sym. on Fusion Tech., Karlsruhe, Germany (1994).
38) Kamada Y., Ushigusa K., Neyatani Y., et al., "Steady-State High Performance in JT-60U", Proc. 15th Int. Conf. on Plasma Physics and Controlled Nuclear Fusion Research, Seville, 1994, A-5-I-5.
39) Kamada Y., Ushigusa K., Naito O., et al., "ELMy H-mode with high-β_N and high β_p in JT-60U", Proc. 4th H-mode Workshop, Plasma Phys. Control. Fusion, **36**, A123 (1994).
40) Kardaun O., and H-mode Database Working Group, "Offset-Linear Scalings Based on the ITER H-mode Confinement Database", Proc. 21st EPS Conf. on Controlled Fusion and Plasma Physics Part I, 90 (1994).
41) Kawasaki A., Ishidzuka H., Watanabe A., et al., "Beam dynamics in a new inductive acceleration structure with multiple electrodes and its relevance to FEL", 16th Int. FEL Conf. Stanford Univ. 1994.
42) Kikuchi M., and the JT-60 Team, "Recent JT-60U Results towards Steady-State Operation of Tokamaks", Proc. 15th Int. Conf. on Plasma Physics and Controlled Nuclear Fusion Research, Seville, 1994, IAEA-CN-60/A-1-I-2.
43) Kikuchi M., "Attractive Fusion Reactor –Present Status and the Future–", Proc. Int. School of Plasma Physics ⟨⟨Piero Caldirola⟩⟩, Varenna, 1994, "Tokamak Concept Improvement", p. 1.
44) Kikuchi M., "Bootstrap Current –Theory and Experiment–", Proc. Int. School of Plasma Physics ⟨⟨Piero Caldirola⟩⟩, Varenna, 1994, "Tokamak Concept Improvement", p. 247.
45) Kimura T., et al., "DSP Application to Fast Parallel Processing in JT-60U Plasma Control," in Proceedings of the 18th Symposium on Fusion Technology, Karlsruhe, August 22-26, 1994, Volume I, 1995, North-Holland, pp.691-694.
46) Kishimoto Y., Tajima T., LeBrun M. J., et al., "Self-Organized Critical Gradient Transport and Shear Flow Effects for Ion Temperature Gradient (ITG) Mode in Toroidal Plasmas" Proc. 15th Int. Conf. on Plasma Physics and Controlled Nuclear Fusion Research, Seville, 1994, D-2-II-3.
47) Koide Y., Ishida S., Kikuchi M., et al., "Improved Confinement and Transport Barrier in JT-60U High-bp H-mode", Proc. 15th Int. Conf. on Plasma Physics and Controlled Nuclear Fusion Research, Seville, 1994, A-2-I-3.
48) Koide Y., Kikuchi M., Ishida S., et al., "Formation of Internal and Edge Transport Barriers in JT-60U", Proc. 4th H-mode Workshop, Plasma Phys. Control. Fusion, **36**, A195 (1994).
49) Koizumi K., Tada E., Takatsu H., et al. "Design Studies and Technology Development of Tokamak Main Components for Fusion Experimental Reactor", The IAEA 15th International Conference on Plasma Physics and Controlled Nuclear Fusion Research, Seville, Spain, September (1994).
50) Kondoh T., Ide S., Naito O., et al., "Current Profile Control by Lower Hybrid Waves and Neutral Beam Injection in JT-60U", Proc. 21st EPS Conf. on Controlled Fusion and Plasma Physics Part III, 1138 (1994).
51) Konishi S., Nagasaki T., Hayashi T., et al., "Improvements in ZrCo Based Tritium Storage Media", ANS 11th Topical Meeting on the Tech. of Fusion Energy, New Oleans, Lousiana, USA (1994).
52) Konishi S., Yamanishi T., Enoeda M., et al., "Operation of a Simulated Non-Steady Tokamak Fuel Loop Using the TSTA", Third Inter. Symp. on Fusion Nucl. Tech., Los Angeles, California, USA (1994).
53) Kurasawa T., Takatsu H., Sato S., et al. "Design and R&D Activities on Ceramic Breeder Blanket for Fusion Experimental Reactors in Japan", 18th Sym. on Fusion Tech., Karlsruhe, Germany (1994)1233-1236.
54) Kurasawa T., Takatsu H., Koizumi K., et al. "Alternative Design of ITER First Wall, Blanket and Shield", The IAEA 15th International Conference on Plasma Physics and Controlled Nuclear Fusion Research, Seville, Spain, September (1994), E-P-13.

55) Kuriyama M. and NBI Group, "Negative-ion based neutral beam injector for JT-60U", in Proceedings of the 18th Symposium on Fusion Technology, Karlsruhe, August 22-26, 1994, Volume 1, 1995, North Holland, pp 621-624.

56) Kusama Y., Tobita K., Nishitani T., et al., "The Effect of Toroidal Field Ripple on Fast-Ion Loss in JT-60U", Proc. 15th Int. Conf. on Plasma Physics and Controlled Nuclear Fusion Research, Seville, 1994, A-2-IV-5.

57) Kusama Y., Tobita K., Kimura H., et al., "Heat Deposition on the First Wall due to ICRF-Induced Loss of Fast Ions in JT-60U", Proc. 11th Int. Conf. on Plasma-Surface Interaction in Controlled Fusion Devices, Mito, 1994, J. Nucl. Mater., **220-222**, 438 (1995).

58) Maebara, S., Imai, T., Nagashima, T., et al., "Development of high RF efficiency 5 GHz klystron for LHRF system in next tokamak machine", 18th Symp. on Fusion Technology, Karlsruhe (1994).

59) Masaki K., Ando T., Kodama K., et al., "Investigation of Plasma Facing Components in JT-60U Operation", Proc. 11th Int. Conf. on Plasma-Surface Interaction in Controlled Fusion Devices, Mito, 1994, J. Nucl. Mater., **220-222**, 390 (1995).

60) Matsuzaki Y. and JT-60 Power Supply Group, "A Dacade Operational Experience of JT-60 Power Supplies", in Proceedings of the 18th Symposium on Fusion Technology, Karlsruhe, August 22-26, 1994, Volume I, 1995, North-Holland, pp. 1001-1004.

61) Miura Y., Nagashima K., Itoh K., et al., "Rapid Change of Ion Energy Distribution and Floating Potential at L/H transition in the JFT-2M Tokamak", Proc. 4th H-mode Workshop, Plasma Phys. Control. Fusion, **36**, A81 (1994).

62) Miya N., Nemoto M., Toyoshima N., "Tritium Release from JT-60U Vacuum Vessel Following High-Power Heated Deuterium Operations", Fusion Technology, **26**, 507 (1994).

63) Miyamoto K., Hanada M., Inoue T., et al., " Development of a 400 keV Multi-stage Electrostatic Accelerator for Neutral Beam Injectors", 18th Symp. on Fusion Technology, Karlsruhe (1994).

64) Mori M., and the JT-60 Team, "Latest Results from JT-60U", Plasma Phys. Control. Fusion, **36**, B181 (1994).

65) Mori M., the JT-60 Team, the JFT-2M Team, "Overview of the Recent Experimental Results in JT-60 and JFT-2M", Proc. 4th H-mode Workshop, Plasma Phys. Control. Fusion, **36**, A39 (1994).

66) Moriyama S., Fujii T., Kimura H., et al., "Design and power test of a new hybrid rf generator composed of a tetrode and solid-state driver for ICRH", in Proc. of 18th Symp. on Fusion Technology , Karlsruhe 1994, (1995) 549.

67) Muraoka K., Miyazaki K., Czarnetzki U., et al., "Diagnostics for the Spatial Distribution of Hydrogen Atoms around the Divertor Region", Proc. 11th Int. Conf. on Plasma-Surface Interaction in Controlled Fusion Devices, Mito, 1994, J. Nucl. Mater., **220-222**, 563 (1995).

68) Nagami M., and the JT-60 Team, "Latest Results from JT-60U Divertor Research", Proc. 11th Int. Conf. on Plasma-Surface Interaction in Controlled Fusion Devices, Mito, 1994, J. Nucl. Mater., **220-222**, 3 (1995).

69) Nagashima K., Shoji T., Tamai H., et al., "Particle and Heat Balance Analysis in Scrape-off and Divertor Regions of the JFT-2M Tokamak", Proc. 11th Int. Conf. on Plasma-Surface Interaction in Controlled Fusion Devices, Mito, 1994, J. Nucl. Mater., **220-222**, 208 (1995).

70) Nagashima T., Hemsworth R.S., Makowski M., et al., "Neutral Beam and Electron Cyclotron Heating and Current Drive Systems for ITER," 15th IAEA Int.Cont.on Plasma physics and controlled nuclear fusion research Seville,Spain [1994].

71) Naito O., Ikeda Y., Seki M., et al., "Launcher Heat Load on High Power LHCD Experiments in JT-60U" Proc. 11th Int. Conf. on Plasma-Surface Interaction in Controlled Fusion Devices, Mito, 1994, J. Nucl. Mater., **220-222**, 425 (1995).

72) Nakajima T., Kitamura A., Fukuyama Y., et al., "Deuterium Analysis by Rotatable Collector Probe in JFT-2M Scrape-off Layer", Proc. 11th Int. Conf. on Plasma-Surface Interaction in Controlled Fusion Devices, Mito, 1994, J. Nucl. Mater., **220-222**, 361 (1995).

73) Nakamura K., Nagase A., Dairaku M., et al., "Sputtering yields of carbon based materials under high particle flux with low energy", Proc. of 11th Int. Conf. PSI, (1994) Mito.

74) Nakamura Y., "Mechanism of Vertical Displacement Event (VDE) during Plasma Current Quench-Axisymmetric Tokamak Simulation-", Proc. Workshop on MHD Computations –Applied to the Controlled Thermonuclear Fusion Research Based on MHD Mathematical Model–, Tokyo, 1994, p. 132.

75) Nemoto M., Shimada M., Miya M., et al., "Behavior of Charge-Exchanged Deuterium Flux and the Relation to Evacuated Tritium in Degassing Discharges on JT-60U", Proc. 11th Int. Conf. on Plasma-Surface Interaction in Controlled Fusion Devices, Mito, 1994, J. Nucl. Mater., **220-222**, 385 (1995).

76) Neyatani Y., et al., "Recent Progress in JT-60U Experiments", Proc. 18th Symposium on Fusion Technology, Karlsruhe, 1994.

77) Ninomiya H., "Overview of the JT-60 Super Upgrade Design", Proc. 18th Symposium on Fusion Technology, Karlsruhe, 1994.

78) Ninomiya H., "Advanced Tokamak Program in Japan", Proc. Int. School of Plasma Physics [Piero Caldirola], Varenna, 1994, "Tokamak Concept Improvement", p. 305.
79) Ninomiya H., Aoyagi T., Azumi M., et al., "Conceptual Design of JT-60 Super Upgrade", Proc. 15th Int. Conf. on Plasma Physics and Controlled Nuclear Fusion Research, Seville, 1994, F-1-I-1.
80) Nishitani T., Ishida S., Kawano Y., et al., "Empirical Scaling Laws of the Neutron Emission in the JT-60U NBI Experiments", Proc. 21st EPS Conf. on Controlled Fusion and Plasma Physics Part I, 94 (1994).
81) Oasa K., Aikawa H., Asahi Y., et al., "Plasma Response on External Rotating Magnetic Fields in the JFT-2M Tokamak", Proc. 15th Int. Conf. on Plasma Physics and Controlled Nuclear Fusion Research, Seville, 1994, A3/5-P-14.
82) Obara K., Kakudate., Oka K., et al. "Development of In-vessel Viewing System for Fusion Experimental Reactor", SPIE The Inter. Society for Optical Engineering, Mol, Belgium, October (1994).
83) Oda Y., Onozuka M., Hasegawa K. et al., "Development of Repetitive Railgum Pellet Accelerator and Steady Hydrogen Extruder", 18th Symposium on Fusion Technology (Karlsruhe).
84) Ogiwara N., Jimbou R., Saidoh M., et al., "Retention and Thermal Release of Oxygen Implanted in Boron Carbide", Proc. 11th Int. Conf. on Plasma-Surface Interaction in Controlled Fusion Devices, Mito, 1994, J. Nucl. Mater., **220-222**, 748 (1995).
85) Oguri H., Okumura Y., Kusano J., "A High Brightness Hydrogen Ion Source for the BTA at JAERI", 17th International Linac Conference, Tsukuba, Aug. 16 - 21 (1994).
86) Ohdachi S., Shoji T., Nagashima K., "Fluctuations and Transport of JFT-2M Scrape-off Plasma", Proc. 4th H-mode Workshop, Plasma Phys. Control. Fusion, **36**, A201 (1994).
87) Okuno K., Konishi S. and The TPL Design Team, "Conceptual Design of a Fuel Cycle for Fusion Devices in the Near Future", Third Inter. Symp. on Fusion Nucl. Tech., Los Angeles, California, USA (1994).
88) Okuno K., Bushnell C.W., Mitchell N., et al., "Status of the ITER magnet R&D program, " 18th Symp.on Fusion Technol.,Karlsruhe, [1994].
89) Ozeki T., Azumi M., Kikuchi M., et al., "Optimization of MHD Stability in Steady-State Tokamak Reactor: SSTR", Proc. 15th Int. Conf. on Plasma Physics and Controlled Nuclear Fusion Research, Seville, 1994, F-P-7.
90) Park H. K., Bell M. G., Yamada M., et al., "Characteristics of Confinement and Fusion Reactivity in JT-60U High-b_p and TFTR Supershot Regimes with Deuterium Neutral Beam Injection", Proc. 15th Int. Conf. on Plasma Physics and Controlled Nuclear Fusion Research, Seville, 1994, A2/4-P-1.
91) Post D., Kukushkin A., Sugihara M., et al., "ITER Divertor Modeling : Predictions and Experimental Validation", Proc. 15th Int. Conf. on Plasma Physics and Controlled Nuclear Fusion Research, Seville, 1994, E-P-7-1(c).
92) Ryter F., and H-mode Database Working Group, "The H-mode Operational Window as Determined from the ITER H-mode Database", Proc. 21st EPS Conf. on Controlled Fusion and Plasma Physics Part I, 334 (1994).
93) Sakamoto, K., Imai, T., "Development of high power and high efficiency gyrotron for electron cyclotron heating", Jarnal of Plasma and Fusion Research, Vol. 71, No.1 (1995), 5-14 (in Japanese).
94) Sakamoto, K., Tsuneoka, M., Kasugai, A., et al., "Development ofhigh power gyrotron with energy recovery system", 18th Sym. on Fusion Tech. Karlsruhe 1994.
95) Saigusa M., Kimura H., Fujii T., et al., "Comprehensive Studies on Second Harmonic ICRF Heating in JT-60U", Proc. 15th Int. Conf. on Plasma Physics and Controlled Nuclear Fusion Research, Seville, 1994, A-3-I-5.
96) Saji G., Bartels H-W., Chuyanov V., et al., "In-vessel Safety in the ITER EDA Design, " 18th Symp.on Fusion Technol.,Karlsruhe, [1994].
97) Sakasai A., Kubo H., Hosogane N., et al., "Transport and Exhaust of Helium Ash in Enhanced Confinement Regimes on JT-60U", Proc. 15th Int. Conf. on Plasma Physics and Controlled Nuclear Fusion Research, Seville, 1994, A2/4-P-12.
98) Sakasai A., Kubo H., Hosogane N., et al., "Helium Transport and Behavior of ELMy H-mode Plasmas on JT-60U", Proc. 11th Int. Conf. on Plasma-Surface Interaction in Controlled Fusion Devices, Mito, 1994, J. Nucl. Mater., **220-222**, 405 (1995).
99) Sato K., Akiba M., Araki M., et al., "Thermal cycling experiment on 1D CFC/W-Cu divertor mock-up", Proc. of US/J Workshop on High Heat Flux Components and Plasma Surface Interactions for Next Fusion Devices, SAND94-0753 (1994) IV-45-50.
100) Sato M., Kikuchi M., Fukuda T., et al., "H-mode of High Toroidal Field Plasmas in JT-60U", Proc. 15th Int. Conf. on Plasma Physics and Controlled Nuclear Fusion Research, Seville, 1994, A-2-II-4.
101) Sato S., Maki M., Seki Y., et al., "Evaluation of Skyshine Dose Rate due to Gamma-rays from Activated on Cooling Water in Fusion Experimental Reactors", 8th International Conference on RADIATION SHIELDING, April 1994.

102) Sato S., Maki M., Seki Y., et al., "Evaluation of Radiation Streaming through the Annular Gaps around Divertor Cooling Pipes in Fusion Experimental Reactors", 8th International Conference on RADIATION SHIELDING, April 1994.

103) Satomi N., Sato S., Tanaka K., et al., "Mechanical Properties of Boron Coatings", Proc. 11th Int. Conf. on Plasma-Surface Interaction in Controlled Fusion Devices, Mito, 1994, J. Nucl. Mater., **220-222**, 752 (1995).

104) Seki Y., "Summary on "New Devices, Reactors, and Technology (including ITER)"", Proc. 15th Int. Conf. on Plasma Physics and Controlled Nuclear Fusion Research, Seville, 1994.

105) Shiho M., Kawasaki A., Watanabe A., et al., "Analysis of Chaotic Behavior in Raman FEL related to the sideband emissons and to the taperd operation", 16th Int. FEL Conf. Stanford Univ. 1994.

106) Shimizu K., Kubo H., Takizuka T., et al., "Impurity Transport Modeling and Simulation Analysis of Impurity Behavior in JT-60U", Proc. 11th Int. Conf. on Plasma-Surface Interaction in Controlled Fusion Devices, Mito, 1994, J. Nucl. Mater., **220-222**, 410 (1995).

107) Shimizu K., Hosogane N., Takizuka T., et al., "Modeling of Impurity and Plasma Transport for Radiative Divertor", Proc. 15th Int. Conf. on Plasma Physics and Controlled Nuclear Fusion Research, Seville, 1994, D-P-I-2.

108) Shimomura Y., Fujisawa N., Kikuchi M., et al., "ITER Operational Capability," 15th International Conf.on Plasma Phyics and Controlled Nuclear Fusion Research Sevilla,Spain Sep.26-Oct.1, [1994].

109) Shirai H., Takizuka T., Kikuchi M., et al., "Nondimensional Transport Scaling and its Correlation with Local Transport Properties in JT-60U Plasmas", Proc. 15th Int. Conf. on Plasma Physics and Controlled Nuclear Fusion Research, Seville, 1994, A-2-III-6.

110) Shoji T., Nagashima K., Tamai H., et al., "Divertor Plasma Modification by Divertor Biasing and Edge Ergodization in JFT-2M", Proc. 11th Int. Conf. on Plasma-Surface Interaction in Controlled Fusion Devices, Mito, 1994, J. Nucl. Mater., **220-222**, 357 (1995).

111) Suzuki S., Akiba M., Araki M., et al., "Heating tests on JT-60 actively coolied divertor mock-up", Proc. of US/J Workshop on High Heat Flux Components and Plasma Surface Interactions for Next Fusion Devices, SAND94-0753 (1994) IV-39-44.

112) Suzuki S., Araki M., Sato K., et al., "Development of the divertor plate at JAERI", Proc. of 18th Symp. Fusion Technology (1994) Karlsruhe.

113) Tada E, Maisonnier D., Herndon J. "Remote Handling Technology Development for Fusion Experimental Reactors", Third Inter. Symp. on Fusion Nucl. Tech., Los Angeles, California, (1994).

114) Takamura S., Sakurai S., Kawashima H., "Transport of High Energy Electrons in Edge Stochastic Magnetic Layer of Tokamaks", Proc. 21st EPS Conf. on Controlled Fusion and Plasma Physics Part II, 890 (1994).

115) Takenaga H., Asakura N., Shimizu K., et al., "Analyses of Neutral Particle Penetration and Particle Confinement", Proc. 11th Int. Conf. on Plasma-Surface Interaction in Controlled Fusion Devices, Mito, 1994, J. Nucl. Mater., **220-222**, 429 (1995).

116) Tamai H., Shoji T., Miura Y., et al., "ELM Control and Boundary Plasma Modification in the JFT-2M Tokamak", Proc. 15th Int. Conf. on Plasma Physics and Controlled Nuclear Fusion Research, Seville, 1994, A-1-II-3.

117) Tamai H., Shoji T., Nagashima K., et al., "Improvement of the Density Limit with an External Helical Field on JFT-2M Tokamak", Proc. 11th Int. Conf. on Plasma-Surface Interaction in Controlled Fusion Devices, Mito, 1994, J. Nucl. Mater., **220-222**, 365 (1995).

118) Toyama H., Ohdachi S., Hanada K., et al., "Observation of Turbulence Suppression and Transport Reduction in the Presence of Sheared Flow", Proc. 15th Int. Conf. on Plasma Physics and Controlled Nuclear Fusion Research, Seville, 1994, A-4-II-3.

119) Tsuji S., Shimizu K., Takizuka T., et al., "Two-dimensional Divertor Simulation on JT-60U", Proc. 11th Int. Conf. on Plasma-Surface Interaction in Controlled Fusion Devices, Mito, 1994, J. Nucl. Mater., **220-222**, 400 (1995).

120) Willms R. S., Konishi S. and Okuno K., "Use of Magnesium for Recovering Hydrogen Isotopes from Tritiated Water", ANS 11th Topical Meeting on the Tech. of Fusion Energy, New Oleans, Lousiana, USA (1994).

121) Yamage M., Sugai H., Saito T., et al., "Hydrogen Content and Isotope Exchange in Boronization", Proc. 11th Int. Conf. on Plasma-Surface Interaction in Controlled Fusion Devices, Mito, 1994, J. Nucl. Mater., **220-222**, 743 (1995).

122) Yamai H., Konishi S. and Okuuno K., "Hydrogen Isotope Separation for Tritiated Water Processing", ANS 11th Topical Meeting on the Tech. of Fusion Energy, New Oleans, Lousiana, USA (1994).

123) Yamaki T., Gotoh Y., Ando T., et al., "Erosion Characteristics of B_4C-Converted CFC Composite", Proc. 11th Int. Conf. on Plasma-Surface Interaction in Controlled Fusion Devices, Mito, 1994, J. Nucl. Mater., **220-222**, 771 (1995).

124) Yamauchi T., et al., "TV Thomson Scattering System on JFT-2M", Proc. 6th Int. Symposium on Advanced Nuclear Energy Research, Mito, 1994, p. 502.
125) Yamauchi Y., Hirohata Y., Hino T., et al., "Hydrogen Retention of B_4C Converted Graphite", Proc. 11th Int. Conf. on Plasma-Surface Interaction in Controlled Fusion Devices, Mito, 1994, J. Nucl. Mater., **220-222**, 851 (1995).
126) Yoshida H., and the JT-60 Team, "Recent Results and Future Prospects on the JT-60U Tokamak", Fusion Technology, **26**, 406 (1994).
127) Yoshida N., Katoh T., Tokunaga K., et al., "Damage and Surface Modification of TiC Coated Mo Divertor of JT-60U", Proc. 11th Int. Conf. on Plasma-Surface Interaction in Controlled Fusion Devices, Mito, 1994, J. Nucl. Mater., **220-222**, 370 (1995).
128) Yoshino R., "Avoidance and Softening of Disruptions by Control of Plasma-Surface Interaction", Proc. 11th Int. Conf. on Plasma-Surface Interaction in Controlled Fusion Devices, Mito, 1994, J. Nucl. Mater., **220-222**, 132 (1995).
129) Yoshino R., Itami K., Sakasai A., "Particle Fueling by Shallow Pellet Injection in JT-60U", Proc. 11th Int. Conf. on Plasma-Surface Interaction in Controlled Fusion Devices, Mito, 1994, J. Nucl. Mater., **220-222**, 433 (1995).
130) Yoshino R., Neyatani Y., Isei N., et al., "Disruption Amelioration Experiments in JT-60U and JET", Proc. 15th Int. Conf. on Plasma Physics and Controlled Nuclear Fusion Research, Seville, 1994, A-5-II-2.

A.1.4 List of other reports

1) Hodgson E., Matoba T., ""CERAMIC" INSULATING MATERIALS (Summary), " ITER/EDA Technical Meeting (Garching).
2) Ikeda K., Tanaka M., Matsuura T.,et al., "State-of-the Art of High Power GTO Converters and Inverters," ITER/EDA Technical Meeting, Naka.
3) Kawashima S., Matsuzaki Y., "Development of power electronics in the industry," ITER/EDA Technical Meeting, Naka.
4) Koizumi K., "Interim report on separate first wall," ITER/EDA Tech.Meeting (Garching).
5) Koizumi K., "Present status of the design work for double-walled separate FW," ITER/EDA Technical Meeting,Garching, April 1994.
6) Kuroda T., "Japanese Proposal on Test Program in ITER," ITER/EDA Technical Meeting,Garching, April 1994.
7) Kuroda T., Takatsu H., "Fabrication procedure of shielding blanket," ITER/EDA Tech.Meeting (Garching).
8) Kuroda T., Takatsu H., "Convertible blanket design proposal," ITER/EDA Tech.Meeting (Garching).
9) Matoba T., "Irradiation Test of Ceramics," ITER/EDA Tech.Meeting (Garching).
10) Matsukawa M., Ninomiya H., Horiike H., et al., "Plasma iginition facility using a multi-winding transformer in a large tokamak device and its application to power supply system for poloidal field magnet," Trans. Institute of Electriacl Engineers of Japan (in Japanese).
11) Matsukawa M., "A Preliminary Scenario," ITER/EDA Tech.Meeting (Naka).
12) Matsuzaki Y., "JT-60 power supply system and possible application to ITER," ITER/EDA Technical Meeting, Naka.
13) Mohri K., "Fabrication for the first wall shield blanket with Pipe Manifold -J.bend Blanket., " ITER/EDA Tech.Meeting (Garching).
14) Mohri K., "Blanket Segmentation/ Fabrication methods/ Welding/ cutting/ inspection," ITER/EDA Tech.Meeting (Garching).
15) Nakamura H., "Wall Conditioning in ITER," International Workshop on Wall Conditioning in large UHV devices, Switzerland, 1995.
16) Nishitani T., "Irradiation Test of Deagnostics Components in Japan," ITER/EDA Tech.Meeting (Garching).
17) Nishitani T., Matoba T., "Application of Optical Fibers in Fusion Diagnostics (in Japanese)," Workshop on Application of Optical Fibers to Quantum Measurement," July 1994.
18) Okuno K., "Status of Model Coils," ITER/EDA Tech.Meeting (Naka).
19) Seki Y., "Radioactivity Safety", Science of Machine, Vol.47, No.1., (1995) (in Japanese).
20) Senda I., Shoji T., "ITER Disruptions Characteristics Obtained by the Deformable Plasma Simulation Code," ITER/EDA Technical Meeting (Garching).
21) Shimada R., Matsuzaki Y., "ITER power from the HV grid combined with the variable-speed constant frequency motor-generator," ITER/EDA Technical Meeting, Naka.
22) Shimizu K., Williamson D., Ioki K., "Electromagnetic Analysis on Vacuum Vessel and In-vessel components," ITER/EDA Tech.Meeting (Garching).
23) Shimizu K., Iizuka T., Ioki K., "Vacuum Vessel Design and Critical Issues," ITER/EDA Tech.Meeting (Garching).

24) Sugihara M., "Status of Edge Database," ITER/EDA Technical Meeting (Garching).
25) Sugihara M., "Initial Considerations on ITER Shot Data Storage System and Edge Database System," ITER/EDA Phys.Expert Group Meeting (San Diego).
26) Tachikawa N., "Back plate design options,coolant pipe layout and remote maintenance/ blanket replacement," ITER/EDA Tech.Meeting (Garching).
27) Takatsu H., "Interim report on shielding blanket design," ITER/EDA Tech.Meeting (Garching).
28) Takatsu H., "Critical issues of modular blanket design concept," ITER/EDA Tech.Meeting (Garching).
29) Takatsu H., "Comments on ITER operation parameters for test program," ITER/EDA Technical Meeting,Garching, April 1994.
30) Takatsu H., "Present Status of Design Tasks for First Wall,Blanket and Shield," ITER/EDA Technical Meeting,Garching, April 1994.
31) Tanaka S., "Evolution of Nuclear Fusion Research and Development of Large Components" 2.4.1 NBI (in Japanese) Technical Report of Institute of Electrical Engineers of Japan 501 (1994).
32) Tsunematsu T., Tada E., Senda I., et al., "Japanese contributions to the first sensitivity analysis meeting,"ITER/EDA 1st Sensitivity Analysis Meeting, San Diego.
33) Tsunematsu T., Tada E., Senda I., et al., "Japanese contributions to the second sensitivity analysis meeting," ITER/EDA 2nd Sensitivity Analysis Meeting, San Diego.
34) Tsunematsu T., Tada E., Senda I., et al., "Japanese contributions to the third sensitivity analysis meeting, " ITER/EDA 3rd Sensitivity Analysis Meeting, San Diego.
35) Tsunematsu T., "Introduction and Exective Summary of Sensitivity Study on ITER, " (St.Petersburg).
36) Yamamoto S., "Introductory Information on ITER Conponents Design,Working Conditions,Requirements for Irradiation Testing,Present and Planned Program.-In Vessel Ancillaries-," ITER/EDA Tech.Meeting (Garching).
37) Yamamoto S., "Activities of In Vessel Diagnostics Group," ITER/EDA Phys.Expert Group Meeting (San Diego).
38) Yamamoto S., "Activities of In Vessel Diagnostics Group for ITER Design and Technology R&D," ITER/EDA Tech.Meeting (Garching).
39) Yamamoto S., "Prospective Products of this meeting," ITER/EDA Tech.Meeting (Garching).
40) Yamamoto S., Matoba T., et al., "Kick-off Meeting Summary on Generic Access Routes for Diagnostics,"ITER/EDA Technical Meeting ,Garching.
41) Yamamoto S., "Evolution of Nuclear Fusion Research and Development of Large Components 2.5 Diagnostics (in Japanese) Technical Report of Institute of Electrical Engineers of Japan 501 (1994).
42) Yoshida K., "Redundancy of PF coils," ITER/EDA Magnet Technical Meeting (Naka).
43) Yoshida K., "Pre-assembly testing of SC magnet," ITER/EDA Magnet Technical Meeting (Naka).

A.2 Personnel and Financial Data

A.2.1 Change in number of personnel and annual budget (FY1988-1994)

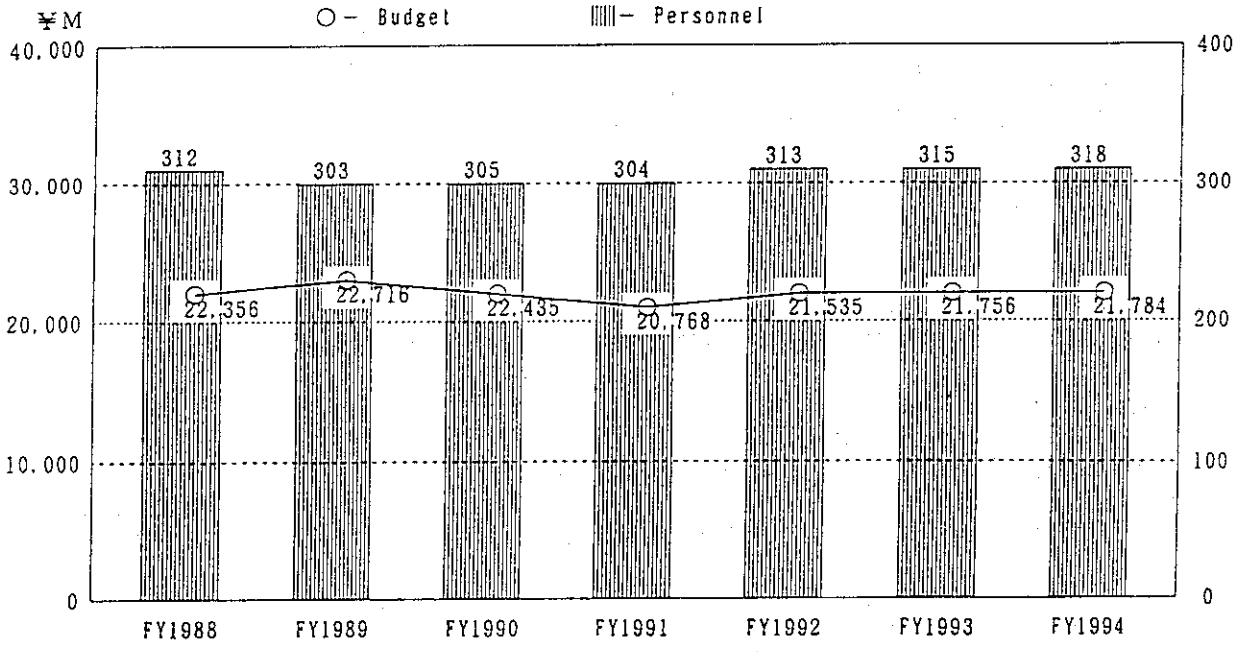

A.2.2 Organization chart (March 31, 1995)

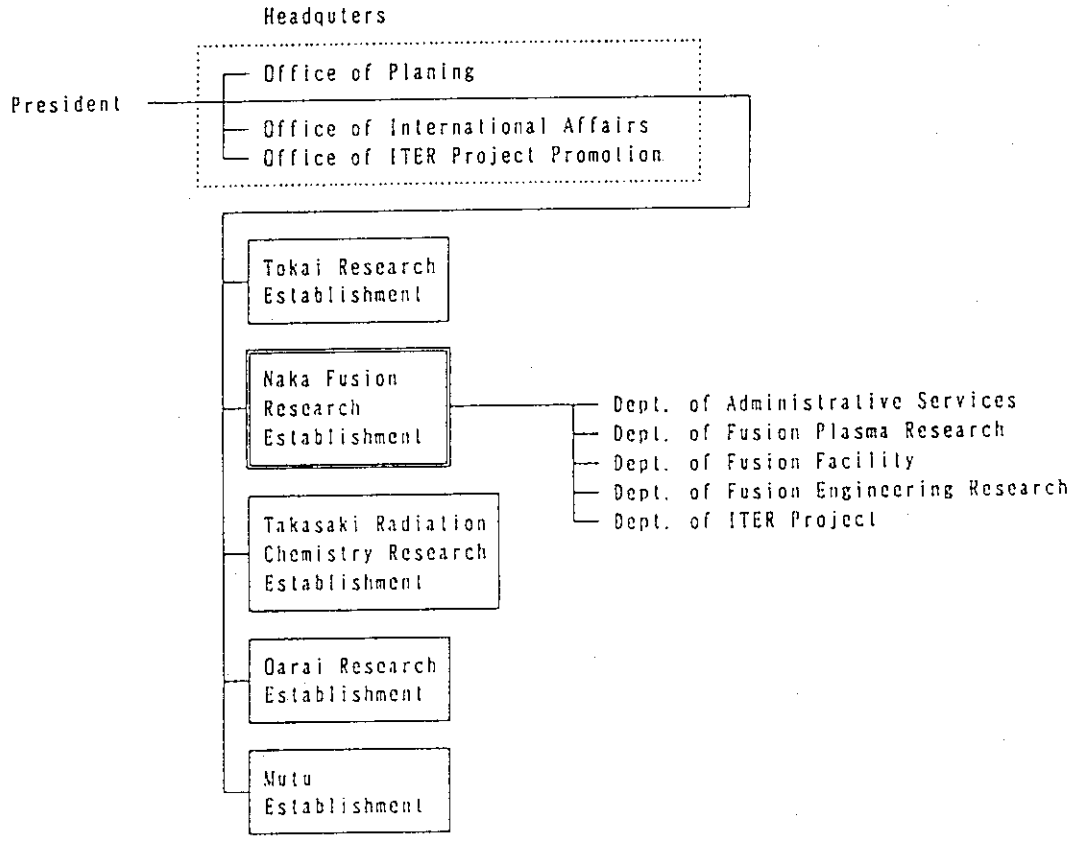

A.2.3 Scientific Staffs in the Naka Fusion Research Establishment (March 31, 1995)

Naka Fusion Research Establishment
TAMURA Sanae (Director General)
MIYAMOTO Goro (Scientific Advisor)
SEKIGUCHI Tadashi (Scientific Advisor)
TANAKA Masatoshi (Scientific Advisor)

Department of Administrative Services
TEZUKA Kihachiro 9Director)

Department of Fusion Plasma Research
KISHIMOTO Hiroshi (Director) NOMURA Fujiyasu (Administrative Manager)

Tokamak Program Division
NAGAMI Masayuki (Head)
KAMADA Yutaka
NAGASHIMA Keisuke
OGURI Shigeru
KIKUCHI Mitsuru
NAKAGAWA Shouji
SAKASAI Akira
MIYA Naoyuki
NAKAJIMA Shinji
TOYOSHIMA Noboru

Plasma Analysis Division
AZUMIMasafumi (Head)
AOYAGI Tetsuo
KIM Jin Yong (*89)
NAKAMURA Yukiharu
SAKATA Shinya
TSUCHIYA Satoru (*85)
TSURUOKA Takuya (*49)
HAGINOYA Hirofumi (*91)
KISHIMOTO Yasuaki
OHSHIMA Takayuki
SATO Minoru
TSUJI Shunji
YAGI Masahiro
HAMAMATSU Kiyotaka
MATSUDA Toshiaki
SAITO Naoyuki
SHIRAI Hiroshi
TSUGITA Tomonori

Large Tokamak Experiment Division I
NINOMIYA Hiromasa (Head)
CHIBA Shinichi
HIGASHIJIMA Satoru
IWAHASHI Takaaki
KITAMURA Shigeru
KONDOH Takashi
NEYATANI Yuzuru
OYEVAAR I. Therdorus (*89)
TAKEJI Satoru
URAMOTO Yasuyuki
YOSHINO Ryuji
FUKUDA Takeshi
ISEI Nobuyuki
KAZAMA Daisuke
KOIDE Yoshihiko
NAGAYA Susumu
OHZEKI Masahiro
SHITOMI Morimasa
TSUCHIYA Katsuhiko
YAMASHITA Osamu
GUNJI Souichi
ISHIDA Shinichi
KAWANO Yasunori
KONOSHIMA Shigeru
NAITO Osamu
ONOSE Yoshiaki
SUNAOSHI Hidenori
TSUKAHARA Yoshimitsu
YOSHIDA Hidetoshi

Large Tokamak Experiment Division II
SHIMADA Michiya (Head)
AFANASSIEV Valeri (*89)
CARLSSON Thomas (*99)
HATAE Takaki
IDE Shunsuke
KOZLOVSKIJ Sergei (*100)
MORIOKA Atsuhiko
NISHITANI Takeo
SAKURAI Shinji
TOBITA Kenji
ASAKURA Nobuyuki
FUJITA Takaaki
HOEK Magnus (*89)
ITAMI Kiyoshi
KUBO Hirotaka
NAGASHIMA Akira
PETROV Sergei (*100)
SHIMIZU Katsuhiro
TUCCILLO Angelo A. (*102)
CARLSSON Mattias (*99)
GASPARINO Ugo (*101)
HOSOGANE Nobuyuki
KIMURA Haruyuki
KUSAMA Yoshiki
NEMOTO Masahiro
PODDA Salvatore (*102)
SUGIE Tatsuo
USHIGUSA Kenkichi

FANG Yude (*90)

Plasma Theory Laboratory
MAEDA Hikosuke (Head)
KAWANOBE Mitsuru (*49) KOGA James (*90) KURITA Gen-ichi
TAKIZUKA Tomonori TOKUDA Shinji TUDA Takashi
YAMAGIWA Mitsuru OZEKI Takahisa

Experimental Plasma Physics Laboratory
MAEDA Hikosuke (Head)
AIKAWA Hiroshi HOSHINO Katsumichi KAWAKAMI Tomohide
KAWASHIMA Hisato MAENO Masaki MIURA Yukitoshi
MORI Masahiro OGAWA Hiroaki OGAWA Toshihide
OASA Kazumi SATO Masayasu SENGOKU Seio
SHIINA Tomio TAMAI Hiroshi UEHARA Kazuya
YAMAUCHI Toshihiko

Department of Fusion Facility
TANAKA Yuji (Director) FUNAHASHI Akimasa (Deputy Director)

Fusion Facility Administration
NOMURA fujiyasu (General Manager)

JT-60 Facility Division I
KIMURA Toyoaki (Head)
AKASAKA Hiromi AKIBA Ken-ichi(*79) ARAKAWA Kiyotsugu
ISAKA Masayoshi KAWAMATA Youichi KIUCHI Shigemi(*30)
KUSAKA Makoto(*28) MATSUZAKI Yoshimi MIYACHI Kengo
NAKAKUKI Riichi(*49) NOBUSKA Hiromichi OKANO Jun
OMORI Shunzo OMORI Yoshikazu SEIMIYA Munetaka
SHIMONO Mitugu TAKAHASHI Minoru TERAKADO Tsunehisa
TOTSUKA Toshiyuki YOSHIDA Michiharu

JT-60 Facility Division II
SHIMIZU Masatsugu (Head)
ANDO Toshiro ARAI Takashi HIRATSUKA Hajime
HONDA Masao ICHIGE Hisashi JIMBOU Ryutaro(*2)
KAMINAGA Atsushi KODAMA Kozo KOIKE Tsuneyuki
KOMURO Ken-ichi(*79) MASAKI Kei MIYO Yasuhiko
OGIWARA Norio OHUCHI Yutaka OKABE Tomokazu
SAIDOH Masahiro SASAJIMA Tadashi SASAKI Noboru(*2)
TAKAHASHI Shoryu(*2) TSURUMI Satoshi(*2) YAGYU Jun-ichi

RF Facility Division
YAMAMOTO Takumi (Head)
ANNOU Katsuto FUJII Tsuneyuki FUKUDA Hiromi (*29)
IKEDA Yoshitaka IKEDA Yukiharu IGARASHI Kouichi (*79)
KITAI Tatsuya (*28) KIYONO Kimihiro MORIYAMA Shinichi
SATO Tomio (*30) SEKI Masami SHINOZAKI Shinichi
SUGANUMA Kazuaki TERAKADO Masayuki YOKOKURA Kenji

NBI Facility Division
KURIYAMA Masaaki (Head)
AKINO Noboru EBISAWA Noboru HONDA Atsushi

HOONOKI Toshio(*31) ISOZAKI Nobumitsu ITOH Takao
KAWAI Mikito KAZAWA Minoru MOGAKI Kazuhiko
OHGA Tokumichi OOHARA Hiroshi SHIMIZU Kazuhiko(*30)
TAKAHASHI Shunji TAKAYASU Toshio(*79) USAMI Hiroji(*2)
USUI Katsutomi YAMAMOTO Masahiro

JFT-2M Facility Division
SUZUKI Norio (Head) TANAKA Takujiro (Deputy Head)
HASEGAWA Koichi KASHIWA Yoshitoshi KIKUCHI Kazuo
KOMATA Masao OKANO Fuminori SAITO Masaya(*30)
SAWAHAATA Masayuki SHIBATA Takatoshi SUZUKI Sadaaki
TANI Takashi TOKUTAKE Toshikuni

Department of Fusion Engineering Research
SHIMAMOTO Susumu (Director) OHTA Mitsuru (Deputy Director)
SHOJI Kuniaki (Administrative Manager)

Plasma Engineering Laboratory
MURAKAMI Yoshio (Head)
ABE Tetsuya HIROKI Seiji KASAI Satoshi
NAKAMURA Jyun-ichi (*103) UEHARA Toshiaki (*30)

NBI Heating Laboratory
OHARA Yoshihiro (Head)
AKIBA Masato ARAKI Masanori DAIRAKU Masayuki
HANADA Masaya INOUE Takashi MIYAMOTO Naoki (*59)
MIYAMOTO Kenji NAGASE Akihito (*2) NAKAMURA Kazuyuki
NISHINO Yoshihiko OKUMURA Yoshikazu SATOH Kazuyoshi
SUZUKI Satoshi WATANABE Kazuhiro YOKOYAMA Kenji

RF Heating Laboratory
IMAI Tsuyoshi (Head)
FUJITA Hideo (*30) FUKUSHIMA Yoshinori KASUGAI Atsushi
KOARAI Tohru (*40) MAEBARA Sunao OGITSU Susumu (*30)
SAIGUSA Mikio SAKAMOTO Keishi SHIHO Makoto
TAKAHASHI Kouji TSUNEOKA Masaki WATANABE Akihiko (*40)

Tritium Engineering Laboratory
OKUNO Kenji (Head)
ARITA Makoto (*35) ENOEDA Mikio HARA Masahide (*23)
HAYASHI Takumi HONMA Takashi ISHIDA Toshikatsu (*16)
ITO Takeshi (*104) KAWAMURA Yoshinori KONISHI Satoshi
MATSUDA Yuji NAKAMURA Hirofumi OBATA Hiroyuki (*16)
O'HIRA Shigeru SUZUKI Takumi TANJI Nobuo (*29)
YAITA Yumi (*4) YAMADA Masayuki YAMAI Hideki (*105)
YAMANISHI Toshihiko

Reactor Structure Laboratory
SEKI Masahiro (Head)
TADA Eisuke OBARA Kenjiro NISHIO Satoshi
KURASAWA Toshimasa KANAMORI Naokazu (*2) KAKUDATE Satoshi
SATO Satoshi OKA Kiyoshi NAKAHIRA Masataka
FURUYA Kazuyuki HORIE Makoto TAGUCHI Kou (*30)
MURAKAMI Shin (*4) TOGAMI Ikuhide (*95) FUKATSU Seiichi (*4)

Fusion Reactor System Laboratory
SEKI Yasushi (Head)
AOKI Isao UEDA Shuzo

Superconducting Magnet Laboratory
TSUJI Hiroshi (Head)

ANDO Toshinari	FUJISAKI Hiroshi (*2)	HAMADA Kazuya
HIYAMA Tadao	ISONO Takaaki	ITO Toshinobu (*4)
KATO Takashi	KAWANO Katsumi	KOIZUMI Norikiyo
MATSUI Kumihiro	NAKAJIMA Hideo	NISHI Masataka
NISHIDA Kazuhiko (*18)	NOZAWA Masanobu (*58)	NUNOYA Yoshihoko
OGATA Hiroshige (*4)	OSHIKIRI Masayuki (*30)	SEKI Syuichi (*30)
SUGIMOTO Makoto	TAKAHASHI Yoshikazu	TAKANO Katsutoshi (*30)
TERASAWA Atsumi (*15)	UNO Yasuhiro (*30)	
WAKABAYASHI Hiroshi (*30)		

Department of ITER Project
MATSUDA Shinzaburo (Director)
TOMABECHI Ken (Invited Researcher) SHIMONURA Yasuo
FUJISAWA Noboru NAGASHIMA Takashi TAKATSU Hideyuki

Administration Group
YAMANE Yoshifumi (Leader)
IIZUKA Koji OHKUBO Keiko YAMASHITATetsuyuki
OZAWA Keiko

Project Management Group
SEKI Syogo (Leader)
MATOBA Tohru

Joint Central Group

SEKI Syogo (Leader)	IIDA Fumio (*2)	KIMURA Haruyuki
HORIKIRI Hitoshi (*97)	OKI Kimihiro (*7)	HANADA Masaya
ISHIMOTO Kazuyuki (*96)	MATSUKAWA Makoto	IIZUKA Takayuki
KONDOH Mitsunori (*4)	MORI Seiji (*16)	ITOH Kazuyoshi (*29)
MIZOGUCHI Tadanori (*2)	SAJI Gen (*7)	MATSUMOTO Hiroshi
NAKANURA Hiroo	SHIMADA Mamoru (*4)	MOHRI Kensuke (*16)
OKUNO Kiyoshi	TANAKA Eiichi (*98)	OIKAWA Akira
SHIBANUMA Kiyoshi	YONEKAWA Izuru	SATO Kouichi (*83)
SUGIHARA Masayashi	TACHIKAWA Nobuo (*4)	SHIMIZU Katsusuke (*23)
YAMAMOTO Shin	TANAKA Shigeru	YOSHIDA Hiroshi
YOSHIDA Kiyoshi		

Home Team Design Group
TSUNEMATSU Toshihide (Leader)
HASHIMOTO Toshiyuki (*16) ODAJIMA Kazuo
HOTTA Masataka (*58)

KOIZUMI Kouichi	SENDA Ikuo (*4)	NOMURA Yukio (*17)
OOKAWA Yoshinao	TADO Shigeru (*15)	SHOJI Akio
YOSHIMURA Kunihiro (*4)	MITSUI Jin (*29)	OZAWA Yoshihiro (*2)
ITOH Yutaka (*2)	HASHIMOTO Masayoshi (*14)	KITAMURA Kazuynori

Safety Evaluation Group
INABE Teruo (Leader)

UDA Tatsuhiko (*2)　　MARUO Takeshi

*1 General Atomics, USA
*2 Hitachi Ltd.
*3 Lawrence Livermore National Laboratory, USA
*4 Toshiba Corp.
*5 Max-Plank Institute fur Plasmaphysik, Germany
*6 Massachusetts Institute of Technology, USA
*7 Mitsubishi Atomic Power Industry Inc.
*8 The University of Tokyo
*9 Nagoya University
*10 Osaka University
*11 Kyoto University
*12 Hiroshima University
*13 Institute fur Reactorbauelements, KfK, Germany
*14 Ishikawajima-Harima Heavy Industries, Ltd.
*15 Mitsubishi Electric Co., Ltd.
*16 Kawasaki Heavy Industries, Ltd.
*17 Hazama-gumi Ltd.
*18 Kobe Steel Ltd.
*19 Oak Ridge National Laboratory, USA
*20 Century Research Center Corp.
*21 Northwestern Laboratory
*22 Institute of Plasma Physics, Nagoya University
*23 Mitsubishi Heavy Industries, Ltd.
*24 NAIG Nuclear Research Laboratory
*25 Japan Atomic Industrial Forum
*26 Central Research Institute for Electric Power
*27 NEC Co.
*28 Kaihatsu Denki Co.
*29 Sumitomo Heavy Industries, Ltd.
*30 Nuclear Engineering Co., Ltd.
*31 Tomoe Shokai
*32 Ibaraki Kohsan
*33 Tokyo Nuclear Service Co., Ltd.
*34 ULVAC Corp.
*35 Kyushu University
*36 Contract Researcher
*37 Princeton Plasma Physics Laboratory, USA
*38 LITEC Co., Ltd.
*39 Japan Expert Clone Corp.
*40 Nissei Sangyo Co., Ltd.
*41 JET Joint Undertaking, UK
*42 Hodaka Seiki Ltd.
*43 Sumitomo Electric Industries, Ltd.
*44 Nikon Corp.
*45 National Laboratory for High Energy Physics
*46 University of Tsukuba
*47 Los Alamos National Laboratory, USA
*48 Japan Radiation Engineering Co.
*49 Nuclear Energy Data Center Co.
*50 Osaka University

*51 IMPRIAL COLLEGE, UK
*52 Institute of Research Hydro-Quebec, Varenns, Canada
*53 KFA-IPP, Germany
*54 Ewic Engineering Co., Ltd.
*55 ORC Manufacturing Co., Ltd.
*56 Koike Sanso Kogyo Co., Ltd.
*57 Hitachi Sanso Co., Ltd.
*58 Fuji Electric Co., Ltd.
*59 Nissin Electric Co., Ltd.
*60 Sandia National Laboratory, USA
*61 JGC Corp.
*62 Tokyo Institute of Technology
*63 Nuclear Research Center Karlsruhe, Germany
*64 Argonne National Laboratory, USA
*65 ITER Team
*66 Yokohama National University
*67 Nihon Software Kaihatsu, Inc.
*68 Kanazawa Computer Service Corp.
*69 University of Calfornia at Los Angeles, USA
*70 University of Texas, USA
*71 Varian Company Co., Ltd.
*72 Nagoya University of Technology
*73 Denki Kogyo Co., Ltd.
*74 The NET Team
*75 National Institute for Fusion Science
*76 I. V. Kurchatov Institute of Atomic Energy
*77 Keio University
*78 Mitsubishi Cable Industries, Ltd.
*79 Nippon Advanced Technology Co., Ltd.
*80 Hamamatsu Photonics KK
*81 University of California at San Diego, USA
*82 University of Maryland
*83 Atomic Data Service Corp.
*84 Nihon Houshasen Engineering Co., Ltd.
*85 ACE
*86 Hitachi Works
*87 Hitachi Cable, Ltd.
*88 Austrian Research Center Seibersdorf
*89 STA Fellowship
*90 JAERI Fellowship
*91 Nuclear Information Service Co.
*92 Tokai University
*93 Ibaraki Software
*94 Ebara Research Co., Ltd.
*95 Kumagai-gumi Ltd.
*96 Shimizu Corparation
*97 Shinryo Corporation
*98 Kajima Corporation
*99 Visiting Researcher
*100 Ioffe Institute, Russian Fed.
*101 IPP Garching, Germany
*102 ENEA, Italy
*103 Osaka Vacuum Ltd.
*104 Kaken Co.
*105 Hitachi Nuclear Engineering Co., Ltd